

## **General Disclaimer**

### **One or more of the Following Statements may affect this Document**

- This document has been reproduced from the best copy furnished by the organizational source. It is being released in the interest of making available as much information as possible.
- This document may contain data, which exceeds the sheet parameters. It was furnished in this condition by the organizational source and is the best copy available.
- This document may contain tone-on-tone or color graphs, charts and/or pictures, which have been reproduced in black and white.
- This document is paginated as submitted by the original source.
- Portions of this document are not fully legible due to the historical nature of some of the material. However, it is the best reproduction available from the original submission.

(NASA-CR-168585) INVESTIGATIONS OF  
FLOWFIELDS FOUND IN TYPICAL COMBUSTOR  
GEOMETRIES Semiannual Status Report, 1 Aug.  
1981 - 31 Jan. 1982 (Oklahoma State Univ.,  
Stillwater.) 138 p HC A07/MF A01

N82-19495

Unclass

G3/34 09249

## ABSTRACT

This is the Third Semi-Annual Status Report on Grant NAG 3-74 and discussion is on those activities undertaken during the first half of the second year of the study. Measurements and computations are being applied to an axisymmetric swirling flow, emerging from swirl vanes at angle  $\phi$ , entering a large chamber test section via a sudden expansion of various side-wall angles  $\alpha$ . New features of the present year's study are: the turbulence measurements are being performed on *swirling* as well as non-swirling flow; and all measurements and computations are also being performed on a confined jet flowfield with realistic *downstream blockage*. Recent activity in the research program falls into three categories:

1. Time-mean flowfield characterization by five-hole pitot probe measurements and by flow visualization.
2. Turbulence measurements by a variety of single- and multi-wire hot-wire probe techniques.
3. Flowfield computations using the computer code developed during the previous year's research program.

Section 1 of this document describes this recent activity in the above subsections of the study, while Section 2 gives a brief summary of the present status and a list of recent publications. Appendices A through E contain a recent report, an M.S. Thesis, and three research papers. Finally, Appendix F contains a report on the first six months of the sub-contract activity at Dynamics Technology.

<u>CONTENTS</u>		Page
	ABSTRACT	ii
1.	<u>RECENT PROGRESS</u>	1
	1.1 Flow Visualization and Time-Mean Velocities	1
	1.2 Hot-Wire Anemometry	1
	1.3 Computer Prediction	4
2.	<u>PRESENT STATUS</u>	6
	2.1 Summary	6
	2.2 Publications	6
3.	FIGURES	10
4.	APPENDICES	
	A. Turbulence Measurements in a Complex Flowfield Using a Six-Orientation Hot-Wire Probe Technique	
	B. Turbulence Measurements in Free and Confined Jet Flows Using Crossed Hot-Wire Probes	
	C. A Simple Finite Difference Procedure for the Vortex Controlled Diffuser	
	D. A Basic Code for the Prediction of Transient Three-Dimensional Turbulent Flowfields	
	E. Computer Modeling in Ramjet Combustors	
	F. Sub-Contract Activity at Dynamics Technology	

## 1. RECENT PROGRESS

### 1.1 Flow Visualization and Time-Mean Velocities

Time-mean flowfield measurements have been performed with a traversing five-hole pitot probe in a confined jet with downstream blockage. These measurements have been performed on a nonswirling confined jet and are currently being done on various swirling flows. It was determined that the downstream blockage had a significant effect on corner recirculation patterns as the blockage position is closer and closer to the inlet. The data obtained from these experiments will be important in evaluating the predictive capability of the  $k-\epsilon$  turbulence model and STARPIC computer code flowfield calculations. They will also assist in turbulence model developments.

As part of this activity, careful measurements of the flowfield immediately downstream of the swirl pack have been made. These measurements have been performed and documented for various blade settings. Briefly, the measurements show that the flowfield typically has a swirl flow angle which is a few degrees smaller than the blade angle. Also, the measurements show a larger axial flow in the outer annular portion of the duct; presumably "thrown" out by centrifugal forces associated with the swirl as the flow passes through the swirler. Reports on these activities will be amalgamated later.

Regarding flow visualization, photography of neutrally-buoyant helium-filled soap bubbles, tufts, and injected smoke helps to characterize the time-mean streamlines, recirculation zones and regions of highly turbulent flow.

### 1.2 Hot-Wire Anemometry

A significant effort has been made in the application of two hot-wire methods to the measurement of time-mean and turbulence properties, and a third method is being readied. The experiments being performed are designed to provide the information necessary for turbulence modeling development in the confined jet facility.

1. One-Wire Method. Single normal hot-wire measurements in non-swirling flow have established that the experimental technique is producing reliable results. Six-orientation hot-wire measurements have been made from which a method has been developed to make estimates of all components of the time-mean velocity vector and the Reynolds stress tensor. A major portion of these measurements are now complete for the nonswirling flowfield, and corresponding measurements in swirling flowfields are currently in progress. The effect of downstream blockage is also to be investigated under nonswirling and swirling conditions. Currently, the nonswirling case without downstream blockage has been extensively evaluated, and the results of this activity are reported in an MS Thesis, which is included as Appendix A of this report.

2. Two-Wire Method. Although the single hot-wire (six-orientation) measurements are convenient and provide a great deal of information on the time-mean velocity and on the kinetic energy of turbulence, they have a shortcoming in that measurements of the Reynolds shear stresses are less accurate than desirable. Consequently, crossed hot-wire capability has been developed to measure turbulence properties. This technique has been used for the nonswirling flow without downstream blockage, and is soon to be used with downstream blockage. A new cross-wire probe is on order which will enable a more accurate evaluation of the turbulent shear stress than currently possible. The results of our present activity is included in the report in Appendix B.

At the moment it seems that application of the crossed-wire method to swirling flowfields will not produce measurements of all the turbulent stresses unless the probe is rotated through multiple orientations. However, the six-orientation single-wire method will yield appropriate estimates. Presently

this technique is being used to measure turbulent stresses in a confined swirling flowfield, and the results will be reported in the next Semi-Annual Status Report.

3. Three-Wire Method. One of the major results of the six-orientation single hot-wire technique was to show that estimates of the turbulent shear stresses typically have large uncertainties. In fact, the uncertainties are probably so large as to preclude a definitive evaluation of turbulence models used in the computations. Believing this to be the case, a series of hot-wire measurements have been planned, using a three-wire, hot-wire probe with direct computer interface and data reduction. These measurements are to be performed by subcontractor Dynamics Technology, Inc. under the direction of Dr. Dennis K. McLaughlin. He is being assisted by Salim I. Janjua who joined the company in January 1982 after completing his MS degree at Oklahoma State University. Dynamics Technology has been assembling a swirling jet facility which will duplicate the flowfield produced by the Oklahoma State University facility. However, it will be instrumented differently, with the three-wire hot-wire probe and its three-degree of freedom probe drive being major constituents. Adequate progress has been made on the facility assembly in order to complete the experiments during the first half of 1982. A report on these activities appears in Appendix F.

### 1.3 Computer Prediction

An advanced computer code is used to predict corresponding confined jet flows. The calculation method includes a stairstep boundary representation of the expansion flow and a conventional  $k-\epsilon$  turbulence model. The predictions include recirculation zone characterization and mean streamline patterns, which are being compared with on-going experimental studies. The general development was discussed in the previous Semi-Annual Status Report, and the details are included in the Ph.D. Thesis of D. L. Rhode and its associated report, NASA CR-3442. Currently, predictions are being made with the standard  $k-\epsilon$  turbulence model and no downstream blockage. These constraints will be removed later. Predictions now include realistic inlet conditions.

An indication of predictive capability is shown in Fig. 1, taking measured  $u$ ,  $v$  and  $w$  profiles very close to the 10-blade variable angle swirler located 4 cm upstream of the expansion  $x/D=0$  location. They may be compared with measurements shown in Fig. 2 [although the experimental data shown at  $x/D=0$  are actually 4 cm downstream of the swirler, and cannot therefore be compared directly with the inlet profiles used in the code and shown in Fig. 1]. The corner recirculation zone is predicted to be slightly too large, and the central recirculation zone slightly too narrow. However, it must be remarked that worse predictions occur if the inlet radial velocity  $v$  is assumed to be zero, or flat inlet profiles, or solid body rotation inflow, is assumed. The present predictions are superior to previous ones by Rhode, who used flat inlet profiles initially, then realistic  $u$  and  $w$  profiles but with  $v$  equal to zero. There is a need for precise inlet flow data to be recorded in experimental work, and clearly turbulence model developments are needed for realistic flow simulation. Similar computations have been generated for other swirl cases, and a complete discussion on these activities is to be prepared.

Oblique to the present research, a simple technique for the solution of transient 2-D and 3-D flowfields has been computerized. The  $k-\epsilon$  turbulence model has recently been added, and species diffusion and buoyancy are included. A paper on the application of the 2-D code to vortex controlled diffusers is given in Appendix C, while Appendix D illustrates two applications of the 3-D turbulent code. Configurations investigated are local destratification near the release structure of a reservoir and deflection of a jet entering normally into a uniform cross-flow, showing good agreement with experimental data in both cases.

## 2. PRESENT STATUS

### 2.1 Summary

There are three major components in the present research program:

1) time-mean flow characterization, 2) turbulence measurements, and 3) flow-field computations. Numerous activities are underway in all three components and results are already being produced and documented. No major difficulties are anticipated in meeting the goals and objectives of the NASA grant and making a substantial contribution to the understanding and prediction capability of complex turbulent swirling flows.

### 2.2 Publications

The following list of publications covers research conducted with the support of the grant, and does not include those listed in previous Semi-Annual Reports:

1. Lilley, D. G., Computer Modeling in Ramjet Combustors. AIAA Journal, Vol. 19, No. 12, Dec. 1981, pp. 1562-1563.
2. Janjua, S. I., Turbulence Measurements in a Complex Flow-field Using a Six-Orientation Hot-Wire Probe Technique. M.S. Thesis, Oklahoma State University, Stillwater, OK, Dec. 1981.
3. Busnaina, A. A. and Lilley, D. G., A Simple Finite Difference Procedure for the Vortex Controlled Diffuser. Paper No. AIAA-82-0109, Orlando, Florida, Jan. 11-14, 1982.
4. Busnaina, A. A. and Lilley, D. G., A Basic Code for the Prediction of Transient Three-Dimensional Turbulent Flow-fields. Paper No. ASME 82-FE27, for presentation at the AIAA/ASME 3rd Joint Thermophysics, Fluids, Plasma and Heat Transfer Conf. to be held in St. Louis, Missouri, June 7-11, 1982.

FIGURE LIST

- Fig. 1 Prediction of axial  $u$  and swirl  $w$  velocities for the sudden expansion  $\alpha=90$  deg flowfield with swirl vane angle  $\phi=45$  deg, using measured inlet values of  $u$ ,  $v$  and  $w$ .
- Fig. 2 Five-hole pitot probe measurements for the corresponding case of Fig. 1.

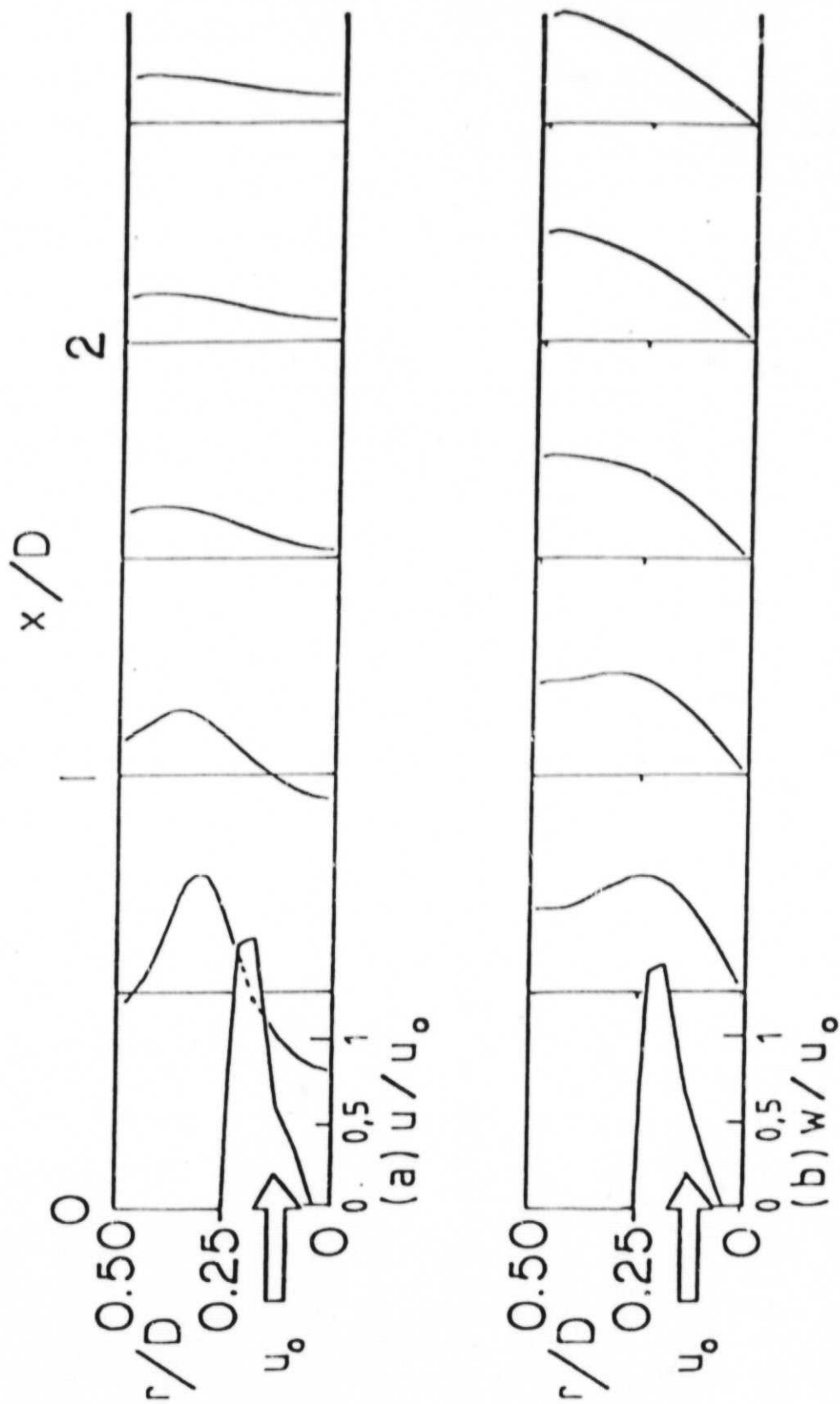


Fig. 1 Prediction of axial  $u$  and swirl  $w$  velocities for the sudden expansion  $\alpha=90$  deg flowfield with swirl vane angle  $\phi=45$  deg, using measured inlet values of  $u$ ,  $v$  and  $w$ .

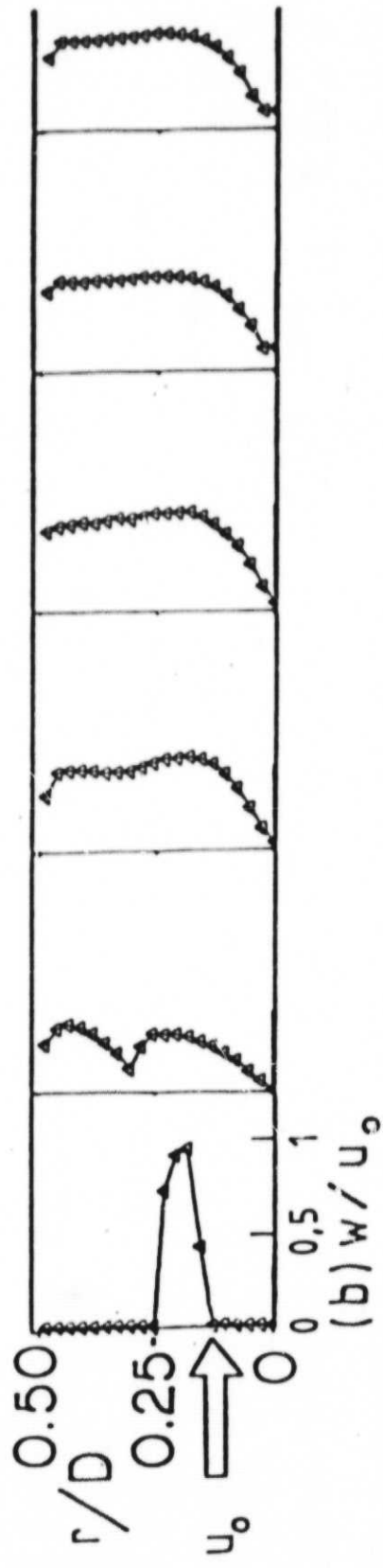
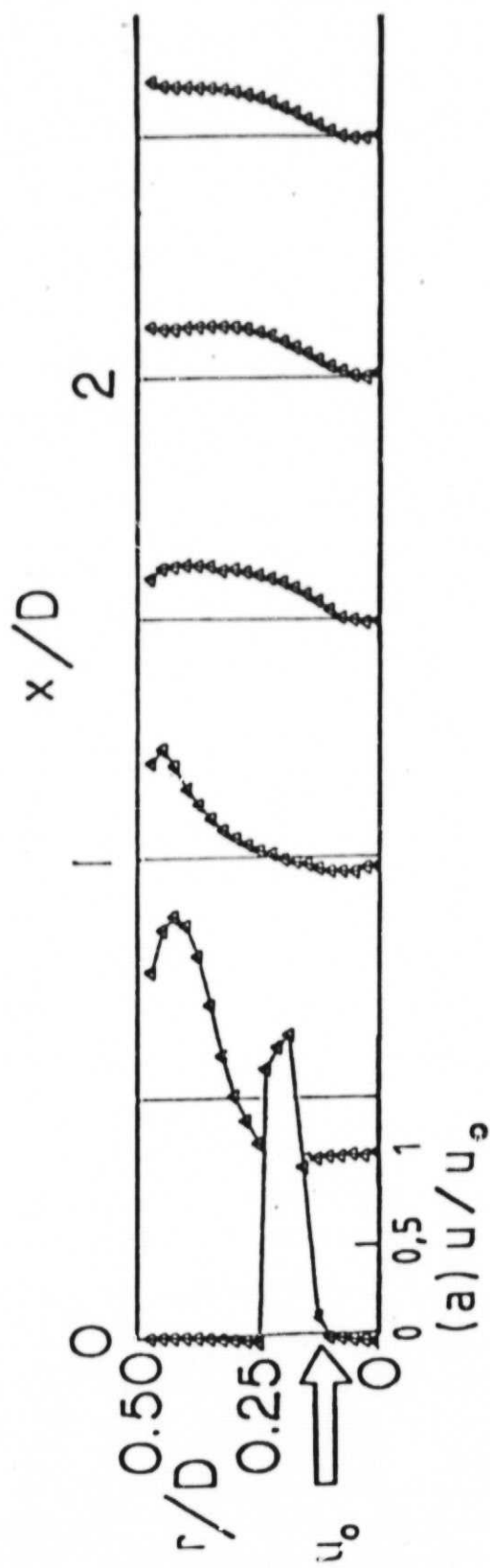


Fig. 2 Five-hole pitot probe measurements for the corresponding case of Fig. 1.

4. APPENDICES

APPENDIX A

TURBULENCE MEASUREMENTS IN A COMPLEX FLOWFIELD  
USING A SIX-ORIENTATION HOT-WIRE PROBE TECHNIQUE

TURBULENCE MEASUREMENTS IN A COMPLEX  
FLOWFIELD USING A SIX-ORIENTATION  
HOT-WIRE PROBE TECHNIQUE

By

SALIM IQBAL JANJUA

Bachelor of Science  
University of Punjab  
Pakistan  
1971

Bachelor of Engineering  
Concordia University  
Montreal, Canada  
1980

Submitted to the Faculty of the Graduate College  
of the Oklahoma State University  
in partial fulfillment of the requirements  
for the Degree of  
MASTER OF SCIENCE  
December, 1981

Name: Salim Iqbal Janjua

Date of Degree: December, 1981

Institution: Oklahoma State University Location: Stillwater, Oklahoma

Title of Study: TURBULENCE MEASUREMENTS IN A COMPLEX FLOWFIELD USING A SIX-ORIENTATION HOT-WIRE PROBE TECHNIQUE

Pages in Study: 74

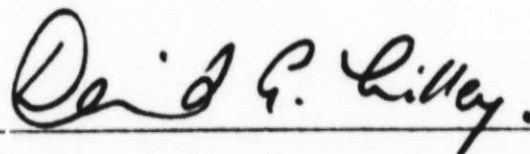
Candidate for Degree of Master of Science

Major Field: Mechanical Engineering

Scope and Method of Study: Measurements of turbulence quantities in a complex three-dimensional, nonreacting, nonswirling, gas turbine combustor flowfield have been carried out using a recently developed six-orientation hot-wire technique. The measurements are done with a single normal hot-wire which is rotated through 150 degrees with an increment of 30 degrees while measuring mean and root-mean-square voltages at each orientation. The data obtained are then processed using a statistical method which assumes turbulence to follow a normal probability distribution having mean voltage as the mean and the squared value of the root-mean-square voltage as the variance. Thus it becomes possible to obtain the three mean velocities, the three turbulence intensities and the three shear stresses. Some of the output quantities are compared with results from a similar study done in the past using a different technique.

Findings and Conclusions: The six-orientation hot-wire technique is found to be a good tool to gather detailed information about turbulence levels in a complex, three dimensional flowfield. Flow in a nonswirling confined jet was found to be primarily dominated by the axial velocity. The six-orientation hot-wire technique is an excellent method to find the mean velocities. It also gives good results for turbulence intensities. An uncertainty analysis done on this technique reveals that certain output parameters such as the axial, radial, and tangential turbulence intensities and shear stresses are extremely sensitive to some input parameters such as yaw factor and mean voltages. The accuracy of measurements can be well judged by the scatter of the values of turbulence quantities among the six different combinations of sets of three mean effective cooling velocities.

ADVISER'S APPROVAL

David G. Lilley.

TURBULENCE MEASUREMENTS IN A COMPLEX  
FLOWFIELD USING A SIX-ORIENTATION  
HOT-WIRE PROBE TECHNIQUE

Thesis Approved:

*David G. Lilley.*

Thesis Adviser

*Troy D. Reed*

*J. M. ...*

Dean of the Graduate College

## ACKNOWLEDGMENTS

The author wishes to express his appreciation to his major adviser, Dr. David G. Lilley for his advice and guidance concerning this work. Gratitude is also extended to other committee members, Dr. John A. Wiebelt and Dr. Troy D. Reed.

Further appreciation is extended to Dr. Dennis K. McLaughlin for his great help and useful advice during major part of this study.

The author also wishes to thank Mrs. Camille Tindall for her expert typing skills and advice in the preparation of this thesis.

Finally, the author recognizes the financial support of National Aeronautics and Space Administration through Grant No. NAG3-74, 1980.

## TABLE OF CONTENTS

Chapter	Page
I. INTRODUCTION . . . . .	1
1.1 The Combustor Flowfield Investigation . . . . .	1
1.2 Previous Experimental Studies on Expansion Flows . . . . .	2
1.3 The Turbulence Measurement Problem . . . . .	2
1.4 The Scope of the Present Study . . . . .	4
II. EXPERIMENTAL FACILITY AND INSTRUMENTATION . . . . .	6
2.1 Idealized Flowfield . . . . .	6
2.2 Hot-Wire Instrumentation . . . . .	7
2.3 Calibration Nozzle . . . . .	8
III. STATISTICAL ANALYSIS PROCEDURE . . . . .	9
3.1 Response Equations . . . . .	9
3.2 Calculation of Covariances . . . . .	15
IV. UNCERTAINTY ANALYSIS . . . . .	19
4.1 Effect of Pitch and Yaw Factors . . . . .	19
4.1.1 Laminar Flow . . . . .	20
4.1.2 Turbulent Flow . . . . .	20
4.2 Effect of Correlation Coefficients . . . . .	20
4.3 Experimental Uncertainty . . . . .	21
4.3.1 Laminar Flow . . . . .	22
4.3.2 Turbulent Flow . . . . .	23
V. RESULTS . . . . .	24
5.1 Mean Velocities . . . . .	25
5.2 Turbulence Intensities . . . . .	25
5.3 Shear Stresses . . . . .	26
VI. CLOSURE . . . . .	28
6.1 Summary . . . . .	28
6.2 Further Work . . . . .	29
REFERENCES . . . . .	30

Chapter	Page
APPENDICES . . . . .	32
APPENDIX A - TABLES . . . . .	33
APPENDIX B - FIGURES . . . . .	38
APPENDIX C - USER'S GUIDE TO COMPUTER CODE FOR SIX- ORIENTATION HOT-WIRE DATA REDUCTION TECHNIQUE . . . . .	53
APPENDIX D - LISTING OF THE COMPUTER PROGRAM . . . . .	62

LIST OF TABLES

Table	Page
I. Values of A0, B0, and C0 in Various Equation Sets . . . . .	34
II. Matrix (T) in Equation 30 . . . . .	35
III. Effect of Input Parameters on Turbulence Quantities . . . . .	36
IV. Scatter Among the Turbulence Quantities When Solved by Six Different Combinations . . . . .	37
V. List of Fortran Variables and Their Meaning in Response Equations . . . . .	59

## LIST OF FIGURES

Figure	Page
1. Typical Axisymmetric Combustion Chamber of a Gas Turbine Engine . . . . .	39
2. The Flowfield Being Investigated . . . . .	40
3. Schematic of Overall Facility . . . . .	41
4. Hot-Wire Constant Temperature Anemometer . . . . .	42
5. Manual Traversing Mechanism Used for Hot-Wire Orientations in the Flowfield . . . . .	43
6. Mounting the Hot-Wire Probe on the Test Section . . . . .	44
7. The Three-Directional Hot-Wire Calibration . . . . .	45
8. Plots of Pitch and Yaw Factors Versus Hot-Wire Voltage . . . . .	46
9. Radial Distribution of Normalized Time-Mean Axial Velocity in Nonswirling Confined Jet . . . . .	47
10. Radial Distribution of Normalized Time-Mean Radial Velocity in Nonswirling Confined Jet . . . . .	48
11. Radial Distribution of Axial Turbulence Intensity in Nonswirling Confined Jet . . . . .	49
12. Radial Distribution of Radial Turbulence Intensity in Nonswirling Confined Jet . . . . .	50
13. Radial Distribution of Azimuthal Turbulence Intensity in Nonswirling Confined Jet . . . . .	51
14. Radial Distribution of Shear Stress $\overline{u'v'}/\overline{u_0}^2$ in Nonswirling Confined Jet . . . . .	52

## NOMENCLATURE

A, B, C	Calibration constants in Equation 1
A0, B0, C0	Cooling velocity functions in Table I
D	Test section diameter
d	Inlet nozzle diameter
E	Hot-wire voltage
F1	Velocity function for axial velocity
F2	Velocity function for azimuthal velocity
F3	Velocity function for radial velocity
G	Pitch factor
K	Yaw factor
$K_{z_p z_q}$	Covariance for cooling velocities $Z_p$ , and $Z_q$
P, Q, R	Selected hot-wire probe positions
T	Matrix given in Table II, Appendix A
u	Axial velocity
v	Radial velocity
w	Azimuthal (swirl) velocity
$\hat{u}, \hat{w}, \hat{v}$	Probe coordinate system defined by Figure 6, Appendix B
x, r, $\theta$	Axial, radial, azimuthal cylindrical polar coordinates
Z	Effective cooling velocity acting on a wire
$\alpha$	Side-wall expansion angle

$c^2$	Variance of a given quantity
$\pi$	Function defined by Equation 31, 32, and 33
$\phi$	Inverse function of calibration equation
$\rho$	Function of selected mean effective cooling velocities given by Equations 34 through 36

#### Subscripts

1, 2, 3, 4, 5, 6	Refer to the six probe measuring positions
i, j, P, Q, R	Refer to the three selected cooling velocities
rms	Root-mean-squared quantity

#### Superscripts

—	Time mean average
'	Fluctuating quantity

## CHAPTER I

### INTRODUCTION

#### 1.1 The Combustor Flowfield Investigation

Understanding the fluid dynamics of the flow in a gas turbine combustion chamber has been of great concern to designers in recent years. A gas turbine combustor, shown in Figure 1, Appendix B, must burn fuel completely, cause little pressure drop, produce gases of nearly uniform temperature, occupy small volume, and maintain stable combustion over a wide range of operating conditions. The designer has a formidable problem in aerothermochemistry, and more thorough and accurate procedures can help in accomplishing the design objectives more quickly and less expensively in the near future.

Intensive research is being carried out at Oklahoma State University on the subject of gas turbine flowfield investigations in the absence of combustion. Figure 2, Appendix B, shows the characteristics of the simplified flowfield being investigated. Flow enters through a jet of diameter  $d$  into a tube of diameter  $D$ , after being expanded through an angle  $\alpha$ . Before entering the tube, the flow may be swirled by a swirler located upstream of the inlet plane. The flowfield is presently being investigated using various methods of approach, such as computer modeling of the flowfield and flow visualization for both swirl and nonswirl conditions (2, 3).

## 1.2 Previous Experimental Studies on Expansion Flows

Several studies on time-mean flowfields of the type just described have been carried out using various turbulence measuring techniques (4-11). Unfortunately, most of the techniques used do not give complete and detailed information about the flow in terms of all its time-mean and turbulence quantities. There is a strong need to obtain all the turbulence quantities in a complex flowfield using a minimum amount of instrumentation and without causing a great deal of interference with the flow.

## 1.3 The Turbulence Measurement Problem

Turbulence measurement in a complex flowfield has always been a complicated problem encountered by engineers. In the past, turbulence phenomena have been discussed by various authors in detail and various methods of turbulence measurement have been suggested (12-15). One of the most widely used instruments to obtain turbulence quantities is the hot-wire anemometer. The most common of all hot-wire anemometers is a single hot-wire. When used at a single orientation and in a two-dimensional flow, a single hot-wire can measure the streamwise components of the time-mean velocity and the root-mean-square velocity fluctuation at a particular location in the flowfield. A two-wire probe can be used to determine the time-mean velocities, streamwise and cross stream turbulence intensities, and the cross correlation between the two components of the velocity fluctuations (16-18). To measure the three velocities and their corresponding fluctuating components in a three-dimensional flowfields such as encountered in combustor simulators, there are two

methods that can be employed at a point in the flowfield:

1. A multi-wire probe used with a single orientation.
2. A single-wire probe used with a multi-orientation.

Multi-wire techniques, with three hot-wires mounted on the same base so that they all lie within the same volume of the flowfield, permit the necessary three sets of readings to be made simultaneously. The requirement is to determine all three components simultaneously. The main disadvantages of such a technique are:

- i. It requires three closely matched anemometer units.
- ii. The probes interfere with each other unless they are carefully placed relative to the time-mean velocity vector.
- iii. The spatial resolution is poor because of the large size of the probe assembly.
- iv. Heat can be convected from one wire to another giving biased readings.

Multi-orientation of a single hot-wire is a novel way to measure the three components of a velocity vector and their fluctuating components. A method devised by Dvorak and Syred (19) uses a single normal hot-wire oriented at three different positions such that the center one is separated by 45 degrees from the other two. The velocity vector at a location is related to the three orthogonal components using pitch and yaw factors as defined by Jorgensen (20). The data are obtained in the form of mean and root-mean-square voltages at each orientation. However, the measurements done with a single wire do not supply all the information needed to obtain the turbulence quantities. Therefore in addition to a single wire, Dvorak and Syred used a cross-wire probe to obtain the covariances between the voltages obtained at adjacent hot-wire

orientations. A cross-wire probe, two wires mounted on the same base and separated by 45 degrees from each other, poses the same problems as already discussed for a multi-wire probe.

King (21) modified the technique developed by Dvorak and Syred. His method calls for a normal hot-wire to be oriented through six different positions, each orientation separated by 30 degrees from the adjacent one. Thus, one measures mean and root-mean-square voltages at each orientation. The data reduction is done using some assumptions regarding the statistical nature of turbulence, making it possible to solve for the three time-mean velocities, the three normal turbulent stresses, and the three turbulent sheer stresses. Having obtained these quantities, one can in addition calculate the kinetic energy of turbulence. Various recent studies discuss the turbulence measurement problem, with emphasis on hot-wire and laser anemometer applications to swirl flows (22-23).

#### 1.4 The Scope of the Present Study

In the present study, the six-orientation single normal hot-wire technique is being employed to obtain the turbulence quantities in the combustor simulation confined jet flowfield. Measurements have been carried out for nonswirling flow with expansion angles of 90 degrees (sudden expansion) and 45 degrees (gradual expansion).

Chapter II gives background information on the various components of the experimental facility and the instruments employed for the hot-wire measurements.

The response equations using King's approach are given in Chapter III. Certain deviations from the procedures suggested by King are also

included in this chapter. A thorough uncertainty analysis of the technique is carried out in order to judge the accuracy and the reliability of the six-orientation hot-wire technique. The salient features of the analysis are discussed in Chapter IV.

Turbulence quantities obtained, using this hot-wire technique, are part of Chapter V which discusses the results in detail. Some of the turbulence quantities are compared with measurements done by Chaturvedi (5) using cross-wire probe in a corresponding flow situation. Chapter VI concludes by summarizing the major achievements of the present study and suggesting some avenues for further research activity.

## CHAPTER II

### EXPERIMENTAL FACILITY AND INSTRUMENTATION

#### 2.1 Idealized Flowfield

The facility, designed and built at Oklahoma State University, is a simulation of a typical axisymmetric combustion chamber of a gas turbine engine shown in Figure 1, Appendix B. The schematic of the test facility with idealized flowfield is shown in Figure 3, Appendix B. Ambient air enters the low-speed wind tunnel through a rubber foam air filter. Next the air flows through an axial flow fan driven by a 5 h.p. varidrive motor. Thus the flow rate can be varied for different test conditions. Then the flow is gradually expanded through the tunnel cross-section without separation because numerous fine mesh screens are encountered by the flow along the way.

Next, the flow goes through a turbulence management section which has two fine-mesh screens, a 12.7 cm length of packed straws, and five more fine-mesh screens. When the flow passes through the turbulence section, small eddies are formed which dissipate much quicker than the large eddies. The turbulence management section thus keeps the turbulence level down.

Having left the turbulence management section, the air enters into a contoured nozzle leading to the test section. This axisymmetric nozzle was designed to produce a minimum adverse pressure gradient on the

boundary layer to avoid flow unsteadiness associated with local separation regions. The area ratio of the cross sections of the turbulence management section to that of the nozzle throat is approximately 22.5. The diameter,  $d$ , of the nozzle throat is approximately 15 cm.

Next, the air enters the test section. The test section is composed of a swirler (optional), an expansion block, and a long plexiglass tube. The swirler currently available is a variable vane-angle type device to impart swirl to the flow entering the test section. The expansion block, attached after the swirler, is a 30 cm diameter disk of wood. At present, there are three expansion blocks, and the appropriate choice gives  $\alpha = 90, 70, \text{ or } 45$  degrees. The flow is expanded into a plexiglass tube of diameter,  $D$ , of 30 cm, thus giving diameter expansion ratio ( $D/d$ ) of 2.

A typical real combustor, shown in Figure 1, Appendix B, is idealized in the present study, as there are no film cooling holes or dilution air holes, and the chamber wall of the test section is a constant diameter pipe. The test section is carefully aligned using a laser beam so that the test section and wind tunnel centerline are colinear.

## 2.2 Hot-Wire Instrumentation

Figure 4, Appendix B, shows the circuit diagram for a constant temperature anemometer. The anemometer used for the present study is DISA type 55M01, CTA standard bridge. A normal hot-wire, type 55P01, manufactured by DISA, is used to carry out the measurements of time-mean and root-mean-square voltages. These probes have two prongs set approximately 3 mm apart and carry 5  $\mu\text{m}$  diameter wire which is gold plated near the prongs to reduce end effects and strengthen the wire. The

time-mean voltage is measured with Hickok Digital Systems, Model DP100, integrating voltmeter and the root-mean-square voltage is measured using Hewlett Packard, Model 400 HR, voltmeter.

The hot-wire is mounted on the facility with the help of a traversing mechanism shown in Figure 5, Appendix B. It consists of a base that is modified to be mounted on the plexiglass tube of the test section at various axial locations. The hot-wire probe is inserted into the tube through a rotary vernier and the base. The rotary vernier is attached to a slide which can traverse up to approximately 14.5 cm. Thus it becomes possible for the probe to be traversed at any location in the combustor flowfield and rotated through 180 degrees. Figure 6, Appendix B, shows the test section with the probe mounted on it.

### 2.3 Calibration Nozzle

The hot-wire is calibrated on a small air jet. The facility consists of a compressed air line, which delivers the desired flow rate through a small pressure regulator and a Fischer and Porter Model 10A1735A rotameter. The jet housing consists of an effective flow management section followed by a contoured nozzle with a 3.5 cm diameter throat.

A rotary table is used to hold the probe while it is being calibrated in three different orientations which are discussed in Chapter III.

## CHAPTER III

### STATISTICAL ANALYSIS PROCEDURE

#### 3.1 Response Equations

The six-orientation hot-wire technique requires a single, straight, hot-wire to be calibrated for three different probe directions in order to determine the directional sensitivity of such a probe. The three directions and the three calibration curves are shown in Figure 7, Appendix B. Each of the three calibration curves is obtained with zero velocity in the other two directions. The calibration curves demonstrate that the hot-wire is most efficiently cooled when the flow is in the  $\hat{v}$  direction. Whereas, the wire is most inefficiently cooled for the flow in  $\hat{w}$  direction. Each of the calibration curves follows a second order, least square fit, of the form:

$$E^2 = A + BZ^{\frac{1}{2}} + CZ \quad (1)$$

where A, B, and C are the calibration constants and Z can take a value of  $\hat{u}$ ,  $\hat{v}$ , and  $\hat{w}$  for the three calibration curves, respectively.

When the wire is placed in a 3-dimensional flowfield, the effective cooling velocity experienced by the hot-wire, in terms of the probe coordinator and pitch and yaw factors (G and K) as defined by Jorgensen (20) is:

$$Z^2 = \hat{v}^2 + G^2\hat{u}^2 + K^2\hat{w}^2 \quad (2a)$$

$$G = \frac{\hat{v}(\hat{w}, \hat{u} = 0)}{\hat{u}(\hat{w}, \hat{v} = 0)}, \quad (2b)$$

$$K = \frac{\hat{v} (\hat{w}, \hat{u} = 0)}{\hat{w} (\hat{v}, \hat{u} = 0)}, \quad (2c)$$

evaluated from the three calibration curves for a constant value of  $E^2$ .

To carry out measurements in the combustor flowfield, the wire is aligned in the flow in such a way that in the first orientation, the wire is normal to the flow in the axial direction and the probe coordinates coincide with the coordinates of the experimental facility. Thus the six equations for the instantaneous cooling velocities at the six orientations, as given by King (21) are:

$$Z_1^2 = v^2 + G^2 u^2 + K^2 w^2 \quad (3)$$

$$Z_2^2 = v^2 + G^2 (u \cos 30^\circ + w \sin 30^\circ)^2 + K^2 (w \cos 30^\circ - u \sin 30^\circ)^2 \quad (4)$$

$$Z_3^2 = v^2 + G^2 (u \cos 60^\circ + w \sin 60^\circ)^2 + K^2 (w \cos 60^\circ - u \sin 60^\circ)^2 \quad (5)$$

$$Z_4^2 = v^2 + G^2 w^2 + K^2 u^2 \quad (6)$$

$$Z_5^2 = v^2 + G^2 (w \sin 120^\circ + u \cos 120^\circ)^2 + K^2 (u \sin 120^\circ - w \cos 120^\circ)^2 \quad (7)$$

$$Z_6^2 = v^2 + G^2 (w \sin 150^\circ + u \cos 150^\circ)^2 + K^2 (u \sin 150^\circ - w \cos 150^\circ)^2 \quad (8)$$

Replacing the sines and cosines and expanding the square brackets:

$$Z_1^2 = v^2 + G^2 u^2 + K^2 w^2 \quad (3a)$$

$$Z_2^2 = v^2 + G^2 \left( u^2 \frac{3}{4} + \frac{w^2}{4} + uw \frac{\sqrt{3}}{2} \right) + K^2 \left( w^2 \frac{3}{4} + \frac{u^2}{4} - uw \frac{\sqrt{3}}{2} \right) \quad (4a)$$

$$Z_3^2 = v^2 + G^2 \left( \frac{u^2}{4} + w^2 \frac{3}{4} + uw \frac{\sqrt{3}}{2} \right) + K^2 \left( \frac{w^2}{4} + u^2 \frac{3}{4} - uw \frac{\sqrt{3}}{2} \right) \quad (5a)$$

$$Z_4^2 = v^2 + G^2 w^2 + K^2 u^2 \quad (6a)$$

$$Z_5^2 = v^2 + G^2 \left( \frac{u^2}{4} + w^2 \frac{3}{4} - uw \frac{\sqrt{3}}{2} \right) + K^2 \left( \frac{w^2}{4} + u^2 \frac{3}{4} + uw \frac{\sqrt{3}}{2} \right) \quad (7a)$$

$$Z_6^2 = v^2 + G^2 \left( u^2 \frac{3}{4} + \frac{w^2}{4} - uw \frac{\sqrt{3}}{2} \right) + K^2 \left( w^2 \frac{3}{4} + \frac{u^2}{4} + uw \frac{\sqrt{3}}{2} \right) \quad (8a)$$

Solving simultaneously any three adjacent equations provides expressions for the instantaneous values of the three velocity components,  $u$ ,  $w$ , and  $v$ , in terms of the equivalent cooling velocities ( $Z_1$ ,  $Z_2$ , and  $Z_3$  for

example, when the first three equations are chosen). King refers to these instantaneous velocity components as F1, F2, and F3 as follows:

$$F1 = \left[ \left\{ AO + (AO^2 + \frac{BO^2}{3})^{\frac{1}{2}} \right\} * \frac{1}{(G^2 - k^2)} \right]^{\frac{1}{2}} \quad (9)$$

$$F2 = \left[ \left\{ -AO + (AO^2 + \frac{BO^2}{3})^{\frac{1}{2}} \right\} * \frac{1}{(G^2 - K^2)} \right]^{\frac{1}{2}} \quad (10)$$

$$F3 = \left[ CO - \frac{(G^2 + k^2)}{(G^2 - k^2)} * (AO^2 + \frac{BO^2}{3})^{\frac{1}{2}} \right]^{\frac{1}{2}} \quad (11)$$

The values of A0, B0, and C0 depend on the set of the three equations chosen and are given in Table 1, Appendix A, for appropriate equation sets.

However, these equations cannot be directly used because it is impossible to obtain  $Z_1$ ,  $Z_2$ , and  $Z_3$  at a single instance in time. Therefore Equation 9 through 11 must be expressed in terms of mean and root-mean-square values. Equation 1 can be written as:

$$\phi(E_i) = Z_i = \left[ \left[ -B + \left\{ B^2 - 4C(A - E_i^2) \right\}^{\frac{1}{2}} \right] / 2C \right]^{\frac{1}{2}} \quad (12)$$

The above equation is in terms of instantaneous velocity  $Z_i$  and instantaneous voltage  $E_i$ . In order to obtain an expression for time-mean velocity as a function of time-mean voltage, a Taylor series expansion of Equation 12 can be carried out.

$$\begin{aligned} \text{Since } Z_i &= \phi(\bar{E}_i + E_i') \\ Z_i &= \phi(\bar{E}_i + E_i') = \phi(\bar{E}_i) + \frac{E_i'}{1!} \cdot \frac{\partial \phi}{\partial E_i} + \frac{E_i'^2}{2!} \cdot \frac{\partial^2 \phi}{\partial E_i^2} \end{aligned} \quad (13)$$

The Taylor series is truncated after second order terms assuming the higher order terms to be relatively small. Time averaging both sides of the above equation and employing the fact that  $\bar{E}' = 0$ , yields:

$$\bar{Z}_i = \bar{\phi} + \frac{1}{2} \frac{\partial^2 \bar{\phi}}{\partial \bar{E}_i^2} \cdot \sigma_{E_i}^2 \quad (14)$$

where  $\bar{\phi}$  indicates that the function is evaluated for  $\bar{E}_i$ . To obtain  $\bar{Z}_i'^2 = \sigma_{Z_i}^2$ , the relationship as given by Hinze (13) is:

$$\bar{Z}_i'^2 = \sigma_{Z_i}^2 = \text{Expec} [Z_i^2] - (\text{Expec} [Z_i])^2 \quad (15)$$

$$\text{Since Expec} [Z_i^2] = \bar{\phi} + \frac{1}{2} \frac{\partial^2 \bar{\phi}}{\partial \bar{E}_i^2} \cdot \sigma_{E_i}^2, \quad (16)$$

the differential in Equation 16 can be evaluated as:

$$\frac{\partial^2 \bar{\phi}^2}{\partial \bar{E}_i^2} = 2 \left( \frac{\partial \bar{\phi}}{\partial \bar{E}_i} \right)^2 + 2 \bar{\phi} \cdot \frac{\partial^2 \bar{\phi}}{\partial \bar{E}_i^2} \quad (17)$$

Then Equation 16 becomes:

$$\text{Expec} [Z_i^2] = \bar{\phi}^2 + \left( \frac{\partial \bar{\phi}}{\partial \bar{E}_i} \right)^2 \cdot \sigma_{E_i}^2 + \bar{\phi} \cdot \frac{\partial^2 \bar{\phi}}{\partial \bar{E}_i^2} \cdot \sigma_{E_i}^2 \quad (18)$$

Squaring Equation 14 and substituting with Equation 18 into Equation 15 gives:

$$\bar{Z}_i'^2 = \sigma_{Z_i}^2 = \frac{\partial \bar{\phi}}{\partial \bar{E}_i}^2 \cdot \sigma_{E_i}^2 - \left( \frac{1}{2} \frac{\partial^2 \bar{\phi}}{\partial \bar{E}_i^2} \cdot \sigma_{E_i}^2 \right)^2 \quad (19)$$

Thus Equations 14 and 19 give the mean and variance of individual cooling velocities in terms of the mean and variance of the appropriate voltage.

In a 3-dimensional flow, it is usually desired to obtain the mean and variance for the individual velocity components in axial, azimuthal, and radial directions, and also their cross correlations.

The procedure to obtain the mean and variance of the individual

velocity components is the same as for the effective cooling velocities except that  $u$ ,  $w$ , and  $v$  are functions of three random variables and there are extra terms in the Taylor expansion to account for the covariances of the cooling velocities. Thus the three mean velocities as given by Dvorak and Syred (19) and King (21) are:

$$\bar{u} = F1(Z_P, Z_Q, Z_R) + \frac{1}{2} \sum_{i=1}^3 \frac{\partial^2 F1}{\partial Z_i^2} \cdot \sigma_{Z_i}^2 + \sum_{i<j}^3 \frac{\partial^2 F1}{\partial Z_i \partial Z_j} \cdot K_{Z_i Z_j} \quad (20)$$

where time-mean values are to be understood on the right side of this and subsequent equations.

$$\bar{w} = F2(Z_P, Z_Q, Z_R) + \frac{1}{2} \sum_{i=1}^3 \frac{\partial^2 F2}{\partial Z_i^2} \cdot \sigma_{Z_i}^2 + \sum_{i<j}^3 \frac{\partial^2 F2}{\partial Z_i \partial Z_j} \cdot K_{Z_i Z_j} \quad (21)$$

and

$$\bar{v} = F3(Z_P, Z_Q, Z_R) + \frac{1}{2} \sum_{i=1}^3 \frac{\partial^2 F3}{\partial Z_i^2} \cdot \sigma_{Z_i}^2 + \sum_{i<j}^3 \frac{\partial^2 F3}{\partial Z_i \partial Z_j} \cdot K_{Z_i Z_j} \quad (22)$$

where  $K_{Z_i Z_j}$  is the covariance of the cooling velocity fluctuations and is defined as:

$$K_{Z_i Z_j} = \frac{1}{T} \int_0^T (Z_i - \bar{Z}_i)(Z_j - \bar{Z}_j) dt \quad (23)$$

Also the normal stresses are given as:

$$\overline{u'^2} = \sum_{i=1}^3 \left( \frac{\partial F1}{\partial Z_i} \right)^2 \cdot \sigma_{Z_i}^2 + \sum_{\substack{i,j \\ i \neq j}}^3 \frac{\partial F1}{\partial Z_i} \cdot \frac{\partial F1}{\partial Z_j} - \left[ \frac{1}{2} \sum_{i=1}^3 \frac{\partial^2 F1}{\partial Z_i^2} \cdot \sigma_{Z_i}^2 + \sum_{i<j}^3 \frac{\partial^2 F1}{\partial Z_i \partial Z_j} \cdot K_{Z_i Z_j} \right]^2 \quad (24)$$

$$\overline{w'^2} = \sum_{i=1}^3 \left( \frac{\partial F2}{\partial Z_i} \right)^2 \cdot \sigma_{Z_i}^2 + \sum_{\substack{i,j \\ i \neq j}}^3 \frac{\partial F2}{\partial Z_i} \cdot \frac{\partial F2}{\partial Z_j} - \left[ \frac{1}{2} \sum_{i=1}^3 \frac{\partial^2 F2}{\partial Z_i^2} \cdot \sigma_{Z_i}^2 + \sum_{i<j}^3 \frac{\partial^2 F2}{\partial Z_i \partial Z_j} \cdot K_{Z_i Z_j} \right]^2 \quad (25)$$

and

$$\overline{v^T v} = \sum_{i=1}^3 \left( \frac{\partial F_3}{\partial Z_i} \right)^2 \cdot \sigma_{Z_i}^2 + \sum_{\substack{i,j \\ i \neq j}}^3 \frac{\partial F_3}{\partial Z_i} \cdot \frac{\partial F_3}{\partial Z_j} \cdot K_{Z_i Z_j} - \left[ \frac{1}{2} \sum_{i=1}^3 \frac{\partial^2 F_3}{\partial Z_i^2} \cdot \sigma_{Z_i}^2 + \sum_{i < j}^3 \frac{\partial^2 F_3}{\partial Z_i \partial Z_j} \cdot K_{Z_i Z_j} \right]^2 \quad (26)$$

Also the shear stresses as given by Dvorak and Syrod (19) are:

$$\overline{u^T w} = \sum_{i=1}^3 \frac{\partial F_1}{\partial Z_i} \cdot \frac{\partial F_2}{\partial Z_i} \cdot \sigma_{Z_i}^2 + \sum_{\substack{i,j \\ i \neq j}}^3 \frac{\partial F_1}{\partial Z_i} \cdot \frac{\partial F_2}{\partial Z_j} \cdot K_{Z_i Z_j} - \left[ \frac{1}{2} \sum_{i=1}^3 \frac{\partial^2 F_1}{\partial Z_i^2} \cdot \sigma_{Z_i}^2 + \sum_{i < j}^3 \frac{\partial^2 F_1}{\partial Z_i \partial Z_j} \cdot K_{Z_i Z_j} \right] \left[ \frac{1}{2} \sum_{i=1}^3 \frac{\partial^2 F_2}{\partial Z_i^2} \cdot \sigma_{Z_i}^2 + \sum_{i < j}^3 \frac{\partial^2 F_2}{\partial Z_i \partial Z_j} \cdot K_{Z_i Z_j} \right] \quad (27)$$

$$\overline{u^T v} = \sum_{i=1}^3 \frac{\partial F_1}{\partial Z_i} \cdot \frac{\partial F_3}{\partial Z_i} \cdot \sigma_{Z_i}^2 + \sum_{\substack{i,j \\ i \neq j}}^3 \frac{\partial F_1}{\partial Z_i} \cdot \frac{\partial F_3}{\partial Z_j} \cdot K_{Z_i Z_j} - \left[ \frac{1}{2} \sum_{i=1}^3 \frac{\partial^2 F_1}{\partial Z_i^2} \cdot \sigma_{Z_i}^2 + \sum_{i < j}^3 \frac{\partial^2 F_1}{\partial Z_i \partial Z_j} \cdot K_{Z_i Z_j} \right] \left[ \frac{1}{2} \sum_{i=1}^3 \frac{\partial^2 F_3}{\partial Z_i^2} \cdot \sigma_{Z_i}^2 + \sum_{i < j}^3 \frac{\partial^2 F_3}{\partial Z_i \partial Z_j} \cdot K_{Z_i Z_j} \right] \quad (28)$$

and finally,

$$\overline{w^T v} = \sum_{i=1}^3 \frac{\partial F_2}{\partial Z_i} \cdot \frac{\partial F_3}{\partial Z_i} \cdot \sigma_{Z_i}^2 + \sum_{\substack{i,j \\ i \neq j}}^3 \frac{\partial F_2}{\partial Z_i} \cdot \frac{\partial F_3}{\partial Z_j} \cdot K_{Z_i Z_j} - \left[ \frac{1}{2} \sum_{i=1}^3 \frac{\partial^2 F_2}{\partial Z_i^2} \cdot \sigma_{Z_i}^2 + \sum_{i < j}^3 \frac{\partial^2 F_2}{\partial Z_i \partial Z_j} \cdot K_{Z_i Z_j} \right] \left[ \frac{1}{2} \sum_{i=1}^3 \frac{\partial^2 F_3}{\partial Z_i^2} \cdot \sigma_{Z_i}^2 + \sum_{i < j}^3 \frac{\partial^2 F_3}{\partial Z_i \partial Z_j} \cdot K_{Z_i Z_j} \right] \quad (29)$$

## 3.2 Calculation of Covariances

Dvorak and Syred (19) used a DISA time correlator (55A06) to find the correlation coefficients between the velocity fluctuations in the three directions. The method adopted by King (21) is to use the information obtained by all six orientations and devise a mathematical procedure to calculate the covariances.

The covariance matrix as derived by King is:

$$\left[ K_{Z_i Z_j} \right] = \left[ \Pi \right] \left[ T \right]^{-1} \quad (30)$$

where

$$K_{Z_i Z_j} = \begin{bmatrix} K_{Z_P Z_Q} \\ K_{Z_P Z_R} \\ K_{Z_Q Z_R} \end{bmatrix} ,$$

and

$$\Pi = \begin{bmatrix} \Pi_1 \\ \Pi_2 \\ \Pi_3 \end{bmatrix}$$

where

$$\Pi_1 = \bar{Z}_{P+3} - \rho_1 - \frac{1}{2} \sum_{i=p}^R \frac{\partial^2 \rho_1}{\partial Z_i^2} \cdot \sigma_{Z_i}^2, \quad (31)$$

$$\Pi_2 = \bar{Z}_{P+4} - \rho_2 - \frac{1}{2} \sum_{i=p}^R \frac{\partial^2 \rho_2}{\partial Z_i^2} \cdot \sigma_{Z_i}^2, \quad (32)$$

and

$$\pi_3 = \bar{Z}_{p+5} - \rho_3 - \frac{1}{2} \sum_{i=p}^R \frac{\partial^2 \rho_3}{2Z_i^2} \cdot \sigma_{Z_i}^2 \quad (33)$$

Also

$$\rho_1 = \bar{Z}_p^2 - 2\bar{Z}_Q^2 + 2\bar{Z}_R^2 \quad (34)$$

$$\rho_2 = 2\bar{Z}_p^2 + 3\bar{Z}_Q^2 + 2\bar{Z}_R^2 \quad (35)$$

and  $\rho_3 = 2\bar{Z}_p^2 - 2\bar{Z}_Q^2 + \bar{Z}_R^2 \quad (36)$

Matrix (T) is a three by three matrix and is given in Table II.

King discovered that matrix (T) is a singular matrix for all cases and hence equation 30 cannot be solved. Therefore, to get covariances one needs extra information. King has made an assumption about the relationship between the covariances in the form:

$$K_{Z_p Z_R} = \eta \frac{K_{Z_p Z_Q} \cdot K_{Z_Q Z_R}}{\sigma_{Z_Q}^2} \quad (37)$$

Where  $\eta$  is given a numerical value of 0.8.

Also  $K_{Z_p Z_Q}$  is obtained from the quadratic equation:

$$K_{Z_p Z_Q}^2 \left[ \frac{-2\bar{Z}_p^2 \cdot \eta}{\sigma_{Z_Q}^2} \right] + K_{Z_p Z_Q} \left[ 6\bar{Z}_p \bar{Z}_Q - \frac{\bar{Z}_p}{\bar{Z}_Q \sigma_{Z_Q}^2} (\pi_1 \cdot \bar{Z}_{R+1}^3 - \pi_3 \cdot \bar{Z}_{R+3}^3) \right] + \left[ \pi_1 \cdot \bar{Z}_{R+1}^3 - 2\pi_3 \cdot \bar{Z}_{R+3}^3 \right] = 0 \quad (38)$$

Equation 38 provides the two values for  $K_{z_p z_Q}$ . The covariance is related to the correlation coefficient as:

$$\gamma_{z_p z_Q} = \frac{K_{z_p z_Q}}{[\sigma_{z_p}^2 \cdot \sigma_{z_Q}^2]^{\frac{1}{2}}} \quad (39)$$

where  $-1 < \gamma_{z_i z_j} < 1$

Therefore, Equation 39 is written in the form:

$$K_{z_p z_Q} = \gamma_{z_p z_Q} \cdot [\sigma_{z_p}^2 \cdot \sigma_{z_Q}^2]^{\frac{1}{2}} \quad (40)$$

The two calculated values of  $K_{z_p z_Q}$  from equation 38 are then substituted in Equation 39, and the two corresponding values of  $\gamma_{z_p z_Q}$  are calculated. The correlation coefficient which lies within the required range of  $\pm 1$ , is used. For the case when the absolute values of both the correlation coefficients are larger than 1, the covariance is given by

$$K_{z_p z_Q} = 0.9 [\sigma_{z_p}^2 \cdot \sigma_{z_Q}^2]^{\frac{1}{2}} \quad (41)$$

Having calculated  $K_{z_p z_Q}$ ,  $K_{z_Q z_R}$  can be calculated from the relationship:

$$K_{z_Q z_R} = \frac{1}{2 \cdot \bar{z}_Q \bar{z}_R} \left[ 2 \cdot \bar{z}_p \cdot \bar{z}_Q \cdot K_{z_p z_Q} + \pi_1 \cdot \bar{z}_{p+3}^3 - \pi_3 \cdot \bar{z}_{p+5}^3 \right] \quad (42)$$

A similar test is applied to ensure that the absolute value of  $\gamma_{z_Q z_R}$  is less than one otherwise  $K_{z_Q z_R}$  is calculated from the relationship:

$$K_{z_Q z_R} = 0.9 [\sigma_Q^2 \cdot \sigma_R^2]^{\frac{1}{2}} \quad (43)$$

$K_{z_p z_R}$  can now be calculated from equation 37. The calculated value of  $K_{z_p z_Q}$ ,  $K_{z_Q z_R}$ , and  $K_{z_p z_R}$  can now be substituted in equations 20 thru 22, and 24 thru 29 to calculate the mean velocities and Reynold stresses.

It was observed during the present study that King's method is not self-consistent in calculating the covariances. The correlation coefficients were found to have values greater than one and therefore it was necessary to have a more consistent method to calculate the covariances. Occasionally, King's method assumed that  $\gamma_{z_p z_Q}$  and  $\gamma_{z_Q z_R}$  had values of 0.9 and  $\gamma_{z_p z_R}$  had a value of 0.648. But this was done only when some of the correlation coefficients were greater than one. The present method assumes constant values of the correlation coefficients. King has suggested that if two wires are separated by an angle of 30 degrees, the fluctuating signals from the wires at the two locations would be such that their contribution to the cooling of the wire would be related by the cosine of the angle between the wires therefore,  $\gamma_{z_p z_Q} = \cos 30^\circ = 0.9$  and similarly we would get

$$\gamma_{z_Q z_R} = 0.9,$$

$$\text{also } \gamma_{z_p z_R} = \eta * \gamma_{z_p z_Q} * \gamma_{z_Q z_R} = 0.648$$

Therefore the present method allows the covariances to be calculated using the following three equations:

$$K_{z_p z_Q} = 0.9 \left[ \sigma_{z_p}^2 \cdot \sigma_{z_Q}^2 \right]^{\frac{1}{2}} \quad (41)$$

$$K_{z_Q z_R} = 0.9 \left[ \sigma_{z_Q}^2 \cdot \sigma_{z_R}^2 \right]^{\frac{1}{2}} \quad (35)$$

$$K_{z_p z_R} = 0.648 \left[ \sigma_{z_p}^2 \cdot \sigma_{z_R}^2 \right]^{\frac{1}{2}} \quad (44)$$

## CHAPTER IV

### UNCERTAINTY ANALYSIS

An uncertainty analysis is presented here with a view to demonstrate the reliability of the six-orientation hot-wire technique and its sensitivity to various input parameters which have major contributions in the response equations. The analysis is done for both laminar and turbulent flow cases. The salient results are tabulated in Tables III and IV of Appendix A.

#### 4.1 Effect of Pitch and Yaw Factors

Pitch and yaw factors ( $G$  and  $K$ ) are used in the response equations described in Chapter III in order to compensate and account for the directional sensitivity of the single hot-wire probe. Figure 8, Appendix B, shows the pitch and yaw factors plotted against the hot-wire mean effective voltage. Both the pitch and yaw factors are functions of the hot-wire mean effective voltage, but the yaw factor is far more sensitive. A 10 percent increase in the voltage reduces the yaw factor by 56 percent and the pitch factor by 13 percent. The value of the pitch factor stays very close to one and hence does not have a major contribution in the response equations. For this reason, it is necessary to further consider the yaw factor, which is now examined for both laminar and turbulent flow conditions.

#### 4.1.1 Laminar Flow

For laminar flow cases, the covariances  $K_{z_i z_j}$  become zero and drop out of the response equations. Then Equations 20, 21, and 22 can be written as:

$$\bar{u} = F1 (\bar{Z}_p, \bar{Z}_Q, \bar{Z}_R)$$

$$\bar{w} = F2 (\bar{Z}_p, \bar{Z}_Q, \bar{Z}_R)$$

$$\bar{v} = F3 (\bar{Z}_p, \bar{Z}_Q, \bar{Z}_R)$$

Experiments were performed on a calibration nozzle free jet in the potential core where the flow can be idealized as being laminar.

As Table III, Appendix A, shows, the effect of yaw factor on time-mean axial and swirl velocities is insignificant for the laminar flow case.

#### 4.1.2 Turbulent Flow

The variation of yaw factor is studied on the turbulence quantities such as mean velocities, turbulence intensities and the shear stress  $\overline{u'v'}$ . As stated in Table III, all turbulence quantities behave differently to the variations in the yaw factor. The effect on all the turbulence quantities, except the mean radial velocity, is insignificant. In the case of mean radial velocity, the term  $(G^2 - K^2)$  in the denominator of Equation 9 changes the value of F3 considerably for small changes in the yaw factor.

### 4.2 Effect of Correlation Coefficients

Correlation coefficients are used in Equation 40 to calculate the

covariances between the fluctuations of the cooling velocities experienced by the hot-wire at adjacent orientations. These are then used in Equations 20 through 29 to calculate various turbulence quantities. A wide range of correlation coefficients ( $\gamma_{z_p z_q}$ ) between 0.1 to 0.9 are used to study the behavior of the turbulence quantities. Among all the turbulence quantities,  $\overline{u'v'}$  was found to be most sensitive to variations in the correlation coefficient ( $\gamma_{z_p z_q}$ ). In view of the sensitivity of  $\overline{u'v'}$  to  $\gamma_{z_p z_q}$  and the assumptions required to estimate  $\gamma_{z_p z_q}$ , it is apparent that this is the major source of the significantly large uncertainty in the estimate of the turbulent shear stress. This appears to be an inherent deficiency of the six-orientation single hot-wire method.

King (21) used a parameter Eta ( $\eta$ ) to relate the covariances between the fluctuations of the effective cooling velocities that are separated by 30 degrees with the covariance of velocities separated by 60 degrees (see Equation 37). He suggested a numerical value of 0.8 for  $\eta$ . Table III shows the effect of  $\eta$  on the turbulence quantities to be insignificant and hence the present study retains this value of 0.8 in all subsequent deductions.

#### 4.3 Experimental Uncertainty

Experimental uncertainty was tested for both laminar and turbulent flow cases. The main reason for these tests was to determine the mean and variance of the output quantities when obtained from the six possible choices of three from among the six possible response equations (Equations 3 through 8 in Chapter III). Another objective of the study was to judge the extent of errors in output quantities because of errors

in measurement of mean and root-mean-square voltages.

#### 4.3.1 Laminar Flow

The calibration free jet facility was used to conduct laminar flow uncertainty experiments. To generate velocities in the axial and azimuthal direction with respect to the wire, the wire was offset by 45 degrees to the main direction of the flow and placed in the potential core region, thereby achieving two equal components of axial and swirl velocities. However, upon data reduction, it was observed that the two components were not equal. The variation among the two components was different for each choice of the six combinations of three adjacent response equations. In general, the variation among the two components was negligible.

Table III shows the effect of variations in measurements of the hot-wire mean voltages on the turbulence quantities. For laminar flow case, the mean axial and swirl velocities are extremely sensitive to errors in measurements of hot-wire mean voltage. This particular test stresses the need for using precise voltmeters. A 10 percent error in measurement of one of the six mean voltages leads to an error of 90 percent in axial velocity deduction for the conditions of this test. At other flow conditions, similar gross sensitivity may be expected.

Turbulence quantities are calculated using six different combinations of the three mean effective cooling velocities experienced by the hot-wire at three adjacent orientations. Table IV, Appendix A, demonstrates good consistency between the six possibilities for mean axial and swirl velocity determination in laminar flow conditions.

#### 4.3.2 Turbulent Flow

As observed for the laminar flow case, errors in mean voltage measurements are extremely magnified in calculations of turbulence quantities. Table III shows these large variations in the turbulence quantities.

For turbulent flows, a large scatter is observed among the six values of turbulence quantities deduced from the six different combinations. To get an estimate of the scatter, the flowfield location  $x/D = 2.0$ ,  $r/D = 0.25$  for the case of side-wall angle  $\alpha = 45$  degrees was selected inside the main test facility. At this location in the flowfield, the turbulence quantities obtained are good representatives of turbulence level in the combustor flowfield.

Table IV shows that for turbulent flow, all the six combinations do not reveal all the turbulence quantities. The omitted items correspond to occasions when the velocity function  $f^3$  attains a complex value via the requirement of the square root of a negative value. Then, no further progress could be made with that particular set of three adjacent orientations in such situations.

Table IV also highlights the scatter among the six values of each turbulent quantity when solved using six different combinations. It is evident that certain quantities (such as mean radial velocity, the radial turbulence intensity, and the shear stress  $\overline{u'v'}$ ) have very large scatter. This shows a great uncertainty in the use of six-orientation hot-wire technique in measurement of these quantities.

## CHAPTER V

### RESULTS

The six-orientation hot-wire technique is employed to measure the turbulence quantities for nonswirling conditions. The experiments have been conducted for expansion angles of 90 degrees (sudden expansion) and 45 degrees (gradual expansion). A computer program, listed in Appendix D, written in Fortran language, is used to process the data on an IBM 370/168 computer. For each location in the flowfield, six combinations of three adjacent orientations are selected and six values of each of the nine turbulence quantities are obtained. So, a decision has to be made about the selection of one of the six values. In nonswirling conditions, the flow is mainly dominated by the axial velocity. When the hot-wire is parallel to the axial direction; it experiences the least cooling effect from the axial velocity, whereas the radial and swirl velocities affect the wire most efficiently. Therefore, a small change in the  $v$  and  $w$  velocities will show a significant change in hot-wire voltage. Hence the set of orientations labeled (3, 4, 5) in Chapter III (orientation 4 having the hot-wire parallel to the  $x$ -direction) is chosen and used in all subsequent results presented, except where noted otherwise. Nevertheless, there are some quantities, such as  $v'_{rms}$  and  $\overline{u'v'}$ , which appear to be better represented by alternative sets of three adjacent orientations, but the appropriate choice is not known a priori.

## 5.1 Mean Velocities

Radial distributions of time-mean axial and radial velocities are plotted in Figures 9 and 10, Appendix B, respectively. Mean axial velocities for different axial locations and expansion angles are compared with measurements done with a crossed hot-wire probe by Chaturvedi (5). A good agreement is found between the two studies.

Because of the inability of the hot-wire to determine the sense of the flow direction, the presence of the corner recirculation zone was observed by a sudden increase in the axial velocity closer to the wall. Mean radial velocity was found to increase at the centerline with an increase in the axial distance. The mean velocity profiles tend to get flatter further downstream from the inlet. For  $\alpha = 45^\circ$ , mean radial velocity at the centerline increased from 5 percent of the maximum inlet mean velocity at  $x/D = 0.5$  to 16 percent of the maximum inlet velocity at  $x/D = 2.0$ . A similar increase was observed for  $\alpha = 90^\circ$ .

## 5.2 Turbulence Intensities

The six-orientation hot-wire technique enables one to measure the axial, radial, and azimuthal turbulence intensities at various axial and radial locations in the confined jet flowfield. The radial distributions of these turbulence intensities are plotted in Figures 11, 12, and 13 of Appendix B. The axial and radial turbulence intensities are compared with Chaturvedi's study (5) and reasonable agreement is found in the case of axial turbulence intensities. However, the two studies are not in good agreement for radial turbulence intensities. The peak values measured in the present study are much lower, in certain cases

being only 50 percent of the previously measured peak values (5). While solving the six sets of combinations of three adjacent orientations, it was found that  $v'_{rms}/\bar{u}_0$  has a large scatter. For example at  $x/D = 2.0$ ,  $r/D = 0.300$ , and  $\alpha = 45^\circ$ , the mean and the standard deviation of  $v'_{rms}/\bar{u}_0$ , among the six sets of readings, were found to be 0.1447 and 0.0330, respectively. This large scatter shows that in nonswirling flow this technique is not a very accurate way of measuring the radial turbulence intensities. Nevertheless, results shown in Figure 11 have been obtained with the set of orientations (3, 4, 5) being used.

### 5.3 Shear Stresses

In nonswirling flow conditions, measurements have been made of the turbulent shear stress  $\overline{u'v'}$ . The radial distribution of  $\overline{u'v'}/u_0^2$  at various axial locations is plotted in Figure 14, Appendix B, and is compared with the earlier study done by Chaturvedi (5). In general, the two studies are in good agreement, but they do differ in two respects: the centerline values far downstream and the peak values near the inlet.

Chaturvedi (5) measured  $\overline{u'v'}$  to be zero at the centerline at all axial locations. However, in the present study,  $\overline{u'v'}$  is found to be non-zero at the centerline at axial locations greater than  $x/D = 0.5$  for both side-wall angles  $\alpha = 45^\circ$  and  $\alpha = 90^\circ$ . A detailed study shows that the scatter for  $\overline{u'v'}/u_0^2$ , when calculated from different sets of adjacent orientations, is quite large. The ratio of standard deviation to the mean is approximately 0.6 and varies with position.

Peak values of  $\overline{u'v'}$  are seen to be in good agreement except close to the inlet. At  $x/D = 0.5$ , Chaturvedi (5) measured peak values approximately 50 percent higher than in the present study. It must be

remembered that there is always difficulty in measuring shear stress values in thin shear layer regions. In the present study, there is also the previously-discussed deficiency, see Chapter IV, because of the assumptions made about the correlation coefficients  $\gamma_{z_i z_j}$ . These assumptions may be the major source of significantly large uncertainty in the calculation of turbulent shear stress values.

## CHAPTER VI

### CLOSURE

#### 6.1 Summary

The six-orientation hot-wire technique is a relatively new method to measure time-mean values and turbulence quantities in complex three-dimensional flowfields. Applied in this study to nonreacting nonswirling axisymmetric flowfields, measurements of time-mean and root-mean-square voltages at six different orientations contain enough information to obtain the time-mean velocities, turbulence intensities and shear stresses. At each location in the flow, there are six different values of each of the above quantities that can be obtained by using six sets of measurements of three adjacent orientations. Because of axial velocity domination, a particular set of orientations was chosen. Nevertheless, the measurement accuracy can be well judged by the scatter of the values of turbulence quantities among the six different combinations of sets of three mean effective cooling velocities. The nonswirling confined jet flow was investigated with this technique. It was found to be an excellent method to find time-mean velocities. It also gave good results for turbulence intensities and shear stresses. An uncertainty analysis done on this technique reveals that certain output parameters such as the axial, radial, and azimuthal turbulence intensities and shear stresses are extremely sensitive to some input

parameters such as yaw factor and mean voltages.

## 6.2 Further Work

The multi-orientation single-wire technique is a useful cost-effective tool for the investigation of complex flowfields. At present, there is a need to check repeatability under nonswirling conditions before progressing to the investigation of flows with moderate and strong swirl. This would lead to further evaluation of reliability and accuracy of the technique in general flowfields. Thus far, there is an *a priori* assumption about the evaluation of covariances, which entails the use of constant values for the correlation coefficients. Further work might call for the development of alternative methods to specify the covariances. Nevertheless, the method has potential for further use in the experimental evaluation of complex flowfields.

## REFERENCES

- (1) Lefebvre, A. H. (ed.). Gas Turbine Combustor Design Problems. New York: Hemisphere-McGraw-Hill, 1980.
- (2) Rhode, D. L., "Predictions and Measurements of Isothermal Flowfields in Axisymmetric Combustor Geometries," Ph.D. Thesis, Oklahoma State University, Stillwater, Oklahoma, 1981.
- (3) Rhode, D. L., D. G. Lilley, and D. K. McLaughlin. "On the Prediction of Swirling Flowfields Found in Axisymmetric Combustor Geometries." Proceedings, ASME Symposium on Fluid Mechanics of Combustion Systems. Boulder, Colo., June 22-24, 1981, pp. 257-266.
- (4) Krall, K. M., and E. M. Sparrow. "Turbulent Heat Transfer in the Separated, Reattached, and Redevelopment Regions of a Circular Tube." Journal of Heat Transfer (Feb., 1966), pp. 131-136.
- (5) Chaturvedi, M. C. "Flow Characteristics of Axisymmetric Expansions." Proceedings, Journal of the Hydraulics Division, ASCE, Vol. 89, No. HY3 (1963), pp. 61-92.
- (6) Phaneuf, J. T., and D. W. Netzer. Flow Characteristics in Solid Fuel Ramjets. Report No. NPS-57Nt74081. Prepared for the Naval Weapons Center by the Naval Postgraduate School, Monterey, California, July, 1974.
- (7) Back, L. H., and E. J. Roschke. "Shear Layer Flow Regimes and Wave Instabilities and Reattachment Lengths Downstream of an Abrupt Circular Channel Expansion." Journal of Applied Mechanics (Sept., 1972), pp. 677-681.
- (8) Roschke, E. J., and L. H. Back. "The Influence of Upstream Conditions on Flow Reattachment Lengths Downstream of an Abrupt Circular Channel Expansion." Journal of Biomechanics, Vol. 9 (1976), pp. 481-483.
- (9) Ha Minh, H., and P. Chassaing. "Perturbations of Turbulent Pipe Flow." Proceedings, Symposium on Turbulent Shear Flows. Pennsylvania State University, April, 1977, pp. 13.9-13.17.
- (10) Moon, L. F., and G. Rudinger. "Velocity Distribution in an Abruptly Expanding Circular Duct." Journal of Fluids Engineering (March, 1977), pp. 226-230.

- (11) Johnson, B. V., and J. C. Bennett. "Velocity and Concentration Characteristics and Their Cross Correlation for Coaxial Jets in a Confined Sudden Expansion; Part II: Predictions." Proceedings, ASME Symposium on Fluid Mechanics of Combustion Systems. Boulder, Colo., June 22-23, 1981, pp. 145-160.
- (12) Goldstein, S. (ed.). "Modern Developments in Fluid Dynamics," Vol. I and II. New York: Dover Publications, 1965.
- (13) Hinze, J. O. "Turbulence," 2nd Edition. New York: McGraw-Hill, 1975.
- (14) Bradshaw, P. "An Introduction to Turbulence and Its Measurement." New York: Pergamon Press, 1971.
- (15) Beer, J. M., and N. A. Chigier. "Combustion Aerodynamics," New York, Halsted Press Division, John Wiley & Sons, Inc., 1972.
- (16) Syred, N., J. M. Beer, and N. A. Chigier. "Turbulence Measurements in Swirling Recirculating Flows." Proceedings, Salford Symposium on Internal Flows. London, England: Inst. of Mechanical Engineering, 1971, pp. B27-B36.
- (17) Wygnanski, I., and H. Fielder. "Some Measurements in the Self Preserving Jet." Journal of Fluid Mechanics, Vol. 38, 1969, p. 577.
- (18) Pratte, B. D., and J. R. Keffer. "The Swirling Turbulent Jet." Journal of Basic Engineering, Vol. 94 (Dec., 1972), pp. 739-748.
- (19) Dvorak, K., and N. Syred, "The Statistical Analysis of Hot Wire Anemometer Signals in Complex Flow Fields," DISA Conference, Univ. of Leicester, 1972.
- (20) Jorgensen, F. E. "Directional Sensitivity of Wire and Fiber Film Probes." DISA Information No. 11, Franklin Lakes, NJ, May 1971.
- (21) King, C. F. "Some Studies of Vortex Devices - Vortex Amplifier Performance Behavior," Ph.D. Thesis, Univ. College of Wales, Cardiff, Wales, 1978.
- (22) Habib, M. A., and J. H. Whitelaw. "Velocity Characteristics of Confined Coaxial Jets With and Without Swirl." ASME Paper 79-WA/FE-21. New York, NY, Dec. 2-7, 1979.
- (23) Gupta, A. K., and D. G. Lilley. Flowfield Modeling and Diagnostics. Tunbridge Wells, England: Abacus Press, 1982 (in press).

APPENDICES

APPENDIX A

TABLES

TABLE I  
VALUES OF AO, BO, AND CO IN VARIOUS EQUATION SETS

Equation Set P,Q,R Choice	AO	BO	CO
1, 2, 3	$(z_2^2 - z_3^2)$	$(-2z_1^2 + 3z_2^2 - z_3^2)$	$(z_1^2 - z_2^2 + z_3^2)$
2, 3, 4	$(z_2^2 - z_3^2)$	$(-z_2^2 + 3z_3^2 - 2z_4^2)$	$(z_2^2 - z_3^2 + z_4^2)$
3, 4, 5	$(z_3^2 - 2z_4^2 + z_5^2)$	$(z_2^2 - z_5^2)$	$(z_3^2 - z_4^2 + z_5^2)$
4, 5, 6	$(-z_5^2 + z_6^2)$	$(-2z_4^2 + 3z_5^2 - z_6^2)$	$(z_4^2 - z_5^2 + z_6^2)$
5, 6, 1	$(-z_5^2 + z_6^2)$	$(-z_5^2 + 3z_6^2 - 2z_1^2)$	$(z_5^2 - z_6^2 + z_1^2)$
6, 1, 2	$(-z_6^2 + 2z_1^2 - z_2^2)$	$(-z_6^2 + z_2^2)$	$(z_5^2 - z_1^2 + z_2^2)$

TABLE II  
Matrix (T) in Equation 30

---

$\frac{2 Z_P Z_Q}{Z_{P+3}^3}$	$\frac{-2 Z_P Z_R}{Z_{P+3}^3}$	$\frac{4 Z_Q Z_R}{Z_{P+3}^3}$
$\frac{6 Z_P Z_Q}{Z_{P+4}^3}$	$\frac{-4 Z_P Z_R}{Z_{P+4}^3}$	$\frac{2 Z_Q Z_R}{Z_{P+4}^3}$
$\frac{4 Z_P Z_Q}{Z_{P+5}^3}$	$\frac{-2 Z_P Z_R}{Z_{P+5}^3}$	$\frac{2 Z_Q Z_R}{Z_{P+5}^3}$

---

TABLE III  
EFFECT OF INPUT PARAMETERS ON TURBULENCE QUANTITIES

PARAMETER	TYPE OF FLOW	% CHANGE IN PARAMETER	% CHANGES IN TURBULENCE QUANTITIES							
			$\bar{u}$	$\bar{w}$	$\bar{v}$	$u'_{rms}$	$w'_{rms}$	$v'_{rms}$	$\overline{u'v'}$	
K	LAM	+10	+0.14	+0.146	--	--	--	--	--	--
K	TURB	+10	-0.17	--	-5.96	-0.18	-0.18	+0.53	--	No Change
$\gamma Z_p Z_Q$	TURB	+10	+0.22	--	+2.76	-3.17	-8.15	-0.57	--	40.28
$\bar{E}_1$	LAM	+10	+89.2	+74.5	--	--	--	--	--	--
ALL $\bar{E}_i$ $i=1,6$	LAM	+10	+65.9	+65.4	--	--	--	--	--	--
$\eta$	TURB	+10	-0.50	--	+1.37	+4.64	+7.02	+0.88	-1.34	--
$\bar{E}_1$	TURB	+10	16.3	--	--	-32.8	--	--	--	+528.3
ALL $\bar{E}_i$ $i=1,6$	TURB	+10	+72.9	--	+97.2	+54.2	+61.7	+64.8	+118.8	--

TABLE IV  
 SCATTER AMONG THE TURBULENCE QUANTITIES WHEN  
 SOLVED BY SIX DIFFERENT COMBINATIONS

TURBULENCE QUANTITY	TYPE OF FLOW	TURBULENCE QUANTITY SOLVED BY SIX COMBINATIONS						MEAN $\bar{x}$	STANDARD DEVIATION $\sigma$	PERCENT $\sigma/\bar{x}$
		1,2,3	2,3,4	3,4,5	4,5,6	5,6,1	6,1,2			
$\bar{u}$ (m/s)	LAM	6.92	6.8566	7.1162	7.0224	6.7273	6.9326	6.9291	0.134	1.9
$\bar{w}$ (m/s)	LAM	7.546	7.4879	7.4093	7.8195	7.557	7.4899	7.5513	0.1414	1.9
$\bar{u}/u_0$	TURB	0.3478	0.3115	0.3343	0.3035	0.3398	0.2382	0.3125	0.0402	12.9
$\bar{v}/u_0$	TURB	--	0.1818	0.1717	0.1795	0.560	0.1835	0.1545	0.0552	35.7
$u'_{rms}/u_0$	TURB	0.1758	0.1781	0.1331	0.1711	0.1680	0.2511	0.1795	0.0387	21.6
$v'_{rms}/u_0$	TURB	--	0.0778	0.0743	0.0783	0.0355	--	0.0665	0.0207	31.1
$[u'v'/u_0^2]^{1/2}$	TURB	--	0.136	0.059	0.100	0.0943	--	0.0973	0.0315	32.4
$u'v'/u_0^2$	TURB	0.0185	0.0035	0.0101	0.0036	--	--	0.0089	0.0071	79.8

APPENDIX B

FIGURES

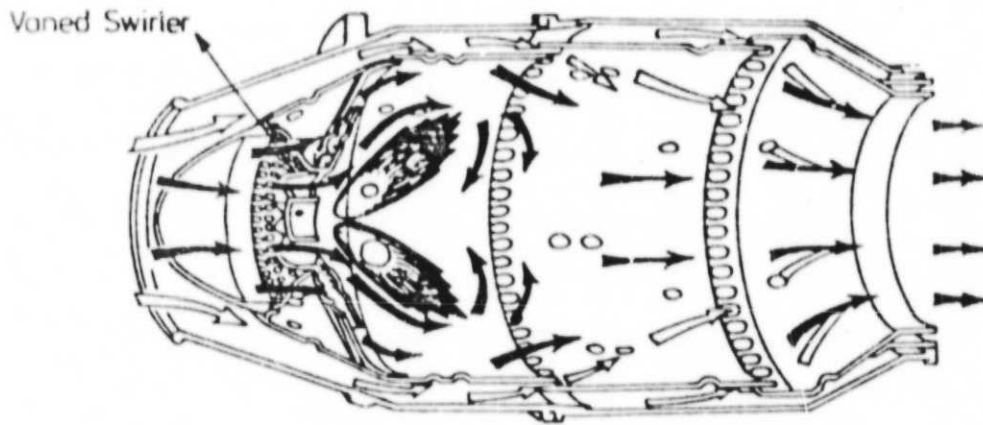


Figure 1. Typical Axisymmetric Combustion Chamber of a Gas Turbine Engine

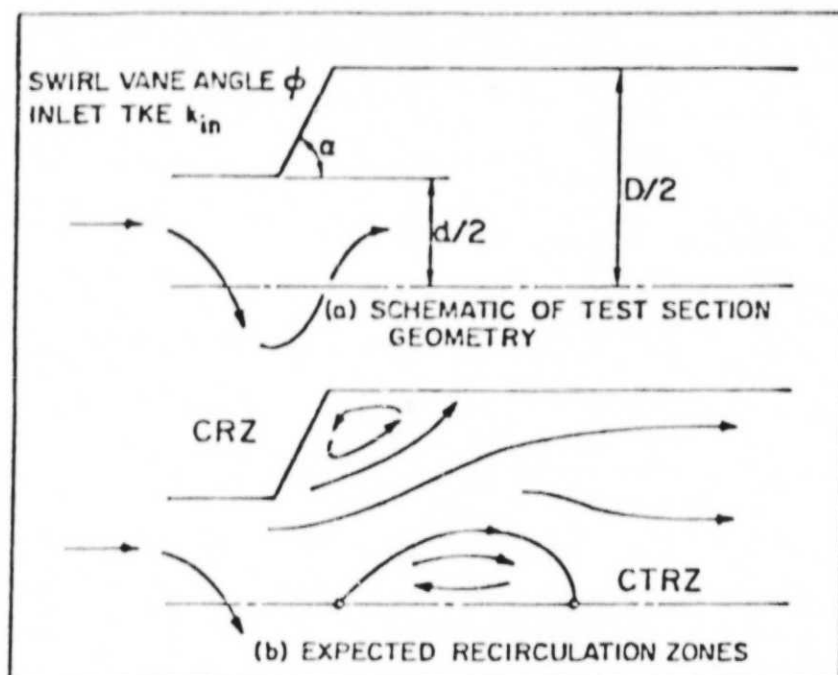


Figure 2. The Flowfield Being Investigated

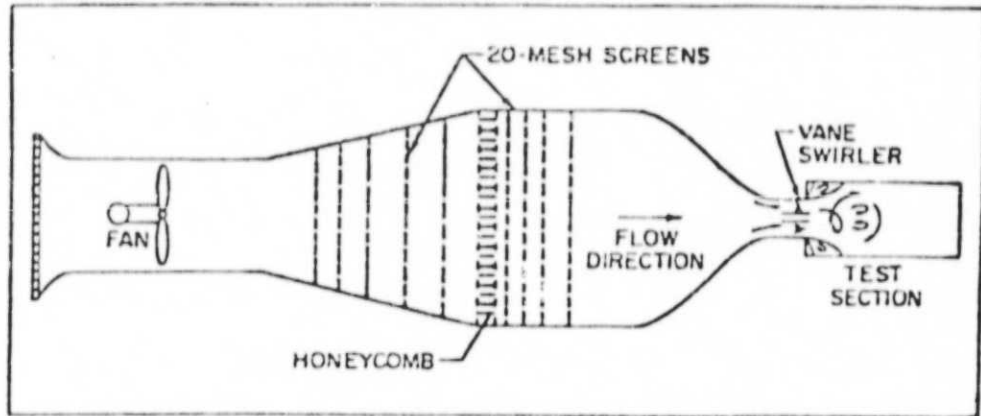


Figure 3. Schematic of Overall Facility

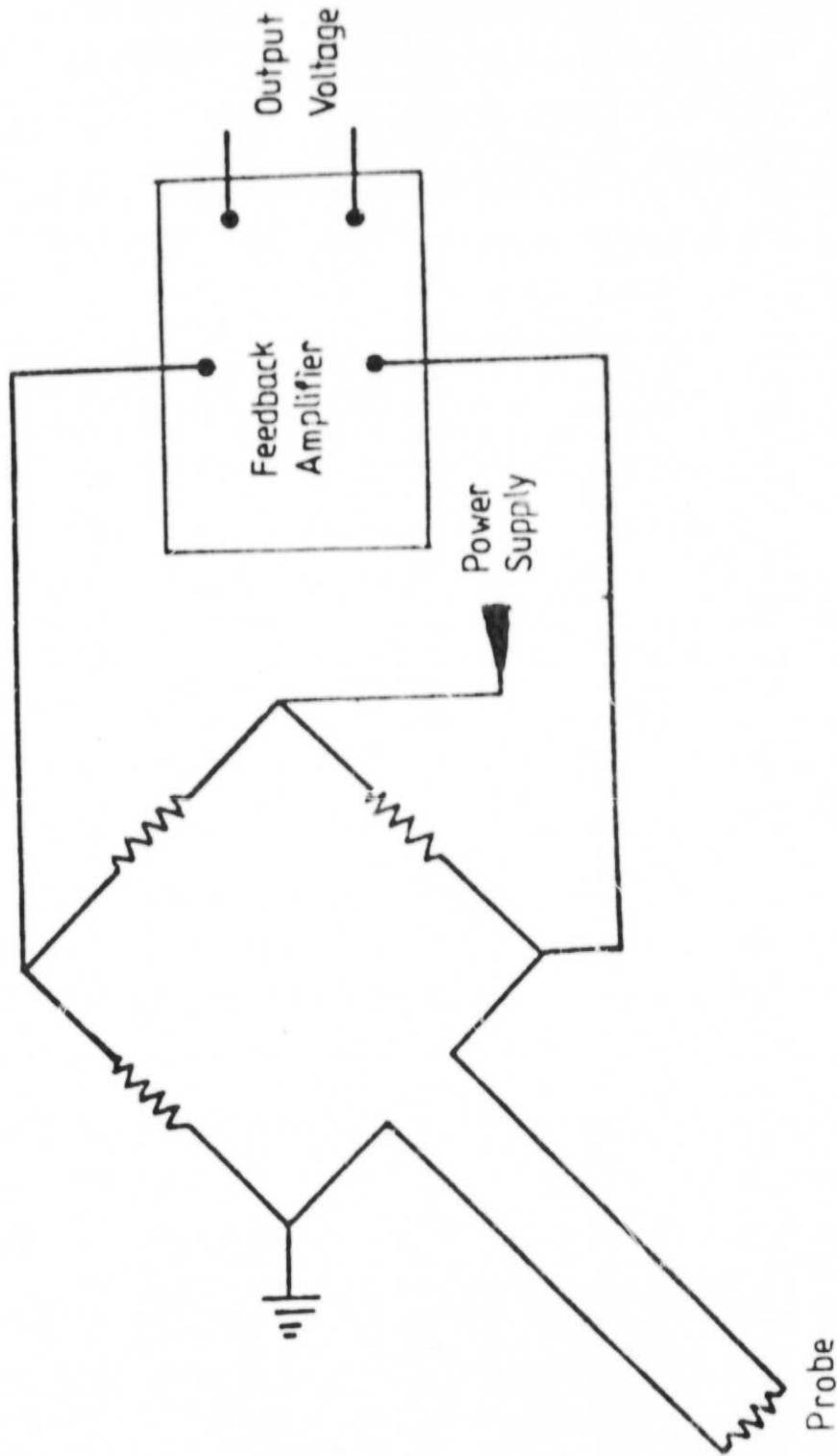


Figure 4. Hot-Wire Constant Temperature Anemometer

ORIGINAL PAGE  
BLACK AND WHITE PHOTOGRAPH

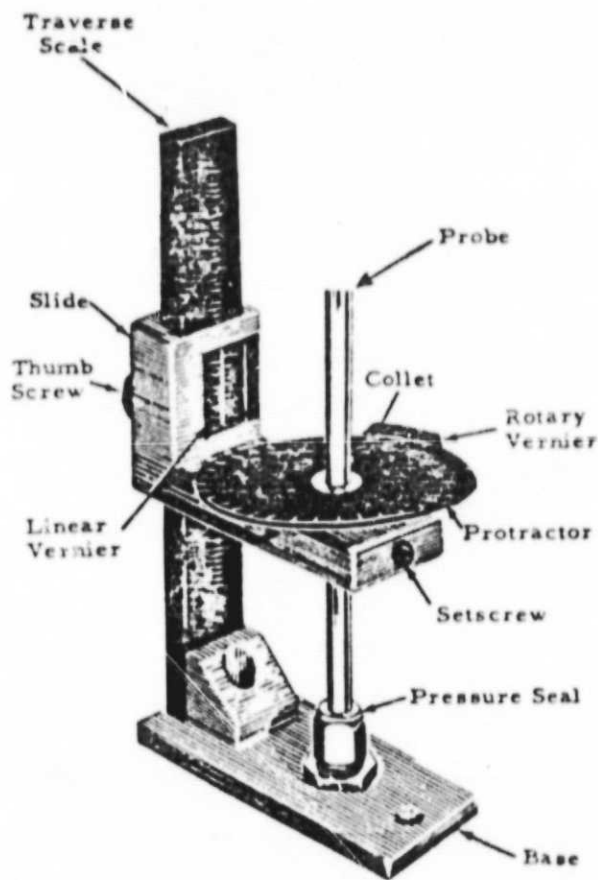


Figure 5. Manual Traversing Mechanism Used for Hot-Wire Orientations in the Flowfield

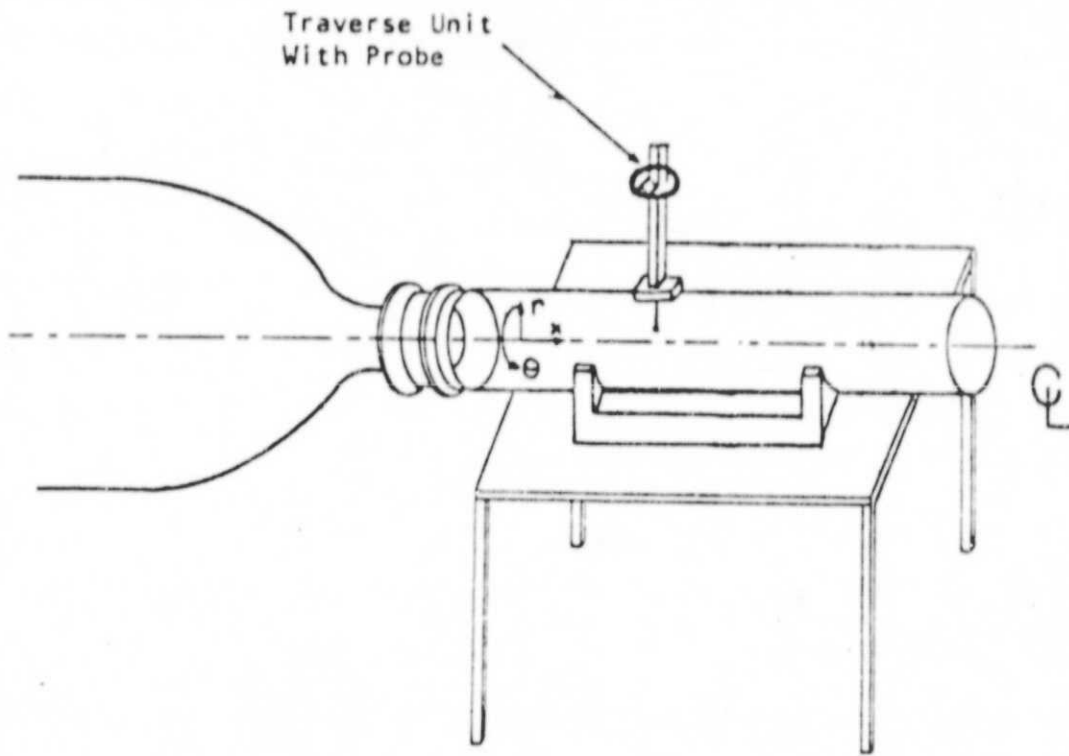


Figure 6. Mounting the Hot-Wire Probe on the Test Section

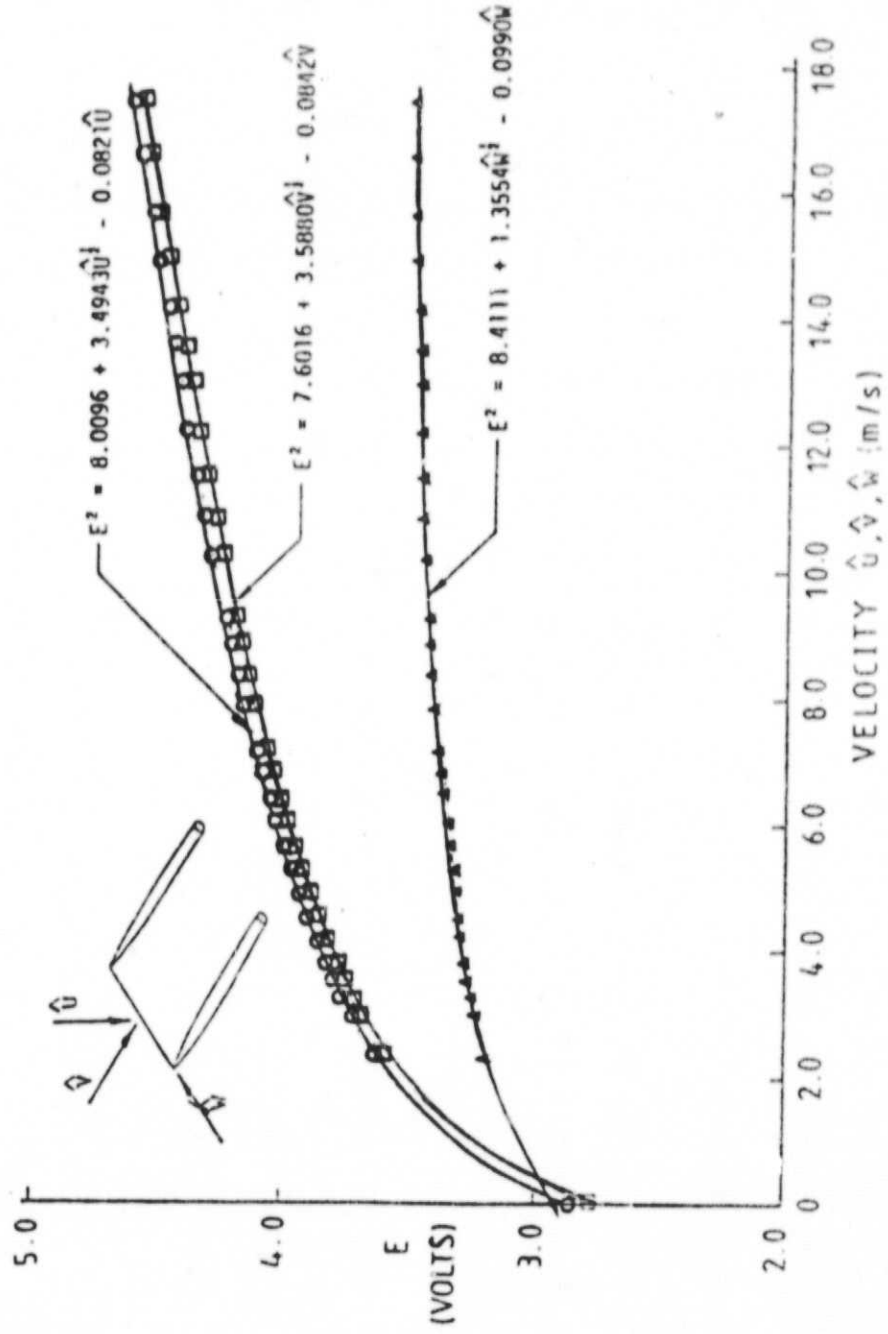


Figure 7. The Three-Directional Hot-Wire Calibration

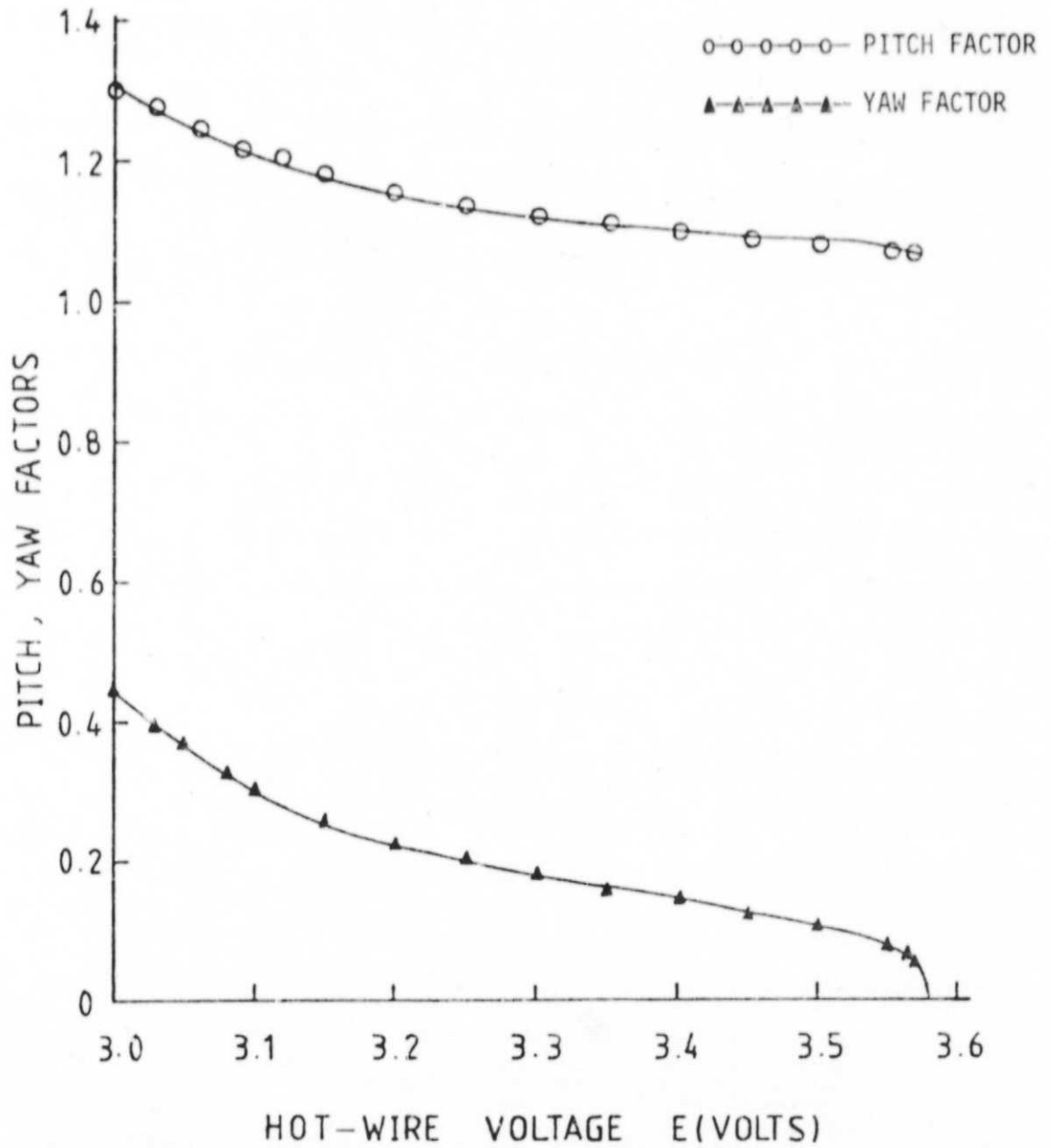


Figure 8. Plot of Pitch and Yaw Factors Versus Hot-Wire Voltage

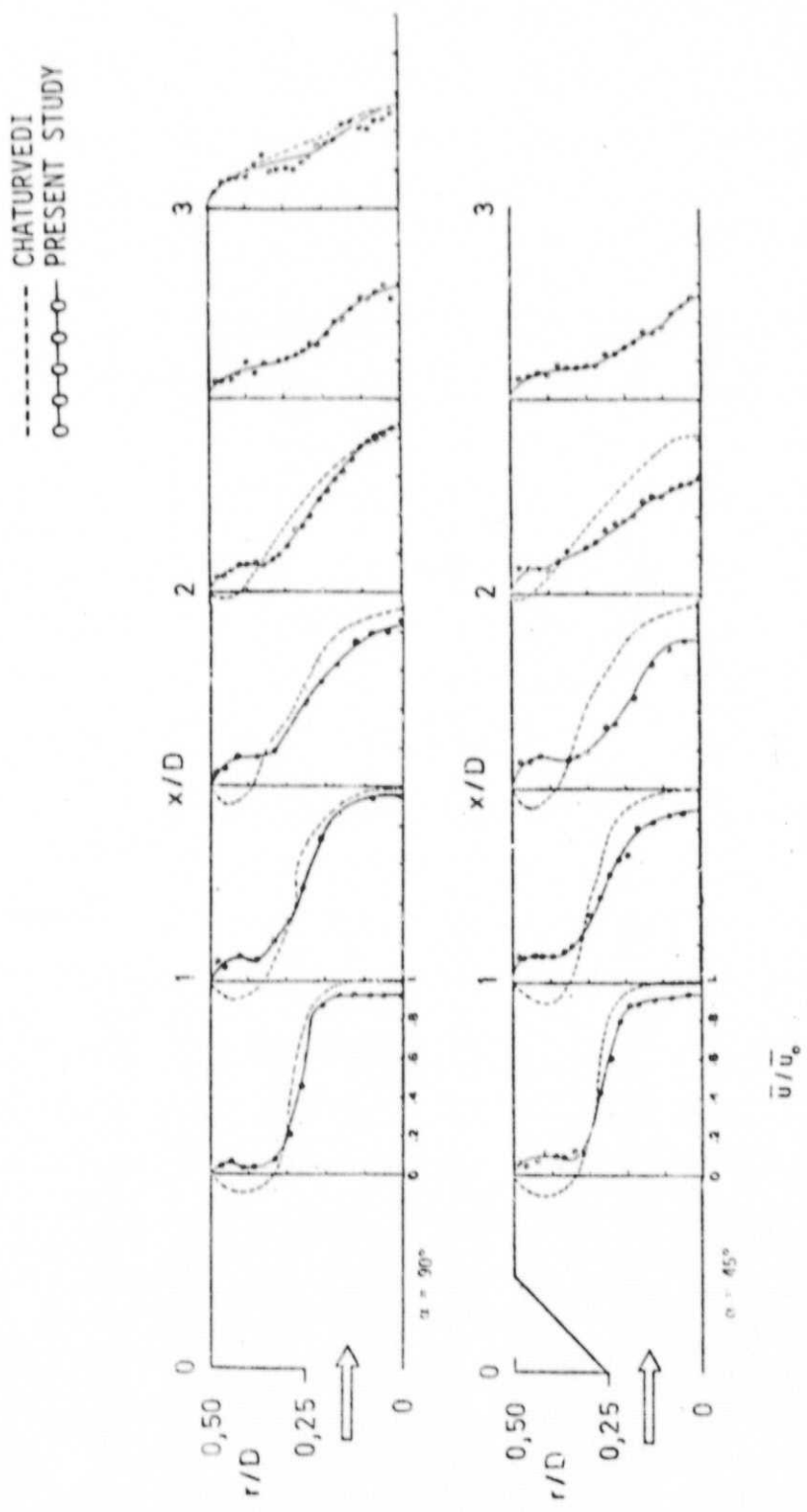


Figure 9. Radial Distribution of Normalized Time-Mean Axial Velocity in Nonswirling Confined Jet

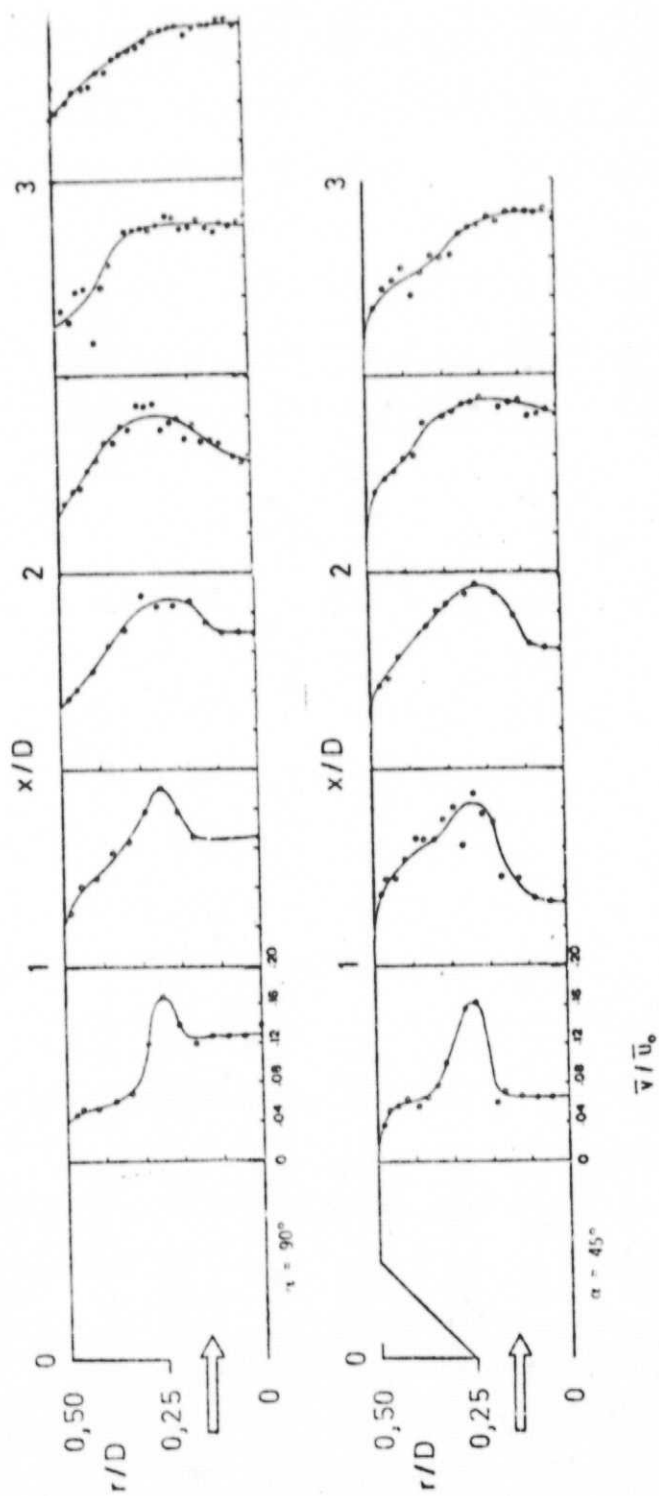


Figure 10. Radial Distribution of Normalized Time-Mean Radial Velocity in Nonswirling Confined Jet

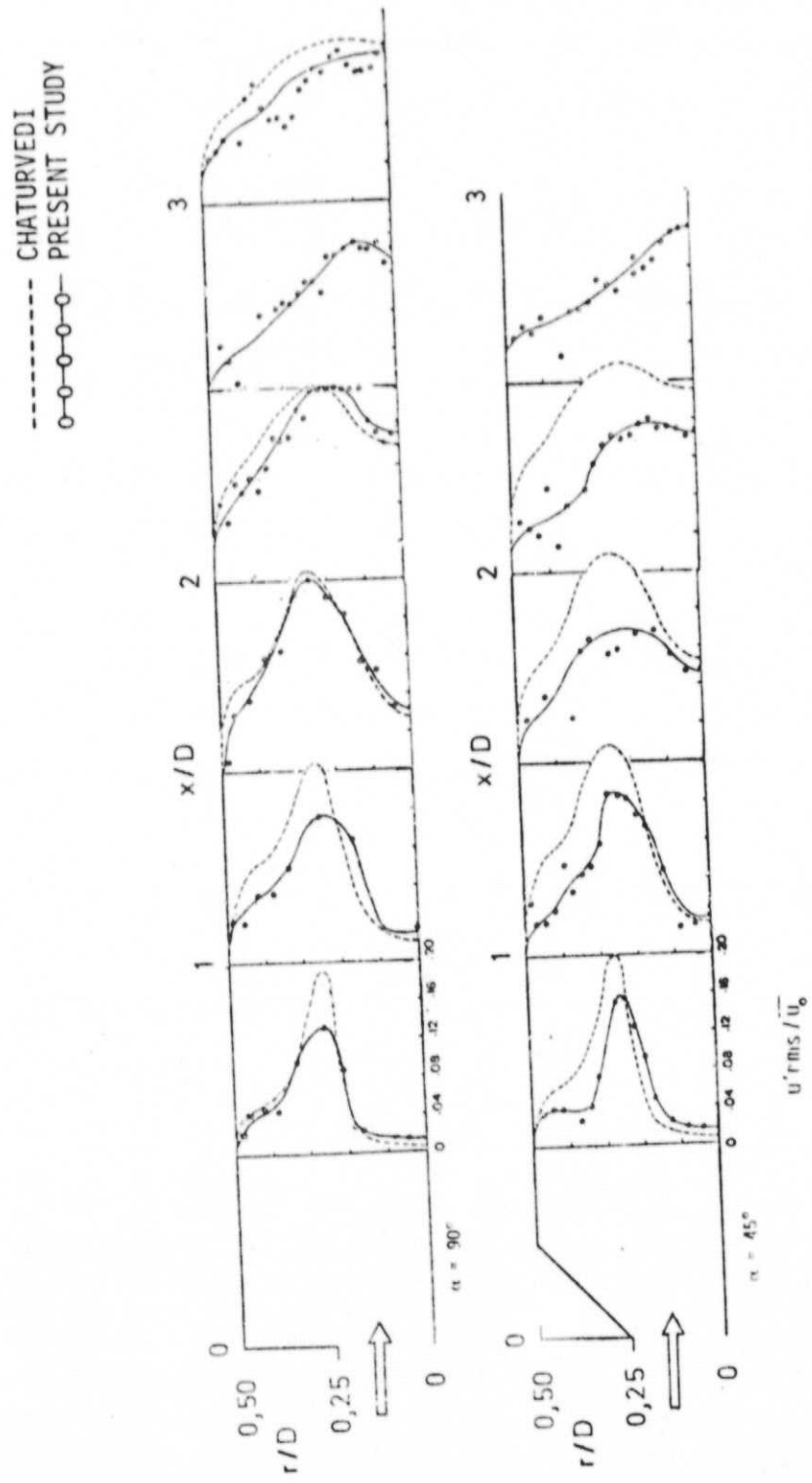


Figure 11. Radial Distribution of Axial Turbulence Intensity in Nonswirling Confined Jet

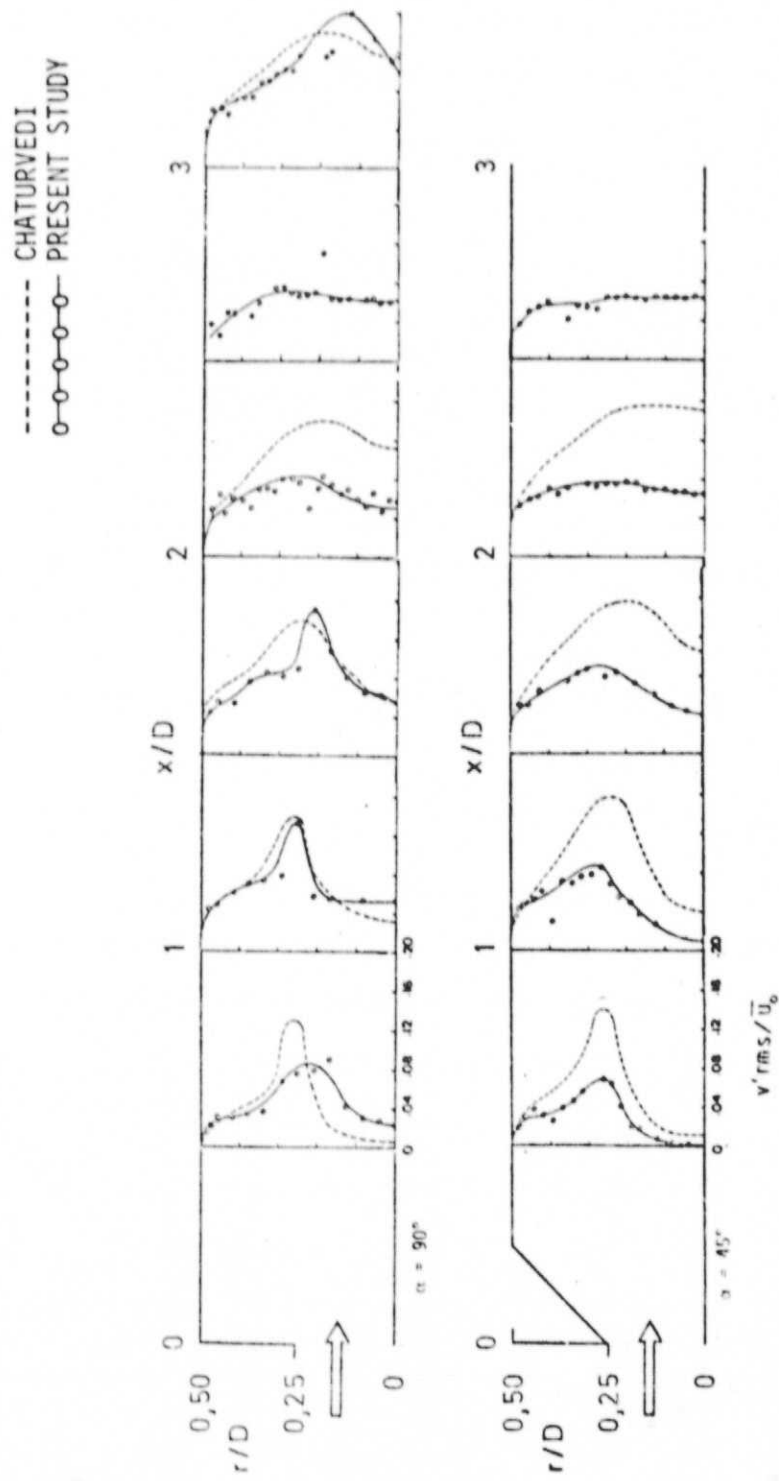


Figure 12. Radial Distribution of Radial Turbulence Intensity in Nonswirling Confined Jet

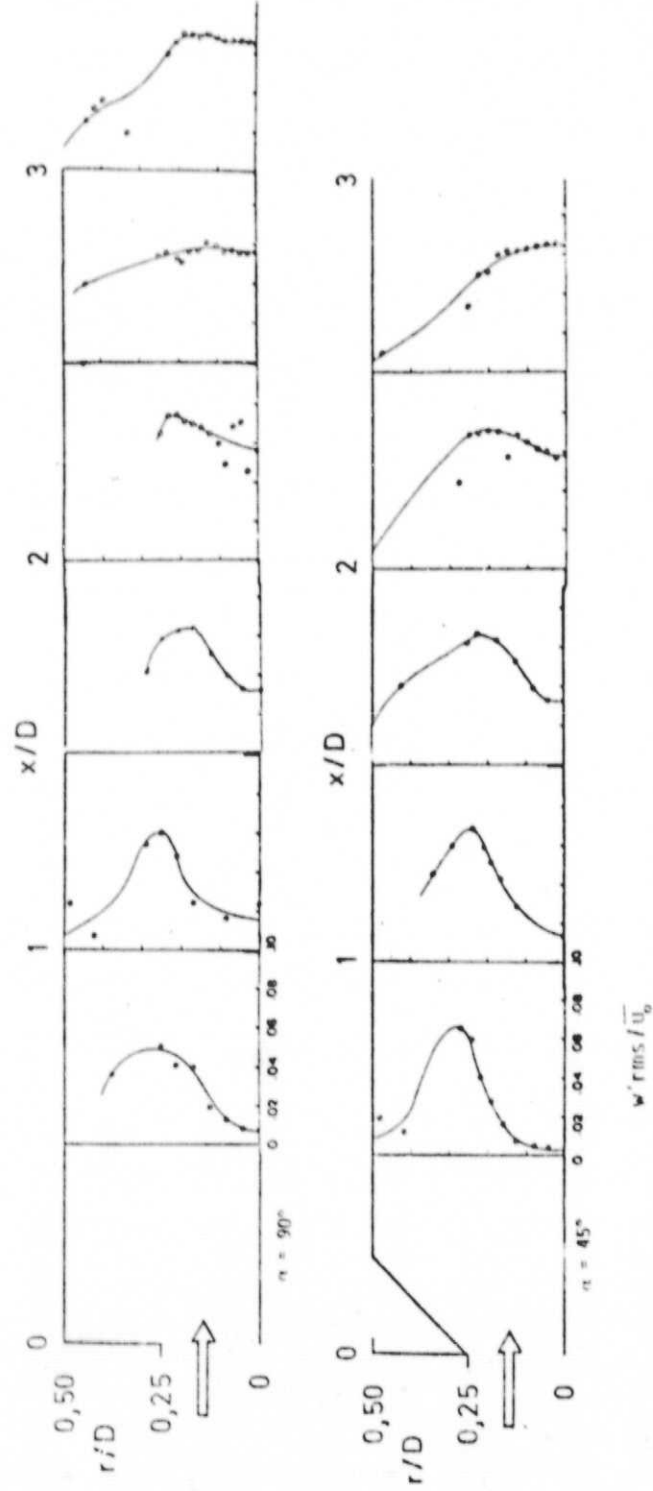


Figure 13. Radial Distribution of Azimuthal Turbulence Intensity in Nonswirling Confined Jet

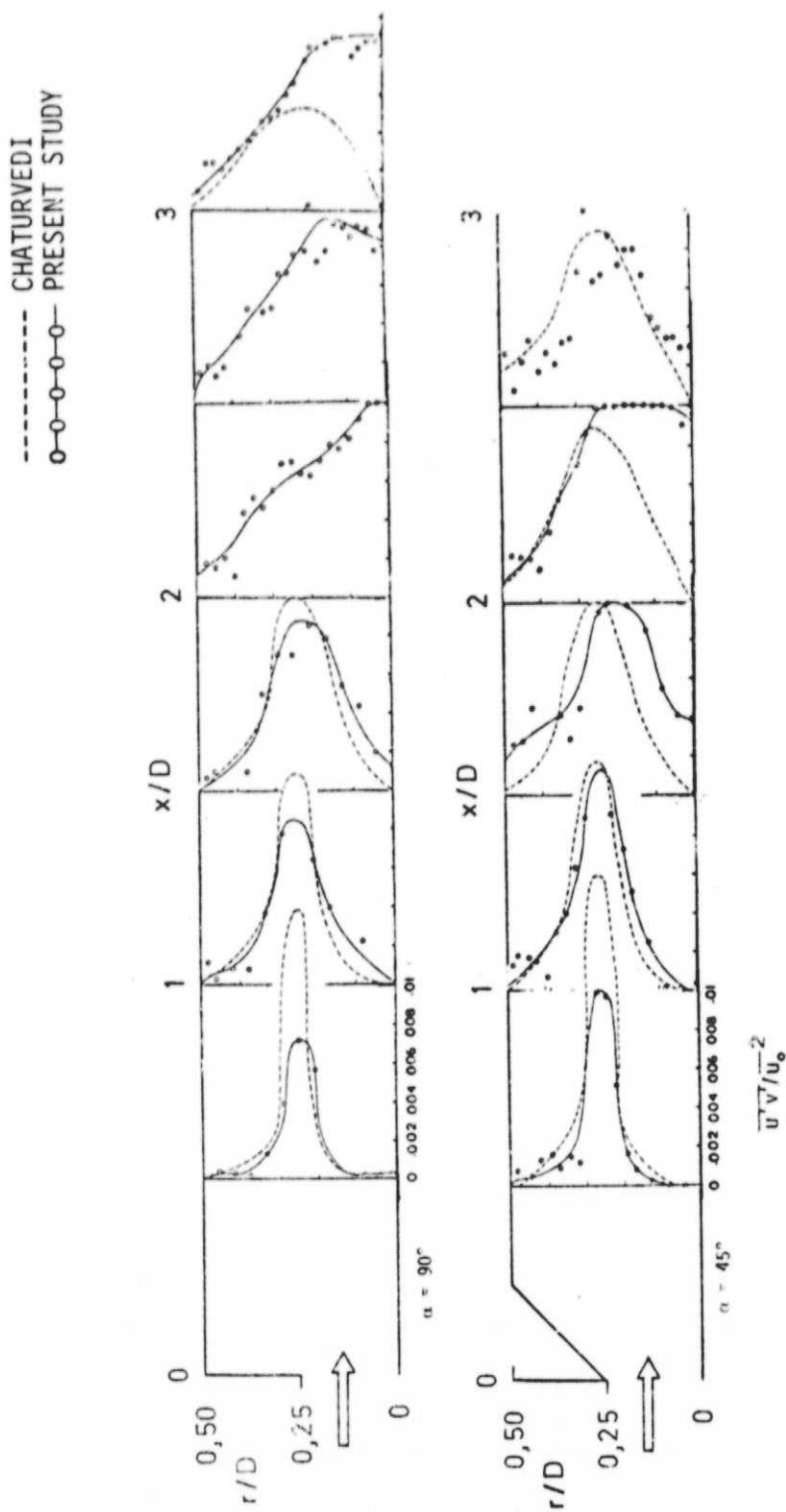


Figure 14. Radial Distribution of Shear Stress  $\overline{u'v'}/u_0^2$  in Nonswirling Confined Jet

APPENDIX C

USER'S GUIDE TO COMPUTER CODE FOR SIX-ORIENTATION  
HOT-WIRE DATA REDUCTION TECHNIQUE

USER'S GUIDE TO COMPUTER CODE FOR SIX-ORIENTATION  
HOT-WIRE DATA REDUCTION TECHNIQUE

A computer code is developed to obtain the turbulence quantities using the technique discussed in Chapter III. Measurements in a turbulent flowfield contain six mean and six root-mean-square voltages. A three-directional hot-wire calibration reveals three calibration constants in each direction. The input to the computer code is the mean, and root-mean-square voltages and also the calibration constants. The experimental data is then processed by the MAIN subprogram and various subroutines to get the output in the form of nine turbulence quantities consisting of the three mean velocities, the three turbulence intensities, and the three shear stresses. To facilitate the use of the computer code, the function of each subprogram is discussed here in detail.

1. The MAIN Subprogram

MAIN is the major part of the computer code which accepts the input in the form of mean and root-mean-square voltages and calibration constants and calls various subroutines to solve the equations listed in chapter III and finally calculates the turbulence quantities.

(8) Calculation of Mean Effective Cooling Velocities and Variances

Main calculates the six mean effective cooling velocities using Equation 14. This equation employs the input values of six mean voltages and calibration constants in  $\hat{u}$ -direction (see Figure 7, Appendix A). The MAIN then calculates the six values of variances using Equation 19. Equations 14 and 19 give mean and variance of individual cooling velocities in terms of the mean and

variance of the appropriate voltage.

(ii) Calculation of Velocity Functions and Differentials

Having calculated the mean effective cooling velocities and variances, the MAIN then calls various subroutines to obtain the necessary information required to calculate velocity functions using Equations 9 through 11. The main then calculates the first and the second differentials of the three velocity functions with respect to the three selected mean effective cooling velocities. The differentials are given as:

$$\frac{\partial \overline{F1}}{\partial \overline{Z}_i} = \frac{\left[ \frac{B0}{3(G^2 - K^2)^2} \frac{\partial B0}{\partial \overline{Z}_i} + \frac{\overline{F1}^2}{(G^2 - K^2)} \frac{\partial A0}{\partial \overline{Z}_i} \right]}{\left[ 2\overline{F1}^3 - 2\overline{F1} \frac{A0}{(G^2 - K^2)} \right]} \quad (1)$$

$$\frac{\partial \overline{F2}}{\partial \overline{Z}_i} = \frac{\left[ \frac{B0}{3(G^2 - K^2)^2} \frac{\partial B0}{\partial \overline{Z}_i} - \frac{\overline{F2}^2}{(G^2 - K^2)^2} \frac{\partial A0}{\partial \overline{Z}_i} \right]}{\left[ 2\overline{F2}^3 + \frac{2A0}{(G^2 - K^2)} \overline{F2} \right]} \quad (2)$$

$$\frac{\partial \overline{F3}}{\partial \overline{Z}_i} = \frac{\left[ \frac{\partial C0}{\partial \overline{Z}_i} \left\{ \overline{F3}^2 - C0 \right\} + \frac{(G^2 + K^2)}{(G^2 - K^2)} \left\{ A0 \frac{\partial A0}{\partial \overline{Z}_i} + \frac{B0}{3} \frac{\partial B0}{\partial \overline{Z}_i} \right\} \right]}{\left[ 2\overline{F3}^3 + 2C0 \overline{F3} \right]} \quad (3)$$

$$\begin{aligned}
\frac{\partial^2 \overline{F1}}{\partial \overline{Z}_i \partial \overline{Z}_j} = & \frac{1}{2 \left[ \overline{F1}^3 - \frac{A0}{(G^2 - K^2)} \overline{F1} \right]} \left[ - \left\{ 6\overline{F1}^2 - \frac{2A0}{(G^2 - K^2)} \right\} \frac{\partial \overline{F1}}{\partial \overline{Z}_i} \cdot \frac{\partial \overline{F1}}{\partial \overline{Z}_j} \right. \\
& + \frac{2\overline{F1}}{(G^2 - K^2)} \left\{ \frac{\partial \overline{F1}}{\partial \overline{Z}_i} \cdot \frac{\partial A0}{\partial \overline{Z}_j} + \frac{\partial A0}{\partial \overline{Z}_i} \cdot \frac{\partial \overline{F1}}{\partial \overline{Z}_j} \right\} + \frac{\overline{F1}^2}{(G^2 - K^2)} \cdot \frac{\partial^2 A0}{\partial \overline{Z}_i \partial \overline{Z}_j} \\
& \left. + \frac{1}{3(G^2 - K^2)^2} \left\{ \frac{\partial B0}{\partial \overline{Z}_i} \cdot \frac{\partial B0}{\partial \overline{Z}_j} + B0 \frac{\partial^2 B0}{\partial \overline{Z}_i \partial \overline{Z}_j} \right\} \right] \quad (4)
\end{aligned}$$

$$\begin{aligned}
\frac{\partial^2 \overline{F2}}{\partial \overline{Z}_i \partial \overline{Z}_j} = & \frac{1}{2 \left[ \overline{F2}^3 + \frac{A0}{(G^2 - K^2)} \overline{F2} \right]} \left[ \left\{ 6\overline{F2}^2 + \frac{2A0}{(G^2 - K^2)} \right\} \frac{\partial \overline{F2}}{\partial \overline{Z}_i} \cdot \frac{\partial \overline{F2}}{\partial \overline{Z}_j} \right. \\
& - \frac{2\overline{F2}}{(G^2 - K^2)} \left\{ \frac{\partial \overline{F2}}{\partial \overline{Z}_i} \cdot \frac{\partial A0}{\partial \overline{Z}_j} + \frac{\partial A0}{\partial \overline{Z}_i} \cdot \frac{\partial \overline{F2}}{\partial \overline{Z}_j} \right\} - \frac{\overline{F2}^2}{(G^2 - K^2)} \cdot \frac{\partial^2 A0}{\partial \overline{Z}_i \partial \overline{Z}_j} \\
& \left. + \frac{1}{3(G^2 - K^2)^2} \left\{ \frac{\partial B0}{\partial \overline{Z}_i} \cdot \frac{\partial B0}{\partial \overline{Z}_j} + B0 \frac{\partial^2 B0}{\partial \overline{Z}_i \partial \overline{Z}_j} \right\} \right] \quad (5)
\end{aligned}$$

$$\begin{aligned}
\frac{\partial \overline{F3}}{\partial \overline{Z}_i \partial \overline{Z}_j} = & \frac{1}{\left[ 2\overline{F3}^3 - 2C0 \cdot \overline{F3} \right]} \left[ \left\{ 6\overline{F3}^2 - 2C0 \right\} \cdot \frac{\partial \overline{F3}}{\partial \overline{Z}_i} \cdot \frac{\partial \overline{F3}}{\partial \overline{Z}_j} \right. \\
& + 2\overline{F3} \cdot \left\{ \frac{\partial \overline{F3}}{\partial \overline{Z}_i} \cdot \frac{\partial C0}{\partial \overline{Z}_j} + \frac{\partial C0}{\partial \overline{Z}_i} \cdot \frac{\partial \overline{F3}}{\partial \overline{Z}_j} \right\} - \frac{\partial C0}{\partial \overline{Z}_i} \cdot \frac{\partial C0}{\partial \overline{Z}_j} \\
& + \left\{ \overline{F3} - C0 \right\} \frac{\partial^2 C0}{\partial \overline{Z}_i \partial \overline{Z}_j} + \frac{(G^2 + K^2)}{(G^2 - K^2)} \left\{ A0 \cdot \frac{\partial A0}{\partial \overline{Z}_i \partial \overline{Z}_j} + \frac{\partial A0}{\partial \overline{Z}_i} \cdot \frac{\partial A0}{\partial \overline{Z}_j} \right. \\
& \left. \left. + \frac{1}{3} \left( \frac{\partial B0}{\partial \overline{Z}_i} \cdot \frac{\partial B0}{\partial \overline{Z}_j} + B0 \frac{\partial^2 B0}{\partial \overline{Z}_i \partial \overline{Z}_j} \right) \right\} \right] \quad (6)
\end{aligned}$$

(iii) Calculation of Covariances

At this stage, the user has the option, whether to calculate the covariances by using King's (21) method or by assuming constant values of correlation coefficients. To get the covariances using King's method, the MAIN has to call the subroutine COVAR, otherwise MAIN calculates covariances using Equations 35, 41, and 44.

(iv) Calculation of the Turbulence Quantities

Now the MAIN has all the information needed to calculate the mean velocities using Equations 20 through 22, also to calculate the turbulence intensities using Equations 24 through 26, and finally to calculate the shear stresses using Equations 27 through 29. The MAIN then prints out the normalized values of the turbulence quantities in the form of nine two by three matrices each containing the six values of a turbulence quantity calculated using six different combinations.

2. Subroutine CPYF

This subroutine calculates the pitch and yaw factors using the calibration constants obtained by three-dimensional calibration. The equations used to calculate these factors are:

$$G = \frac{\hat{v}}{\hat{u}} \begin{pmatrix} \hat{w}, \hat{u} = 0 \\ \hat{w}, \hat{v} = 0 \end{pmatrix}$$

$$K = \frac{\hat{v}}{\hat{w}} \begin{pmatrix} \hat{w}, \hat{u} = 0 \\ \hat{v}, \hat{u} = 0 \end{pmatrix}$$

evaluated at a constant value of  $E^2$ .  $u$ ,  $v$ , and  $w$  are obtained using equation 12 for their respective calibration constants. The value of  $E^2$  can be adjusted to obtain an interval  $\Delta E$  to get appropriate values of

G, and K.

3. Subroutine FMCV

The task of this subroutine is to find the mean effective cooling velocity which has minimum value among the six calculated by the MAIN. FMCV also finds the two mean effective cooling velocities which are adjacent to the minimum mean effective cooling velocity and returns the set of the three to be used by MAIN for further data processing.

4. Subroutine SEABC

SEABC recognizes the three selected mean effective cooling velocities  $Z_p$ ,  $Z_Q$ , and  $Z_R$ , and sets the three appropriate equations for  $A_0$ ,  $B_0$ , and  $C_0$  in terms of  $\bar{Z}_p$ ,  $\bar{Z}_Q$ , and  $\bar{Z}_R$ , using Table V.  $A_0$ ,  $B_0$ , and  $C_0$  are used by MAIN to calculate the three velocity functions given by Equations 9 through 11.

5. Subroutine CDABC

CDABC calculates the first and second differentials of  $A_0$ ,  $B_0$ , and  $C_0$  with respect to  $\bar{Z}_p$ ,  $\bar{Z}_Q$ , and  $\bar{Z}_R$ . It is evident from Table V that  $A_0$ ,  $B_0$ , and  $C_0$  are functions of  $\bar{Z}_p$ ,  $\bar{Z}_Q$ , and  $\bar{Z}_R$  and so are their first and second differentials.

6. Subroutine COVAR

This subroutine calculates covariances using a method suggested by King (21). This method calls for employing Equations 40 through 43. This subroutine can be called only when one desires to calculate covariances using King's method. Otherwise, the covariances are calculated within MAIN by the procedure already described.

TABLE V  
LIST OF FORTRAN VARIABLES AND THEIR  
MEANING IN RESPONSE EQUATIONS

<u>Input Values</u>	
EM	$\bar{E}$
ER	E'rms
<u>Mean Effective Cooling Velocities and Variances</u>	
AMECV	$\bar{Z}$
VAR	$\sigma_Z^2$
<u>Pitch and Yaw Factors</u>	
PF	G
YF	K
<u>Set of Three Cooling Velocities Chosen</u>	
ZP	$\bar{Z}_P$
ZQ	$\bar{Z}_Q$
ZR	$\bar{Z}_R$
<u>Derivatives of Functions A0, B0, and C0</u> (Definitions for B and C are analogous to those for A defined here)	
A1	$\frac{\partial A0}{\partial Z_P}$
A2	$\frac{\partial A0}{\partial Z_Q}$
A3	$\frac{\partial A0}{\partial Z_R}$
A21	$\frac{\partial^2 A0}{\partial Z_P^2}$
A22	$\frac{\partial^2 A0}{\partial Z_Q^2}$
A23	$\frac{\partial^2 A0}{\partial Z_R^2}$

TABLE V (Continued)

---

 Derivatives of Velocity Functions F1, F2, and F3
 

---

DF1P	$\frac{\partial \bar{F}_1}{\partial Z_P}$
DF1Q	$\frac{\partial \bar{F}_1}{\partial Z_Q}$
DF1R	$\frac{\partial \bar{F}_1}{\partial Z_R}$
D2F1P	$\frac{\partial^2 \bar{F}_1}{\partial Z_P^2}$
D2F1Q	$\frac{\partial^2 \bar{F}_1}{\partial Z_Q^2}$
D2F1R	$\frac{\partial^2 \bar{F}_1}{\partial Z_R^2}$
D2F1PQ	$\frac{\partial^2 \bar{F}_1}{\partial Z_P \partial Z_Q}$
D2F1QR	$\frac{\partial^2 \bar{F}_1}{\partial Z_Q \partial Z_R}$
D2F1PR	$\frac{\partial^2 \bar{F}_1}{\partial Z_P \partial Z_R}$

Covariances

AKPQ	$K_{Z_P Z_Q}$
AKQR	$K_{Z_Q Z_R}$
AKPR	$K_{Z_P Z_R}$

TABLE V (Continued)

---

 Output Variables Calculated
 

---

UMEAN	$\bar{u}$
WMEAN	$\bar{w}$
VMEAN	$\bar{v}$
UPRMS2	$\bar{u}'^2$
WPRMS2	$\bar{w}'^2$
VPRMS2	$\bar{v}'^2$
UVPB	$\overline{u'v'}$
UWPB	$\overline{u'w'}$
VWPB	$\overline{v'w'}$
UDUMO	$\bar{u}/\bar{u}_0$
WMDUMO	$\bar{w}/\bar{u}_0$
VMDUMO	$\bar{v}/\bar{u}_0$
UPDUMO	$\sqrt{\bar{u}'^2}/\bar{u}_0$
WPDUMO	$\sqrt{\bar{w}'^2}/\bar{u}_0$
VPDUMO	$\sqrt{\bar{v}'^2}/\bar{u}_0$
UVDUMO	$\overline{u'v'}/\bar{u}_0^2$
UWDUMO	$\overline{u'w'}/\bar{u}_0^2$
VWDUMO	$\overline{v'w'}/\bar{u}_0^2$

---

APPENDIX D

LISTING OF THE COMPUTER PROGRAM

```

60 C      *
70 C      *
80 C      *
90 C      *      COMPUTER PROGRAM TO CALCULATE TURBULENCE
100 C     *      QUANTITIES USING THE EXPERIMENTAL DATA
110 C     *      OBTAINED BY SIX ORIENTATION HOT-WIRE TECHNIQUE.
120 C     *
130 C     *
140 C     *
150 C     *      VERSION OF OCT, 1961
160 C     *
170 C     *
180 C     *
190 C     *      PREPARED BY:
200 C     *      SALIM I. JANJUA
210 C     *      SCHOOL OF MECHANICAL AND AEROSPACE ENGINEERING
220 C     *      OKLAHOMA STATE UNIVERSITY
230 C     *      STILLWATER OK. 74078
240 C     *
250 C     *
260 C     *
270 C     *
280 C     *
290 C     *
300 C     *
310     DIMENSION EM(12),EP(12),AMECV(12),VAP(12)
320     DIMENSION UDUMD(6),UPDUMD(6),VVDUMD(6),VPDUMD(6)
330     DIMENSION WMDUMD(6),WPDUMD(6),UVDUMD(6),WPDUMD(6),
340     *VVDUMD(6)
350     DATA DIA,EITA/12.0,0.8/
360     FEWIND 30
370     NS=1
380     908 IF(NS.EQ.0) GO TO 909
390     READ(30,*) A,B,C
400     READ(30,*) A1,B1,C1
410     READ(30,*) A2,B2,C2
420     WRITE(6,1111)
430     1111 FORMAT(///,4X,'THE CALIBRATION CONSTANTS ARE:')
440     WRITE(6,*) A,B,C
450     WRITE(6,*) A1,B1,C1
460     WRITE(6,*) A2,B2,C2
470     909 READ(30,*,END=559) X,R,EMC,NS
480     READ(30,*) (EM(I), I=1,6)
490     READ(30,*) (ER(I), I=1,6)
500     WRITE(6,1112)
510     1112 FORMAT(///,9X,'THE MEAN AND R.M.S. VOLTAGES ARE:')
520     WRITE(6,1100) (EM(I), I=1,6)
530     WRITE(6,1200) (ER(I), I=1,6)
540     1100 FORMAT(6F9.4)
550     1200 FORMAT(6F9.4)
560     FC(DIA)=R/DIA
570     XD(DIA)=X/DIA

```

```

580      U*CI=(-B+SQRT(B**2-4.*C*(A-EM**2)))/(2.*C)
590      UM1=(-B+SQRT(B**2-4.*C*(A-EM(1)**2)))/(2.*C)
600      U*CI=UM1*UM1
610      U*CI=UM1*UM1
620      DEU=0/(4.*EM(1)*UM1)+C/(2.*E*(1))
630      U*CI=U*DEU
640      U*CI=57(1)/U*DEU
650      U*CI=UM1*UM1
660      U*CI=UM1*UM1
670      DC 30 I=1,6
680      ER2=EM(1)*EM(1)
690      ER2=ER(1)*ER(1)
700      D=SQRT(D**2-(4.*C*(A-EM**2)))
710      PHE=(1-B*D)/(2.*C)**2
720      DPHE=(2.*EM(1)/C)*(1-(1/D))
730      D2PHE=(1/EM(1))*DPHE+(1.*D**2)/D**2
740 C-----
750 C-----LOCAL MEAN EFFECTIVE COOLING VELOCITY IS CALCULATED
760 C-----
770      AMECV(1)=PHE+0.5*D2PHE*ER2
780 C-----
790 C-----VARIANCE, VAR IS CALCULATED-----
800 C-----
810      VAR(1)=(DPHE**2)*(ER2)-((0.5*D2PHE*ER2)**2)
820      AMECV(1+C)=AMECV(1)
830      VAR(1+C)=VAR(1)
840      WRITE(6,112)
850      WRITE(6,110) AMECV(1),VAR(1)
860 110  FORMAT(//,7X,'AMECV=',F7.4,5X,'VAR=',F7.4)
870 30  CONTINUE
880 C-----
890 C-----MAIN CALLS THE SUBROUTINE CRYF TO CALCULATE
900 C-----THE PITCH AND YAW FACTORS.-----
910 C-----
920      CALL CRYF(A,B,C,A1,B1,C1,A2,B2,C2,PF,YF)
930 C-----
940 C-----PITCH FACTOR AND YAW FACTOR-----
950 C-----
960      WRITE(6,543) PF,YF
970 543  FORMAT(///,7X,'PITCH FACTOR=',F7.4,3X,'YAW FACTOR=',F7.4)
980      AL=PF*PF-YF*YF
990      C=PF*PF+YF*YF
1000     WRITE(6,444) U*CI,UM1
1010 444  FORMAT(///,7X,'AXIAL MEAN VEL/INLET MAX VEL=',F8.4,4X,
1020     *'AXIAL TURB INTEN=',F8.4)
1030     WRITE(6,515) U*CI
1040 515  FORMAT(//,12X,'MAX INLET VELOCITY=',F8.4)
1050     DC 222 I=1,6
1060     II=III-1
1070     N=50
1080     CALL STOTZ(U*CI,UM1,VM*CI,UM1,UP*CI,UM1,VP*CI,UM1,
1090     *U*CI,UM1,V*CI,UM1,N,III)
1100 C-----
1110 C-----MAIN CALLS THE SUBROUTINE FNCV TO FIND THE
1120 C-----THE MINIMUM COOLING VELOCITY AND THE TWO
1130 C-----ADJACENT GNS
1140 C-----

```

```

1150      CALL FMCV(AMFCV,N,IP,IG,IF,II)
1160      ZP=AMECV(IP)
1170      ZQ=AMECV(IQ)
1180      ZR=AMECV(IF)
1190      IF(IG.GT.6) IQ=IQ-6
1200      IF(IF.GT.6) IR=IF-6
1210 C-----
1220 C-----MAIN CALLS THE SUBROUTINE,SEARC TO SET UP
1230 C-----THE EQUATIONS FOR AG,BC,AND C-----
1240 C-----
1250      CALL SEABC(ZP,ZQ,ZR,IP,AQ,BC,CC)
1260      F=SQRT((AQ**2)+(BC**2)/3)
1270      IF(CC.LT.F*O/AL) GO TO 222
1280 C-----
1290 C-----VELOCITY FUNCTIONS F1,F2,AND F3 ARE CALCULATED-----
1300 C-----
1310      F1=SQRT((1/AL)*(AQ+F))
1320      IF((1/AL)*(-AQ+F).LT.0) GO TO 222
1330      F2=SQRT((1/AL)*(-AQ+F))
1340      F3=SQRT(CC-(O/AL)*F)
1350      IF(F2.FQ.0) GO TO 222
1360 C-----
1370 C-----MAIN CALLS THE SUBROUTINE CDABC TO CALCULATE
1380 C-----THE FIRST AND SECOND DIFFERENTIALS OF AQ,BQ,
1390 C-----AND CQ-----
1400 C-----
1410      CALL CDABC(DAP,DBF,DCF,D2AP,D2BP,D2CP,CAQ,DBQ,DCQ,D2AQ,D2BQ,
1420      *D2CQ,DAR,DER,DCR,D2AR,D2BR,D2CR,DZF,ZP,ZQ,ZR,IP)
1430 C-----MAIN CALCULATES THE FIRST AND SECOND
1440 C-----DIFFERENTIALS OF THE VELOCITY FUNCTIONS
1450 C-----F1,F2,AND F3 WITH RESPECT TO THE
1460 C-----SELECTED SET OF THE THREE COOLING VELO
1470 C-----CITIES.-----
1480 C-----
1490      X1=F1*F1
1500      X2=X1*F1
1510      X3=EC/(3*AL*AL)
1520      X4=X1/AL
1530      X5=(2*X2)-(2*F1*AQ/AL)
1540      X6=-(6*X1-2*AQ/AL)
1550      Y1=F2*F2
1560      Y2=Y1*F2
1570      Y3=2.0*Y2+2.0*F2*AC/AL
1580      Y4=Y1/AL
1590      Y5=-(6*Y1+(2.0*AC/AL))
1600      Z1=F3*F3
1610      Z2=Z1*F3
1620      Z3=2.0*Z2-2.0*CO*F3
1630      Z4=-(6.0*Z1-2.0*CO)
1640      DF1P=(X3*DRP+X4*DAP)/X5
1650      DF2P=(X3*DRP-Y4*DAP)/Y3
1660      DF3P=(DCP*(Z1-CO)+(O*O)/(AL*AL))*(AQ*CAP+(BO*DBQ)/3)/Z3
1670      DF1C=(X3*CEC+X4*CAQ)/X5
1680      DF2C=(X3*DEC-Y4*AC)/Y3
1690      DF3C=(DCO*(Z1-CO)+(O*O)/(AL*AL))*(AO*DAQ+(BO*DBQ)/3)/Z3
1700      DF1F=(X3*DRF+X4*DAP)/X5
1710      DF2F=(X3*DRF-Y4*DAR)/Y3

```

ORIGINAL PAGE IS  
OF POOR QUALITY

```

1720 DF25=(DCR*(Z1-CD)+(C*C)/(AL*AL))*((A*DA)+(BD*DF)/Z3)/Z3
1730 D2F1P=((X6*DF1P*DF1P)+(2.0*F1/AL)*(DAP*DF1P+DAP*DF1P)+(D2AP
1740 **X1/AL)+(1/(3.0*AL*AL))*(D2AP*DF1P+D2AP*DF1P))/X5
1750 D2F2P=((Y5*DF2P*DF2P)-(2.0*F2/AL)*(DF2P*DA+DAP*DF2P)-(Y1*D2
1750 *AP/AL)+(D2P*DF2P+D2P*DF2P)/(3.0*AL*AL))/Y3
1770 D2F3P=((Z4*DF3P*DF3P)+2.0*F3*(DF3P*DC+DC*DF3P)-(DC*DC)+(Z1
1780 *-CC)*D2CP+(C*C)/(AL*AL))*((AC*D2AP+DAP*DA)+(D2P*DF
1790 **E*(D2PP)/Z3)/Z3
1800 D2F1Q=((X6*DF1Q*DF1Q)+(2.0*F1/AL)*(DAP*DF1Q+DAP*DF1Q)+(D2AQ
1810 **X1/AL)+(1/(3.0*AL*AL))*(D2AQ*DF1Q+D2AQ*DF1Q))/X5
1820 D2F1Q=((Y5*DF2Q*DF2Q)-(2.0*F2/AL)*(DF2Q*DA+DAP*DF2Q)-(Y1*D2
1830 *AQ/AL)+(D2Q*DF2Q+D2Q*DF2Q)/(3.0*AL*AL))/Y3
1840 D2F3Q=((Z4*DF3Q*DF3Q)+2.0*F3*(DF3Q*DC+DC*DF3Q)-(DC*DC)+(Z1
1850 **-(Z1-CD)*D2CQ+(C*C)/(AL*AL))*((AD*D2AQ+DAP*DA)+(
1860 *D2Q*DF2Q+D2Q*DF2Q)/Z3)/Z3
1870 D2F1R=((X6*DF1R*DF1R)+(2.0*F1/AL)*(DAP*DF1R+DAP*DF1R)+(D2AR
1880 **X1/AL)+(1/(3.0*AL*AL))*(D2AR*DF1R+D2AR*DF1R))/X5
1890 D2F2R=((Y5*DF2R*DF2R)-(2.0*F2/AL)*(DF2R*DA+DAP*DF2R)-(Y1*D2
1900 *AR/AL)+(D2R*DF2R+D2R*DF2R)/(3.0*AL*AL))/Y3
1910 D2F3R=((Z4*DF3R*DF3R)+2.0*F3*(DF3R*DC+DC*DF3R)-(DC*DC)+(Z1
1920 **-(Z1-CD)*D2CR+(C*C)/(AL*AL))*((AD*D2AR+DAP*DA)+(
1930 *D2R*DF2R+D2R*DF2R)/Z3)/Z3
1940 D2F1Q=((X6*DF1Q*DF1Q)+(2.0*F1/AL)*(DAP*DF1Q+DAP*DF1Q)+(X1
1950 **D2APC/AL)+(1/(3.0*AL*AL))*(D2APC*DF1Q+D2APC*DF1Q))/X5
1960 D2F1QR=((X6*DF1Q*DF1R)+(2.0*F1/AL)*(DAP*DF1Q+DAP*DF1R)+(X1
1970 **D2APR/AL)+(1/(3.0*AL*AL))*(D2APR*DF1Q+D2APR*DF1R))/X5
1980 D2F1PR=((X6*DF1R*DF1R)+(2.0*F1/AL)*(DAP*DF1R+DAP*DF1R)+(X1
1990 **D2APR/AL)+(1/(3.0*AL*AL))*(D2APR*DF1R+D2APR*DF1R))/X5
2000 D2F2PQ=((Y5*DF2P*DF2Q)-(2.0*F2/AL)*(DF2P*DA+DAP*DF2Q)-(Y1
2010 **D2APQ/AL)+(1/(3.0*AL*AL))*(D2P*DF2Q+D2P*DF2Q))/Y3
2020 D2F2QR=((Y5*DF2Q*DF2R)-(2.0*F2/AL)*(DF2Q*DA+DAP*DF2R)-(Y1
2030 **D2AQF/AL)+(1/(3.0*AL*AL))*(D2Q*DF2R+D2Q*DF2R))/Y3
2040 D2F2PR=((Y5*DF2P*DF2R)-(2.0*F2/AL)*(DF2P*DA+DAP*DF2R)-(Y1
2050 **D2APR/AL)+(1/(3.0*AL*AL))*(D2P*DF2R+D2P*DF2R))/Y3
2060 D2F3PQ=((Z4*DF3P*DF3Q)+2.0*F3*(DF3P*DC+DC*DF3Q)-(DC*DC)+(Z1
2070 **-(Z1-CD)*D2CPQ+(C*C)/(AL*AL))*((AD*D2APQ+DAP*DA)+(
2080 *D2P*DF2Q+D2P*DF2Q)/Z3)/Z3
2090 D2F3QR=((Z4*DF3Q*DF3R)+2.0*F3*(DF3Q*DC+DC*DF3R)-(DC*DC)+(Z1
2100 **-(Z1-CD)*D2CQR+(C*C)/(AL*AL))*((AC*D2APQ+DAP*DA)+(
2110 *D2Q*DF2R+D2Q*DF2R)/Z3)/Z3
2120 D2F3PR=((Z4*DF3P*DF3R)+2.0*F3*(DF3P*DC+DC*DF3R)-(DC*DC)+(Z1
2130 **-(Z1-CD)*D2CPR+(C*C)/(AL*AL))*((AC*D2APR+DAP*DA)+(
2140 *D2P*DF2R+D2P*DF2R)/Z3)/Z3
2150 C-----
2160 C-----MAIN CALLS THE SUBROUTINE COVAR TO
2170 C-----CALCULATE THE COVARIANCE BETWEEN THE
2180 C-----REFLECTED COOLING VELOCITIES.-----
2190 C-----
2200 AKQ=0.9*SQRT(VAR(IP)*VAR(IP+1))
2210 AKQF=0.9*SQRT(VAR(IP+1)*VAR(IP+2))
2220 AKQR=0.5*ETA*SQRT(VAR(IP)*VAR(IP+2))
2230 AKGP=AKQG
2240 AKQC=AKQR
2250 AKQB=AKQR
2260 C-----
2270 C-----MAIN CALCULATES THE AXIAL,RADIAL,AND
2280 C-----TANGENTIAL MEAN VELOCITIES.-----

```

```

2290 (-----)
2300 UMEAN=F1+0.5*(D2F1P*VAR(IP)+D2F1G*VAI(IP+1)+D2F1R*VAR(IP+2))
2310 **D2F1PQ*AKPQ+D2F1GR*AKGR+D2F1FR*AKFR
2320 KPEAK=F2+0.5*(D2F2P*VAI(IP)+D2F2G*VAI(IP+1)+D2F2R*VAI(IP+2))
2330 **D2F2PQ*AKPQ+D2F2GR*AKGR+D2F2FR*AKFR
2340 VMEAN=F3+0.5*(D2F3P*VAR(IP)+D2F3G*VAI(IP+1)+D2F3R*VAR(IP+2))
2350 **D2F3PQ*AKPQ+D2F3GR*AKGR+D2F3FR*AKFR
2360 UP1=DF1P*DF1P*VAI(IP)+DF1G*DF1G*VAI(IP+1)+DF1R*DF1R*VAI(IP
2370 **2)
2380 UF2=DF1P*DF1G*AKPG+DF1P*DF1R*AKPR+DF1G*DF1P*AKGP+DF1G*DF1R*AK
2390 **GR+DF1R*DF1P*AKRP+DF1R*DF1G*AKRG
2400 UF3=0.5*(D2F1P*VAR(IP)+D2F1G*VAI(IP+1)+D2F1R*VAR(IP+2))
2410 UP4=D2F1PQ*AKPQ+D2F1GR*AKGR+D2F1FR*AKFR
2420 UF5=UP3+UP4
2430 UPRMS2=UP1+UF2-UF5**2
2440 WP1=DF2P*DF2P*VAR(IP)+DF2G*DF2G*VAI(IP+1)+DF2R*DF2R*VAR(IP
2450 **2)
2460 VF2=DF2P*DF2G*AKPG+DF2P*DF2R*AKPR+DF2G*DF2P*AKGP+DF2G*DF2R*AK
2470 **GR+DF2R*DF2P*AKRP+DF2R*DF2G*AKRG
2480 WF3=0.5*(D2F2P*VAR(IP)+D2F2G*VAI(IP+1)+D2F2R*VAR(IP+2))
2490 WP4=D2F2PQ*AKPQ+D2F2GR*AKGR+D2F2FR*AKFR
2500 WP5=WP3+WP4
2510 WPRMS2=WP1+WP2-WP5**2
2520 VP1=DF3P*DF3P*VAR(IP)+DF3G*DF3G*VAI(IP+1)+DF3R*DF3R*VAR(IP
2530 **2)
2540 VF2=DF3P*DF3G*AKPG+DF3P*DF3R*AKPR+DF3G*DF3P*AKGP+DF3G*DF3R*AK
2550 **GR+DF3R*DF3P*AKRP+DF3R*DF3G*AKRG
2560 VP2=0.5*(D2F3P*VAR(IP)+D2F3G*VAI(IP+1)+D2F3R*VAR(IP+2))
2570 VP4=D2F3PQ*AKPQ+D2F3GR*AKGR+D2F3FR*AKFR
2580 VP5=VP3+VP4
2590 VPRMS2=VP1+VP2-VP5**2
2600 UV1=DF1P*DF3P*VAR(IP)+DF1G*DF3G*VAI(IP+1)+DF1R*DF3R*VAR(IP
2610 **2)
2620 UV2=DF1P*DF3G*AKPG+DF1P*DF3R*AKPR+DF1G*DF3P*AKGP+DF1G*DF3R*AK
2630 **GR+DF1R*DF3P*AKRP+DF1R*DF3G*AKRG
2640 UV3=0.5*(D2F1P*VAR(IP)+D2F1G*VAI(IP+1)+D2F1R*VAR(IP+2))
2650 UV4=D2F1PQ*AKPQ+D2F1GR*AKGR+D2F1FR*AKFR
2660 UV2=0.5*(D2F3P*VAR(IP)+D2F3G*VAI(IP+1)+D2F3R*VAR(IP+1))
2670 UV6=D2F3PQ*AKPQ+D2F3GR*AKGR+D2F3FR*AKFR
2680 UVPB=UV1+UV2-((UV3+UV4)*(UV5+UV6))
2690 VK1=DF3P*DF2P*VAR(IP)+DF3G*DF2G*VAI(IP+1)+DF3R*DF2R*VAR(IP
2700 **2)
2710 VK2=DF3P*DF2G*AKPG+DF3P*DF2R*AKPR+DF3G*DF2P*AKGP+DF3G*DF2R*AK
2720 **GR+DF2R*DF3P*AKRP+DF2R*DF2G*AKRG
2730 VK3=0.5*(D2F3P*VAI(IP)+D2F2G*VAI(IP+1)+D2F2R*VAI(IP+2))
2740 VK4=D2F3PQ*AKPQ+D2F2GR*AKGR+D2F2FR*AKFR
2750 VK5=0.5*(D2F2P*VAR(IP)+D2F2G*VAI(IP+1)+D2F2R*VAI(IP+1))
2760 VK6=D2F2PQ*AKPQ+D2F2GR*AKGR+D2F2FR*AKFR
2770 VKPB=VK1+VK2-((VK3+VK4)*(VK5+VK6))
2780 UM1=DF1P*DF2P*VAR(IP)+DF1G*DF2G*VAI(IP+1)+DF1R*DF2R*VAI(IP
2790 **2)
2800 UM2=DF1P*DF2G*AKPG+DF1P*DF2R*AKPR+DF1G*DF2P*AKGP+DF1G*DF2R*AK
2810 **GR+DF1R*DF2P*AKRP+DF1R*DF2G*AKRG
2820 UM3=0.5*(D2F1P*VAR(IP)+D2F1G*VAI(IP+1)+D2F1R*VAI(IP+2))
2830 UM4=D2F1PQ*AKPQ+D2F1GR*AKGR+D2F1FR*AKFR
2840 UM5=0.5*(D2F2P*VAR(IP)+D2F2G*VAI(IP+1)+D2F2R*VAI(IP+1))
2850 UM6=D2F2PQ*AKPQ+D2F2GR*AKGR+D2F2FR*AKFR

```

```

2550      U*P=U*14U*2-((U*7+U*4)*(U*5+U*6))
2570      UDUMD(111)=UMCAK/ZUMD
2580      WPDUMD(111)=WMA AN/ZUMD
2590      VPDUMD(111)=VMA AN/ZUMD
2593      IF(UPRMS2.GT.0.0) UFDUMD(111)=SQRT(UPRMS2)/ZUMD
2594      IF(WPRMS2.GT.0.0) WPDUMD(111)=SQRT(WPRMS2)/ZUMD
2595      IF(VPRMS2.GT.0.0) VPDUMD(111)=SQRT(VPRMS2)/ZUMD
2596      UVDUMD(111)=UVPB/ZUMD**2
2597      WVDUMD(111)=WVPB/ZUMD**2
2598      UWDUMD(111)=UWPB/ZUMD**2
2599      112 FORMAT(' ')
2600      222 CONTINUE
2610      WRITE(6,113) XDIA
2620      WRITE(6,114) XDIA
3000      114 FORMAT(///,20X,'AXIAL DISTANCE X/D=',F7.2)
3010      113 FORMAT(/,20X,'RADIAL DISTANCE R/D=',F5.4)
3020      WRITE(5,112)
3030      WRITE(6,112)
3040      WRITE(6,1000) (UDL4D(I),I=1,3)
3050      WRITE(6,1000) (UDUMD(I),I=4,6)
3060      WRITE(5,112)
3070      WRITE(6,112)
3080      WRITE(6,2000) (WPDUMD(I),I=1,3)
3090      WRITE(6,2000) (WPDUMD(I),I=4,6)
3100      WRITE(5,112)
3110      WRITE(6,112)
3120      WRITE(6,3000) (VMDUMD(I),I=1,3)
3130      WRITE(6,3000) (VMDUMD(I),I=4,6)
3140      WRITE(5,112)
3150      WRITE(6,112)
3160      WRITE(6,4000) (UPDUMD(I),I=1,3)
3170      WRITE(6,4000) (UPDUMD(I),I=4,6)
3180      WRITE(5,112)
3190      WRITE(6,112)
3200      WRITE(6,5000) (WPDUMD(I),I=1,3)
3210      WRITE(6,5000) (WPDUMD(I),I=4,6)
3220      WRITE(5,112)
3230      WRITE(6,112)
3240      WRITE(6,6000) (VPDUMD(I),I=1,3)
3250      WRITE(6,6000) (VPDUMD(I),I=4,6)
3260      WRITE(5,112)
3270      WRITE(6,112)
3280      WRITE(6,7000) (UVDUMD(I),I=1,3)
3290      WRITE(6,7000) (UVDUMD(I),I=4,6)
3300      WRITE(5,112)
3310      WRITE(6,112)
3320      WRITE(6,8000) (UWDUMD(I),I=1,3)
3330      WRITE(6,8000) (UWDUMD(I),I=4,6)
3340      WRITE(5,112)
3350      WRITE(6,112)
3360      WRITE(5,112)
3370      WRITE(6,9000) (VWDUMD(I),I=1,3)
3380      WRITE(6,9000) (VWDUMD(I),I=4,6)
3390      WRITE(5,112)
3400      WRITE(6,112)
3410      1000 FORMAT(/,7X,'UDUMD=',F9.4,5X,'UDUMD=',F9.4,5X,'UDUMD=',
3420      *F5.4)

```

```

3430 2000 FCFMATT(/,7X,'WDUMC=',F9.4,5X,'WDUMC=',F9.4,5X,'WDUMC=',
3440 *F9.4)
3450 3000 FCFMATT(/,7X,'VDUMC=',F9.4,5X,'VDUMC=',F9.4,5X,'VDUMC=',
3460 *F9.4)
3470 4000 FCFMATT(/,7X,'UPDUMC=',F9.4,4X,'UPDUMC=',F9.4,4X,'UPDUMC=',
3480 *,'= ',F9.4)
3490 5000 FCFMATT(/,7X,'WPDUMC=',F9.4,4X,'WPDUMC=',F9.4,4X,'WPDUMC=',
3500 *,'= ',F9.4)
3510 6000 FCFMATT(/,7X,'VPDUMC=',F9.4,4X,'VPDUMC=',F9.4,4X,'VPDUMC=',
3520 *,'= ',F9.4)
3530 7000 FCFMATT(/,7X,'UVDUMC=',F9.4,4X,'UVDUMC=',F9.4,4X,'UVDUMC=',
3540 *,F9.4)
3550 8000 FCFMATT(/,7X,'LWUMC=',F9.4,4X,'LWUMC=',F9.4,4X,'LWUMC=',
3560 *,F9.4)
3570 9000 FCFMATT(/,7X,'VWUMC=',F9.4,4X,'VWUMC=',F9.4,4X,'VWUMC=',
3580 *,F9.4)
3590 GC TO 909
3600 999 STOP
3610 END

```

```

3620 C
3630 C
3640 C
3650 C
3660 C
3670 C*****
3680 C-----THIS SUBROUTINE SETS TURBULENT QUANTITIES TO
3690 C-----ZERO AT THE BEGINNING OF EACH ITERATION
3700 C*****
3710 SUBROUTINE STOTZ(UDUMC,WUMC,VDUMC,UPDUMC,WPUMC,
3720 *VPUMC,UVDUMC,LWUMC,VWUMC,N,I)
3730 DIMENSION UDUMC(6),WUMC(6),VDUMC(6),UPDUMC(6),WPUMC(6)
3740 DIMENSION VPUMC(6),UVDUMC(6),LWUMC(6),VWUMC(6)
3750 UDUMC(I)=0.0
3760 WUMC(I)=0.0
3770 VDUMC(I)=0.0
3780 UPDUMC(I)=0.0
3790 WPUMC(I)=0.0
3800 VPUMC(I)=0.0
3810 UVDUMC(I)=0.0
3820 LWUMC(I)=0.0
3830 VWUMC(I)=0.0
3840 RETURN
3850 END

```

```

3560 C
3570 C
3580 C
3590 C .....
3600 C
3610 C   THIS SUBROUTINE FINDS THE MINIMUM MEAN EFFECTIVE
3620 C   COOLING VELOCITY AND THE TUBE ADJACENT TO IT.
3630 C
3640 C .....
3650 C
3660 C
3670 C
3680 C
3690 C   SUBROUTINE FMCV(CV,N,IX,IY,IZ,II)
4000 C   DIMENSION CV(50)
4010 C   IF(CV(2).LT.CV(1)) GO TO 20
4020 C   IF(CV(3).LT.CV(1)) GO TO 30
4030 C   IF(CV(4).LT.CV(1)) GO TO 40
4040 C   IF(CV(5).LT.CV(1)) GO TO 50
4050 C   IF(CV(5).LT.CV(1)) GO TO 60
4060 C   IX=6
4070 C   IY=1
4080 C   IZ=2
4090 C   GO TO 100
4100 C 20 IF(CV(3).LT.CV(2)) GO TO 30
4110 C   IF(CV(4).LT.CV(2)) GO TO 40
4120 C   IF(CV(5).LT.CV(2)) GO TO 50
4130 C   IF(CV(5).LT.CV(2)) GO TO 60
4140 C   IX=1
4150 C   IY=2
4160 C   IZ=3
4170 C   GO TO 100
4180 C 30 IF(CV(4).LT.CV(3)) GO TO 40
4190 C   IF(CV(5).LT.CV(3)) GO TO 50
4200 C   IF(CV(5).LT.CV(3)) GO TO 60
4210 C   IX=2
4220 C   IY=3
4230 C   IZ=4
4240 C   GO TO 100
4250 C 40 IF(CV(5).LT.CV(4)) GO TO 50
4260 C   IF(CV(5).LT.CV(4)) GO TO 60
4270 C   IX=3
4280 C   IY=4
4290 C   IZ=5
4300 C   GO TO 100
4310 C 50 IF(CV(5).LT.CV(5)) GO TO 60
4320 C   IX=4
4330 C   IY=5
4340 C   IZ=6
4350 C   GO TO 100
4360 C 60 IX=5
4370 C   IY=6
4380 C   IZ=1
4390 C 100 IX=IX+II
4400 C   IF(IX.GT.6) IX=IX-6
4410 C   IF(IY.GT.6) IY=IY-6
4420 C   IF(IZ.GT.6) IZ=IZ-6
4430 C   IY=IX+1
4440 C   IZ=IX+7
4450 C   RETURN
4460 C   END

```

```

4470 C
4480 C*****
4490 C
4500 C THIS SUBROUTINE CALCULATES THE PITCH AND YAW
4510 C FACTORS USING THE THREE-DIRECTIONAL CALIBRATION
4520 C CONSTANTS.
4530 C
4540 C*****
4550 C
4560 C SUBROUTINE CPYE (A,B,C,A1,B1,C1,A2,B2,C2,PF,YF)
4570 C E=3.0
4580 C 10 W1=E1**2-A.0*C1*(A1-E**2)
4590 C IF(W1.LT.0.) GO TO 20
4600 C E=E+0.05
4610 C GO TO 10
4620 C 20 E=E-0.10
4630 C W1=(-B1+SQRT(B1**2-4.0*C1*(A1-E**2)))/(2.0*C1)
4640 C W1=1/W1
4650 C V1=(-B2+SQRT(B2**2-4.0*C2*(A2-E**2)))/(2.0*C2)
4660 C V=V1*V1
4670 C U1=(-B3+SQRT(B3**2-4.0*C3*(A-E**2)))/(2.0*C3)
4680 C U=U1*U1
4690 C PF=V/U
4700 C YF=V/W
4710 C RETURN
4720 C END
4730 C*****
4740 C
4750 C THIS SUBROUTINE SETS EQUATIONS FOR AC,BC,AND CD
4760 C DEPENDING UPON THE SET OF THE THREE COOLING
4770 C VELOCITIES CHOSEN.
4780 C
4790 C
4800 C*****
4810 C
4820 C SUBROUTINE SEABC(A1,A2,A3,K,X,Y,Z)
4830 C IF(K.EQ.1) GO TO 10
4840 C IF(K.EQ.2) GO TO 25
4850 C IF(K.EQ.3) GO TO 35
4860 C IF(K.EQ.4) GO TO 45
4870 C IF(K.EQ.5) GO TO 55
4880 C IF(K.EQ.6) GO TO 65
4890 C 15 X=A2**2-A3**2
4900 C Y=-2.0*A1**2+3.0*A2**2-A3**2
4910 C Z=A1**2-A2**2+A3**2
4920 C GO TO 105
4930 C 25 X=A1**2-A2**2
4940 C Y=-(A1**2)+3.0*A2**2-2.0*A3**2
4950 C Z=A1**2-A2**2+A3**2
4960 C GO TO 115
4970 C 35 X=A1**2-2.0*A2**2+A3**2
4980 C Y=A1**2-A3**2
4990 C Z=A1**2-A2**2+A3**2
5000 C GO TO 105
5010 C 45 X=-(A2**2)+A3**2
5020 C Y=-2.0*A1**2+3.0*A2**2-A3**2
5030 C Z=A1**2-A2**2+A3**2
5040 C GO TO 105
5050 C 55 X=-(A1**2)+A2**2
5060 C Y=-(A1**2)+3.0*A2**2-2.0*A3**2
5070 C Z=A1**2-A2**2+A3**2
5080 C GO TO 105
5090 C 65 X=-(A1**2)+2.0*A2**2-A3**2
5100 C Y=-(A1**2)+A3**2
5110 C Z=A1**2-A2**2+A3**2
5120 C 105 RETURN
5130 C END

```

```

5140 C
5150 C *****
5160 C
5170 C   THIS SUBROUTINE CALCULATES THE FIRST AND SECOND
5180 C   DIFFERENTIALS OF THE FUNCTIONS AL, AC, AND CD WITH
5190 C   RESPECT TO THE THREE CHOSEN MEAN EFFECTIVE COOLING
5200 C   VELOCITIES.
5210 C
5220 C *****
5230 C
5240   SUBROUTINE CDABC(A1,B1,C1,A21,B21,C21,A2,B2,C2,A22,B22,C22,
5250 *A3,B3,C3,A23,B23,C23,C24,X,Y,Z,K)
5260   IF(K.EQ.1) GO TO 10
5270   IF(K.EQ.2) GO TO 20
5280   IF(K.EQ.3) GO TO 30
5290   IF(K.EQ.4) GO TO 40
5300   IF(K.EQ.5) GO TO 50
5310   IF(K.EQ.6) GO TO 60
5320   10  A1=0.0
5330     B1=-4*X
5340     C1=2*X
5350     A21=0.0
5360     B21=-4.0
5370     C21=2.0
5380     A2=2.0*Y
5390     B2=6.0*Y
5400     C2=-2.0*Y
5410     A22=2.0
5420     B22=6.0
5430     C22=-2.0
5440     A3=-2.0*Z
5450     B3=-2.0*Z
5460     C3=2.0*Z
5470     A23=-2.0
5480     B23=-2.0
5490     C23=2.0
5500     GO TO 100
5510   20  A1=2.0*X
5520     B1=-2.0*X
5530     C1=2.0*X
5540     A21=2.0
5550     B21=-2.0
5560     C21=2.0
5570     A2=-2.0*Y
5580     B2=6.0*Y
5590     C2=-2.0*Y
5600     A22=-2.0
5610     B22=6.0
5620     C22=-2.0
5630     A3=0.0
5640     B3=-4.0*Z
5650     C3=2.0*Z
5660     A23=0
5670     B23=-4.0
5680     C23=2.0
5690     GC TO 100
5700   30  A1=2.0*X

```

ORIGINAL PAGE IS  
OF POOR QUALITY

5710		D1=2.0
5720		C1=2.0 X
5730		A21=2.0
5740		B21=2.0
5750		C21=2.0
5760		A2=-4.0*Y
5770		B2=0.0
5780		C2=-2.0*Y
5790		A22=-4.0
5800		B22=0.0
5810		C22=-2.0
5820		A3=2.0*Z
5830		B3=-2.0*Z
5840		C3=2.0*Z
5850		A23=2.0
5860		B23=-2.0
5870		C23=2.0
5880		GC TC 106
5890	46	A1=0.0
5900		B1=-2.0*Y
5910		C1=2.0*Y
5920		A21=0.0
5930		B21=-4.0
5940		C21=2.0
5950		A2=-2.0*Y
5960		B2=6.0*Y
5970		C2=-2.0*Y
5980		A22=-2.0
5990		B22=0.0
6000		C22=-2.0
6010		A3=2.0*Z
6020		B3=-2.0*Z
6030		C3=2.0*Z
6040		A23=2.0
6050		B23=-2.0
6060		C23=2.0
6070		GC TC 106
6080	56	A1=-2.0*Y
6090		B1=-2.0*Y
6100		C1=2.0*Y
6110		A21=-2.0
6120		B21=-2.0
6130		C21=2.0
6140		A2=2.0*Y
6150		B2=6.0*Y
6160		C2=-2.0*Y
6170		A22=2.0
6180		B22=0.0
6190		C22=-2.0
6200		A3=0.0
6210		B3=-2.0*Z
6220		C3=2.0*Z
6230		A23=0.0
6240		B23=-4.0
6250		C23=2.0
6260		GC TC 106
6270	66	A1=-2.0*Y
6280		C1=-2.0*Y
6290		C1=2.0*Y
6300		A21=-2.0
6310		B21=-2.0
6320		C21=2.0
6330		A2=4.0*Y
6340		B2=0.0
6350		C2=-2.0*Y
6360		A22=4.0

ORIGINAL PAGE IS  
OF POOR QUALITY

```

0370      P2=-0.0
0380      C22=-2.0
0390      A3=-2.0*Z
0400      H3=2.0*Z
0410      C3=2.0*Z
0420      A23=-2.0
0430      B23=2.0
0440      C23=2.0
0450      104 RETURN
0460      END
0520 C *****
0530 C      THIS SUBROUTINE CALCULATES THE COVARIANCES BETWEEN THE
0540 C      VELOCITY FLUCTUATIONS USING A METHOD SUGGESTED BY KING.
0550 C *****
0560 C *****
0620      SUBROUTINE COVAR(CV,V,N,IP,ZP,ZC,ZF,AKPC,AKPK,AKQP,AKQR,AKRP
0630      * ,AKRQ,PI TA)
0640      DIMENSION CV(5),V(5)
0650      EITA=0.5
0660      DC IS I=1,6
0670      CV(I+6)=CV(I)
0680      V(I+6)=V(I)
0690      15 CONTINUE
0700      IF(V(IP).LE.0.002) GO TO 100
0710      ZETA1=SQRT(ZP**2-2.0*ZC**2+2.0*ZP**2)
0720      ZETA3=SQRT(2.0*ZF**2-2.0*ZC**2+ZF**2)
0730      P11=CV(IP+3)-ZETA1-0.5*((1/CV(IP+3)-ZP**2/CV(IP+3)**3)*V(IP)
0740      *- (4.0*ZC**2/CV(IP+3)**3+2.0/CV(IP+3))*V(IP+1))+(-4.0*ZF**2
0750      */CV(IP+3)**3+2.0/CV(IP+3))*V(IP+2))
0760      P13=CV(IP+5)-ZETA3-0.5*((2.0/CV(IP+5)-4.0*ZP**2/CV(IP+5)**3
0770      *)*V(IP)+(-2.0/CV(IP+5)-4.0*ZC**2/CV(IP+5)**3)*V(IP+1)+(1/CV
0780      * (IP+5)-ZP**2/CV(IP+5)**3)*V(IP+2))
0790      A1=-2.0*ZP**2*EITA/V(IP+1)
0800      B1=6.0*7P*ZQ-(ZP*EITA/(ZQ*V(IP+1)))*(P11*CV(IP+3)**3-P13*CV
0810      *(IP+5)**3)
0820      C1=P11*CV(IP+3)**3-2.0*PI2*CV(IP+5)**3
0830      IF(P1**2-4.0*A1*C1.LT.C) GO TO 57
0840      AKPQ1=(-P1+SQRT(B1**2-4.0*A1*C1))/(2.0*A1)
0850      AKPQ2=(-P1-SQRT(B1**2-4.0*A1*C1))/(2.0*A1)
0860      FPQ1=AKPQ1/SQRT(V(IP)*V(IP+1))
0870      FPQ2=AKPQ2/SQRT(V(IP)*V(IP+1))
0880      IF(ABS(FPQ1).GT.1) GO TO 17
0890      GO TO 27
0900      17 IF(ABS(FPQ2).GT.1) GO TO 37
0910      AKPQ=AKPQ2
0920      27 AKPQ=AKPQ1
0930      GO TO 47
0940      37 AKPQ=0.9*SQRT(V(IP)*V(IP+1))
0950      47 AKQR=(7.0*CV(IP)*CV(IP+1)*KQ+PI1*CV(IP+3)**3-P13*CV(IP+5)
0960      **3)/(7.0*CV(IP+1)*CV(IP+2))
0970      FCR=AKQR*SQRT(V(IP+1)*V(IP+2))
0980      IF(ABS(FCR).GT.1) AKQR=0.9*SQRT(V(IP+1)*V(IP+2))
0990      AKPR=EITA*AKPQ*AKQR/V(IP+1)
1000      GO TO 107
1010      57 AKPC=0.9*SQRT(V(IP)*V(IP+1))
1020      AKQP=0.5*SQRT(V(IP+1)*V(IP+2))
1030      AKPR=EITA*AKPQ*AKQR/V(IP+1)
1040      GO TO 107
1050      103 AKPC=0.0
1060      AKQP=0.0
1070      AKPR=0.0
1080      107 AKQR=AKPQ
1090      AKRQ=AKQR
1100      AKR=AKPR
1110      RETURN
1120      END

```

C-2

VITA

Salim Iqbal Janjua

Candidate for the Degree of

Master of Science

Thesis: TURBULENCE MEASUREMENTS IN A COMPLEX FLOWFIELD USING A SIX-ORIENTATION HOT-WIRE PROBE TECHNIQUE

Major Field: Mechanical Engineering

Biographical:

Personal Data: [REDACTED] the son of Mr. and Mrs. M. Aslam Janjua.

Education: Graduated from Punjab University with a Bachelor of Science degree in Physics and Mathematics in 1971; received the Bachelor of Engineering degree from Concordia University at Montreal, Canada in May, 1980; completed requirements for the Master of Science degree at Oklahoma State University in December, 1981.

Professional Societies: Member of American Institute of Aeronautics and Astronautics.

APPENDIX B

TURBULENCE MEASUREMENTS IN FREE AND CONFINED  
JET FLOWS USING CROSSED HOT-WIRE PROBES

TURBULENCE MEASUREMENTS IN FREE AND CONFINED  
JET FLOWS USING CROSSED HOT-WIRE PROBES

T. W. Jackson, D. G. Lilley and D. K. McLaughlin

School of Mechanical and Aerospace Engineering  
Oklahoma State University  
Stillwater, OK 74078

February, 1982

## ABSTRACT

The general aim of the present study is to investigate axisymmetric, nonreacting flow in sudden expansions. This configuration simulates the typical geometries found in can-type gas turbine and ramjet combustion chambers. The turbulence quantities reported here are used to understand the complex flowfield in question. They are also to be used to recommend appropriate turbulence model advances in the simulation of combustor chamber flowfields. In the present contribution, data are obtained with a hot-wire probe, with two inclined wires, and specialized electronics capable of instantaneously adding and subtracting the two voltages.

Initially measurements were taken in a free shear flow, in the form of a free axisymmetric jet. The main results reported are properties of the axisymmetric confined turbulent jet in the sudden enlargement [side-wall angle  $\alpha=90$  deg] test facility. Experimental measurements of mean and fluctuating velocities are presented at several axial stations under nonswirling conditions. Results are compared with those of previous researchers where possible, and good agreement is to be noted.

## CONTENTS

	Page
ABSTRACT	ii
1. INTRODUCTION	1
2. EXPERIMENTAL FACILITIES	3
2.1 Confined Jet Flowfield	3
2.2 Free Jet Calibration Facility	4
2.3 Hot-Wire Instrumentation	4
3. EXPERIMENTAL TECHNIQUES	6
3.1 Data Reduction	6
3.2 Calibration	7
3.3 Free Jet Measurements - Proof of Principle	8
3.4 Confined Jet Measurements	9
4. CONFINED JET RESULTS	11
5. CONCLUSIONS	13
6. REFERENCES	14
7. NOMENCLATURE	15
8. FIGURE LIST	16
FIGURES	

## 1. INTRODUCTION

A major objective of the combustion aerodynamics research at Oklahoma State University is to perform detailed turbulence measurements in an isothermal swirling confined jet. The geometry is a simplified simulation of an aircraft can combustor. This report discusses measurements made with a crossed hot-wire probe in this flowfield.

Two independent hot-wires on one probe inclined at  $\pm 45^\circ$  to the flow direction were used as early as 1951 by Corrsin and Uberoi,<sup>1</sup> where they measured the power spectra of velocity and temperature fluctuations in heated and unheated jets. Further work by Davies et al<sup>2</sup> and Koplin<sup>3</sup> consisted of using single and double crossed wires in the measurement of turbulence intensity and shear stress in the mixing region of a round jet. Corrsin and Uberoi<sup>1,4</sup> and Wygnanski and Fiedler<sup>5</sup> performed measurements in the self-preserving region of the jet. More recently, Bradshaw et al<sup>6</sup> measured turbulence properties in the noise producing region of the jet, that is, up to 7.5 downstream of the jet exit. As all jets have somewhat different nozzle configurations, this study concentrated on free jet measurements far downstream of the jet exit in the self-preserving region of the jet. The data of Corrsin<sup>7</sup> were used as a basis of comparison of the present hot-wire measurements to provide an independent check on the data acquisition and interpretation technique. Measurements of mean and fluctuating properties were taken at an axial distance of 20 diameters downstream of the jet exit.

Several research groups have made measurements in axisymmetric, sudden expansion flowfields similar to the one being studied.<sup>8-10</sup> Ha Minh and Chassaing<sup>8</sup> made pitot probe and hot-wire measurements in various sudden expansion flowfields. The expansion ratios  $D/d$ , they used were 0.6, 2 and

1.6 but the axial locations they measured at were not compatible to those of the present study. Ha Minh and Chassaing<sup>8</sup> successfully managed to measure the Reynolds stresses using the rotating, inclined, single hot-wire technique. Moon and Rudinger<sup>9</sup> measured mean velocities and recirculation region geometries with the use of Laser Doppler anemometry equipment but the expansion ratio differed from the one used in the present experiments. Chaturvedi<sup>10</sup> performed mean velocity and turbulence measurements in an axisymmetric sudden expansion flowfield with an expansion ratio  $D/d = 2$ , which is identical to that used in our experiments. Consequently his measurements can be compared directly with those made in the present study. Also comparable are single-wire six-orientation measurements,<sup>11</sup> recently obtained in the same test facility as used in the present study.

Experimental facilities and instrumentation are described in Section 2. The measurement procedure is dealt with in Section 3, which includes calibration and data reduction techniques, and preliminary proof of principle measurements in a free jet with results compared with Corrsin.<sup>7</sup> Confined jet measurements are given in Section 4, where validation of techniques is further demonstrated by way of comparison with earlier results of Chaturvedi<sup>10</sup> and Janjua.<sup>11</sup>

## 2. EXPERIMENTAL FACILITIES

### 2.1 Confined Jet Flowfield

The experiments have been conducted in the confined jet facility shown schematically in Fig. 1. The facility has an axial flow fan whose speed can be changed by altering the drive pulley combination. Numerous fine screens and straws produce flow in the settling chamber of low turbulence intensity. The contraction section leading to the test section has been designed by the method of Morel<sup>12</sup> to produce a minimum adverse pressure gradient on the boundary layer and thus avoid unsteady problems associated with local separation regions. The sudden expansion consists of a 15 cm diameter nozzle, exiting abruptly into a 30 cm diameter test section. The substantial size of this test model will provide good probe resolution for the hot-wire measurements. The test section is constructed of plexiglass to facilitate flow visualization and ease of location of measuring probes.

Flow at abrupt expansions is a typical example of the problem of separation of a flowing fluid from the boundary. The flow is separated at the sudden expansion and causes a region of reverse flow. This is called the corner recirculation zone (CRZ). This region is associated with a large pressure drop which adversely affects the performance of a can combustor. On the shear layer between the two regions the turbulence levels are high, which would indicate that good combustion could be achieved at this position. Reacting flows in actual can combustors would have points of high heat transfer at the area of impingement of the dividing streamline. This, of course, could lead to rapid deterioration of the combustor and is therefore of great interest to combustor designers.

## 2.2 Free Jet Calibration Facility

It was necessary to calibrate the crossed hot-wires in a flow of known characteristics. This was achieved by means of a round free jet issuing horizontally into a quiescent atmosphere. The jet was formed by using a seamless contoured nozzle of 34 mm exit diameter,  $d$ . The nozzle was fed by a thermally stabilized compressed air generator which was regulated by an upstream control valve to provide the correct flow rate through the calibration nozzle. The sensitivity to angulation was obtained by usage of a rotary table (see section 2.2) on the jet centerline to rotate the probe from  $-10^\circ$  to  $+10^\circ$  to the free stream flow direction.

The usual hot-wire instrumentation was used to calibrate the probe as described in section 1.3.

## 2.3 Hot-Wire Instrumentation

The probe used in this study consisted of two independent inclined hot-wires. The wires were inclined at  $\pm 45^\circ$  to the flow direction and were made from 5  $\mu\text{m}$  tungsten wire soldered onto the tips of round jewellers broaches. The broaches were supported by a perforated ceramic insulator.

The mean and fluctuating flow measurements were made using separate constant temperature anemometer electronics for each of the hot-wires. The anemometers consisted of a DISA 55M01 main frame with a 55M10 standard bridge. In addition to this it was necessary to instantaneously add and subtract the wire rms outputs. This was achieved by the construction of commercially available integrated circuits. The multiplication of these voltages was obtained by using a Saicor model SAI 43 correlation and probability analyzer. The fluctuating signals were also amplified, with a Hewlett Packard amplifier with 20 dB gain on each of the signals. Normally the frequency response of the hot-wires and the associated electronics was

approximately 40 kHz based on square wave response tests. A schematic of the electronics layout is shown in Figure 2.

Experience in the use of crossed hot-wire has been gained at Oklahoma State University by researchers such as Swearingen<sup>13</sup> and Morrison.<sup>14</sup> though the majority of their measurement dealt with compressible flow, knowledge of the crossed-wire technique was first developed in subsonic jets. It was through their previous experience that the use of linearizers was judged unnecessary for the measured quantities in the report.

### 3. EXPERIMENTAL TECHNIQUES

#### 3.1 Data Reduction

Following the ideas of Corrsin and Uberoi<sup>1</sup> the instantaneous velocity fluctuations measured from an inclined hot-wire can be represented by the following expression.

$$\frac{e'}{E} = A_m \frac{u'}{u} + A_v \frac{v'}{u}$$

where  $A_m$  and  $A_v$  are the sensitivity coefficients for axial velocity fluctuations and radial velocity fluctuations respectively. The coefficients can be evaluated as follows:

$$A_m = \left. \frac{\partial \ln E}{\partial \ln u} \right|_{R_w, \phi \text{ constant}}$$

$$A_v = \left. \frac{\partial \ln E}{\partial \phi} \right|_{u, R_w \text{ constant}}$$

The two oppositely inclined wires of a crossed hot-wire probe give outputs that can be instantaneously added and subtracted to result in:

$$(e_1' + e_2') = (E_1 A_{m_1} + E_2 A_{m_2}) \frac{u'}{u} + (E_1 A_{v_1} - E_2 A_{v_2}) \frac{v'}{u}$$

$$(e_1' - e_2') = (E_1 A_{m_1} - E_2 A_{m_2}) \frac{u'}{u} + (E_1 A_{v_1} + E_2 A_{v_2}) \frac{v'}{u}$$

The crossed hot-wires are suitably matched so that the sensitivity coefficients  $A_m$  and  $A_v$  are approximately the same for each wire. These simplifications result in two voltages proportional to  $u'/u$  and  $v'/u$  respectively

$$(e_1' + e_2') = D_m \frac{u'}{u}$$

where

$$D_m = (E_1 A_{m_1} + E_2 A_{m_2})$$

and

$$(e_1' - e_2') = B_\phi \frac{v'}{u}$$

where

$$B_{\phi} = (E_1 A_{V_1} + E_2 A_{V_2})$$

Additionally, the major shear component of the Reynolds stress tensor in a shear flow may be determined by the multiplication of the voltages proportional to  $u'/u$  and  $v'/u$  and using the following relation

$$\frac{\overline{u'v'}}{u_0^2} = \frac{\text{correlator output}}{B_{\phi} \cdot D_m} \left| \frac{u^2}{u_0^2} \right|$$

### 3.2 Calibration

The calibration is performed by placing the crossed hot-wire probe on the free jet calibration facility centerline near the nozzle exit within the potential core region. The axial velocity is then varied by an upstream control valve and a Rotometer is used to determine the flow rate through the calibration nozzle. The corresponding voltage from each of the wires for each Rotometer setting is then noted. Curves of  $E$  versus  $u$  can then be drawn for each wire, Fig. 3. The derivative  $\partial \ln E / \partial \ln u$  is needed to obtain the sensitivity coefficient, that is

$$A_m = \frac{\partial \ln E}{\partial \ln u} = \frac{u}{E} \frac{\partial E}{\partial u}$$

A certain number of points are then taken from each of the two curves to obtain  $A_{m_1}$  and  $A_{m_2}$ . For each velocity a certain  $D_m$  exists, knowing this a graph can be drawn of  $D_m$  against velocity and can be approximated by a straight line (Fig. 6). From this, any  $D_m$  is known within the range of velocities encountered.

To obtain the sensitivity to angulation,  $A_v$ , the probe is located on the  $x$ - $z$  plane of the jet (see Fig. 4). The probe is then rotated between  $+10^\circ$  and  $-10^\circ$  incidence angle ( $\phi$ ) to the free stream flow direction in increments of  $2^\circ$ . This is repeated at the same velocities at which

the  $D_m$ 's are calculated. A sample of these readings are shown in Fig. 5. It is noticed that these curves do not intersect at the zero degree point as one might expect, due to the inexact matching of the wires - slight differences in individual wire output for identical flow conditions. From the plots of E against  $\phi$ , the derivative  $\partial \ln E / \partial \phi$  is obtained, hence the sensitivity coefficient is also obtained.

$$A_v = \frac{\partial \ln E}{\partial \phi} = \frac{1}{E} \frac{\partial E}{\partial \phi}$$

From each of these graphs  $A_{v_1}$  and  $A_{v_2}$  can be calculated, therefore leading to  $B_\phi$ . This again is plotted against velocity and can be approximated by a straight line as shown in Fig. 6.

### 3.3 Free Jet Measurements - Proof of Principle

Preliminary measurements were made in a free jet for which much published data exist. This is necessary to validate the experimental procedure and data reduction discussed earlier, as little published data concerning confined jet fluctuating flow data using the present method are available. As mentioned previously, measurements were made of mean velocity and turbulence intensities in the self preserving region of the jet i.e. at an axial distance,  $x/d$ , of 20. These results were then compared with those of Corrsin.<sup>7</sup> Corrsin<sup>7</sup> used a one inch diameter jet issuing into still air at a velocity of 10 m/s while the present jet consisted of a contoured nozzle with an area contraction ratio of 16:1 and an exit velocity of 14 m/s.

Initially, traverses for mean velocity were made across the jet at  $x/d$  equal to 20 to indicate if the jet used in this study is similar to the one used by Corrsin.<sup>7</sup> Figure 7 indicates that the present jet is very

comparable with the previous researcher's jet. The differences that occur at the large radial distances can be expected due to the difficulties in measuring very low velocities.

Presented in Figs. 8 and 9 are measurements of  $u'_{rms}/u_m$  and  $v'_{rms}/u_m$  at  $x/d = 20$ . As can be seen all the jet measurements have been non-dimensionalized with regard to the station maximum axial velocity, i.e. on the jet centerline. This is because non-dimensionalizing with the jet exit velocity would be very insignificant at such a distance downstream from the nozzle exit. As can be seen from the plots fair agreement with Corrsin<sup>7</sup> was achieved, especially for  $u'_{rms}/u_m$ . The  $v'_{rms}/u_m$  values measured here tend to be slightly lower than those presented by Corrsin<sup>7</sup> but this again can be explained by the difficulty in measuring turbulent, low speed flows.

#### 3.4 Confined Jet Measurements

Before any measurements were made in the test facility the crossed hot-wire probes had to be calibrated in the free jet facility as described in section 2.2. This was to study the angular sensitivity of the probe and to ensure that no 'drifting' of the electronics had occurred. The resistances of the hot-wires were also checked after the final measurements for the same reason.

The measurements of mean and fluctuating components of velocity were made in an isothermal model of a can combustor. The expansion ratio  $D/d$  was equal to 2 with an expansion angle,  $\alpha$ , of  $90^\circ$ . The measurements were made at axial locations in the test section of  $x/D$  of 0, 0.5, 1, 1.5, 2 and 2.5. The fluctuating components of the flow were normalized with the jet nozzle exit velocity,  $u_0$ . This quantity was measured prior to the commencement of any test.

Measurements of  $u'_{rms}$  and  $v'_{rms}$  were achieved by placing the crossed wires of the probe in the x-y plane (see Fig. 4) at the required x/D location and instantaneously adding and subtracting the rms voltages from each of the wires. The  $w'_{rms}$  component of the fluctuating velocity was measured by rotating the crossed hot-wires through  $90^\circ$  until they were on the x-z plane. The subtraction of the two instantaneous rms voltages is then used in the calculation of  $w'_{rms}/u_0$ .

The probe was traversed radially across the test facility by means of a probe drive built at OSU. This probe drive made it possible to make measurements at 18 positions radially across the test section.

#### 4. CONFINED JET RESULTS

The results presented here are measured values of the mean axial velocity, axial, radial, and tangential velocity fluctuations found in isothermal airflows of axisymmetric combustor geometries. As noted earlier the diameter expansion ratio  $D/d = 2$ , inlet Reynolds number  $Re_d = 1.26 \times 10^5$  and wall expansion angle,  $\alpha$ , is  $90^\circ$ . Measurements were taken at axial locations of  $x/D$  equal to 0, 0.5, 1.0, 2.0 and 2.5.

Figures 10 (a) - (f) show measured values of the time-mean axial velocity at all of the axial locations. The axial location of  $x/D$  of zero is actually a distance of approximately 5 mm between the wires and the enlargement face to insure that the wires were not damaged. The measurements at this location show that the shear layer is very thin, in the region of 3 mm. Comparisons have been made with Chaturvedi<sup>10</sup> at all axial locations except at positions of  $x/D$  equal to 0 and 2.5. Chaturvedi<sup>10</sup> did not take measurements at these locations. Both sets of axial velocities show good agreement except in the region of the recirculation zone. This is due to the hot-wire not being unable to sense flow direction, but an increase in flow velocity was detected as the probe was traversed further across the recirculation bubble. Therefore, indicating that a flow reversal did take place.

The plots depicting  $u'_{rms}/u_0$  are shown in Fig. 11 (a) - (f). As can be seen, good comparisons can be noted for most of the measured values with those of Chaturvedi. The curves of radial velocity fluctuations are shown in Fig. 12 (a) - (f). The two studies are in fair agreement except in regions of high turbulence where the present study gives higher values compared to Chaturvedi.<sup>10</sup> Fig. 12 (a) ( $v'_{rms}/u_0$  at  $x/D = 0$ ) indicates that the radial velocity fluctuations are damped due to the presence of the enlargement wall.

The final curves, Fig. 13 (a) - (f) show the tangential velocity fluctuations ( $w'_{rms}/u_0$ ). Chaturvedi<sup>10</sup> only made preliminary measurements of these fluctuations and concluded that  $v' = w'$ . The figures shown here tend to support this fact with very similar peak and centerline turbulence intensities between  $v'_{rms}/u_0$  and  $w'_{rms}/u_0$ . Fig. 13(a) again shows the damping effect of the wall, which tends to provide further proof of Chaturvedi's<sup>10</sup> observation. The small discrepancies that do occur between the present results and those of Chaturvedi<sup>10</sup> could be caused by slight drifting of the electronics and differing nozzle geometries.

The results shown here show the high level of turbulence in zones of separation, the conditions of nonhomogeneity and the variation of turbulence characteristics as the flow proceeds. Chaturvedi<sup>10</sup> noted that centerline values of turbulence intensities reached a maximum at an axial location of approximately  $x/D = 2.5$ . This result agrees favorably with that of the present study. Also shown on Figs. 10-12 are single-wire six-orientation measurements, recently obtained in the same test facility at Oklahoma State University.<sup>14</sup> Again the agreement is generally satisfactory.

## 5. CONCLUSIONS

Application of the crossed hot-wire anemometry technique to turbulent nonswirling flows has been discussed, together with the calibration and data reduction procedures. Great care has to be taken during calibration of the probe and, in conjunction with this, 'drifting' of the electronics has to be kept to a minimum. The method has been applied initially to free jet flows in order to justify the technique; results are in good agreement with Corrsin.<sup>7</sup> The main application of the method is to axisymmetric confined jets in the Oklahoma State University test facility. Results are given for the nonswirling flow in the sudden expansion configuration. Measurements of time-mean and fluctuating velocities are presented at several axial stations and compared with those of Chaturvedi<sup>10</sup> and Janjua.<sup>11</sup> Good agreement is to be noted.

6. REFERENCES

1. Corrsin, S., and Uberoi, M. S., "Spectrums and Diffusion in a Round Turbulent Jet", NASA Rep. 1040, 1949.
2. Davies, P. O. A. L., Fisher, M. J., and Barrett, M. J., "Turbulence in the Mixing Region of a Round Jet", Journal of Fluid Mechanics, Vol. 15, 1963, pp. 337-367.
3. Kopylov, M. A., "The Flow in the Mixing Region of a Jet", Journal of Fluid Mechanics, Vol. 18, 1964, pp. 529-548.
4. Corrsin, S., and Uberoi, M. S., "Further Experiments on the Flow and Heat Transfer in a Heated Turbulent Jet", NACA TN 1895, 1949.
5. Wagnanski, I., and Fielder, H., "Some Measurements in the Self-Preserving Jet", Journal of Fluid Mechanics, Vol. 38, 1969, pp. 577-612.
6. Bradshaw, P., Ferris, D. H., and Johnson, R. F., "Turbulence in the Noise Producing Region of a Circular Jet", Journal of Fluid Mechanics, Vol. 19, 1964, pp. 591-624.
7. Corrsin, S., "Investigation of Flow in an Axially Symmetrical Heated Jet of Air", NACA wartime Report W94, 1943.
8. Ha Minh, H., and Chassaing, P., "Perturbations of Turbulent Pipe Flow", Proc. Symposium on Turbulent Shear Flows, Pennsylvania State University, April 1977, pp. 13.9-13.17.
9. Moon, L. F., and Rudinger, G., "Velocity Distribution in an Abruptly Expanding Circular Duct", Journal of Fluids Engineering, March 1977, pp. 226-230.
10. Chaturvedi, M. C., "Flow Characteristics of Axisymmetric Expansions", Proc., Journal Hydraulics Division, ASCE, Vol. 89, May 1963, pp. 61-92.
11. Janjua, S. I., Turbulence Measurements in a Complex Flowfield Using a Six-Orientation Hot-Wire Probe Technique, M.S. Thesis, Oklahoma State University, Stillwater, OK, Dec. 1981.
12. Morel, T., "Comprehensive Design of Axisymmetric Wind Tunnel Contractions", ASME Paper 75-FE-17, Minneapolis, May 5-7, 1975.
13. Morrison, G. L., "Flow Instability and Acoustic Radiation Measurements of Low Reynolds Number Supersonic Jets", Ph.D. Thesis, Oklahoma State University, 1977.
14. Swearingen, J. D., "Crossed Hot-Wire Measurements in Low Reynolds Number Supersonic Jets", M.S. Thesis, Oklahoma State University, 1979.

## 7. NOMENCLATURE

$A_m$	axial velocity fluctuation sensitivity coefficient
$A_v$	radial velocity fluctuation sensitivity coefficient
$B_\phi$	$(E_1 A_{v_1} + E_2 A_{v_2})$
$D$	chamber diameter
$d$	nozzle exit diameter
$D_m$	$(E_1 A_{m_1} + E_2 A_{m_2})$
$E$	mean voltage
$e'$	voltage fluctuation
$r$	radial distance
$r_o$	free jet nozzle radius
$R_w$	hot-wire resistance
$u$	time-mean axial velocity
$u_m$	station maximum velocity
$u_o$	nozzle exit velocity
$u'_{rms}$	rms axial velocity fluctuation
$v'_{rms}$	rms radial velocity fluctuation
$w'_{rms}$	rms tangential velocity fluctuation
$\overline{u'v'}$	rx component of Reynolds stress tensor
$x$	axial distance
$x,r,\theta$	axial, radial, polar co-ordinates
$x,y,z$	Cartesian coordinates
$\alpha$	wall expansion angle
$\phi$	yaw angle of cross wire probe relative to jet centerline

## 8. FIGURE LIST

- Fig. 1. Schematic of confined jet facility
- Fig. 2. Schematic of instrumentation layout
- Fig. 3. Calibration plot of E versus u
- Fig. 4. Coordinate system of free and confined jet
- Fig. 5. Calibration plot for sensitivity to angulation
- Fig. 6. Parameters  $D_m$  and  $B_\theta$  versus u
- Fig. 7. Radial distribution of time-mean axial velocity at  $x/d = 20$  in nonswirling free jet [----- Ref. 7]
- Fig. 8. Radial distribution of axial velocity fluctuation at  $x/d = 20$  in nonswirling free jet [----- Ref. 7]
- Fig. 9. Radial distribution of radial velocity fluctuation at  $x/d = 20$  in nonswirling free jet [----- Ref. 7]
- Fig. 10. Time-mean axial velocity profiles in nonswirling confined jet [o—o present study, ----- Ref. 10, --- Ref. 11]
- Fig. 11. Axial velocity fluctuation profiles in nonswirling confined jet [o—o present study, ----- Ref. 10, --- Ref. 11]
- Fig. 12. Radial velocity fluctuation profiles in nonswirling confined jet [o—o present study, ----- Ref. 10, --- Ref. 11]
- Fig. 13. Tangential velocity fluctuation profiles in nonswirling confined jet

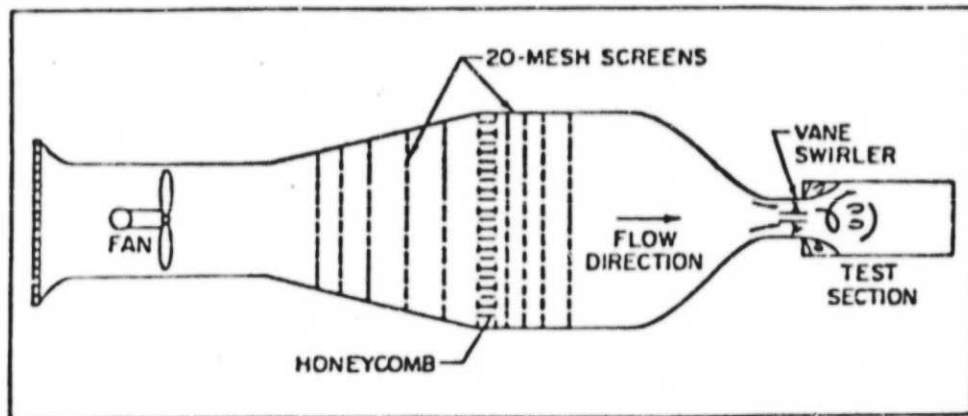


Fig. 1 Schematic of confined jet facility

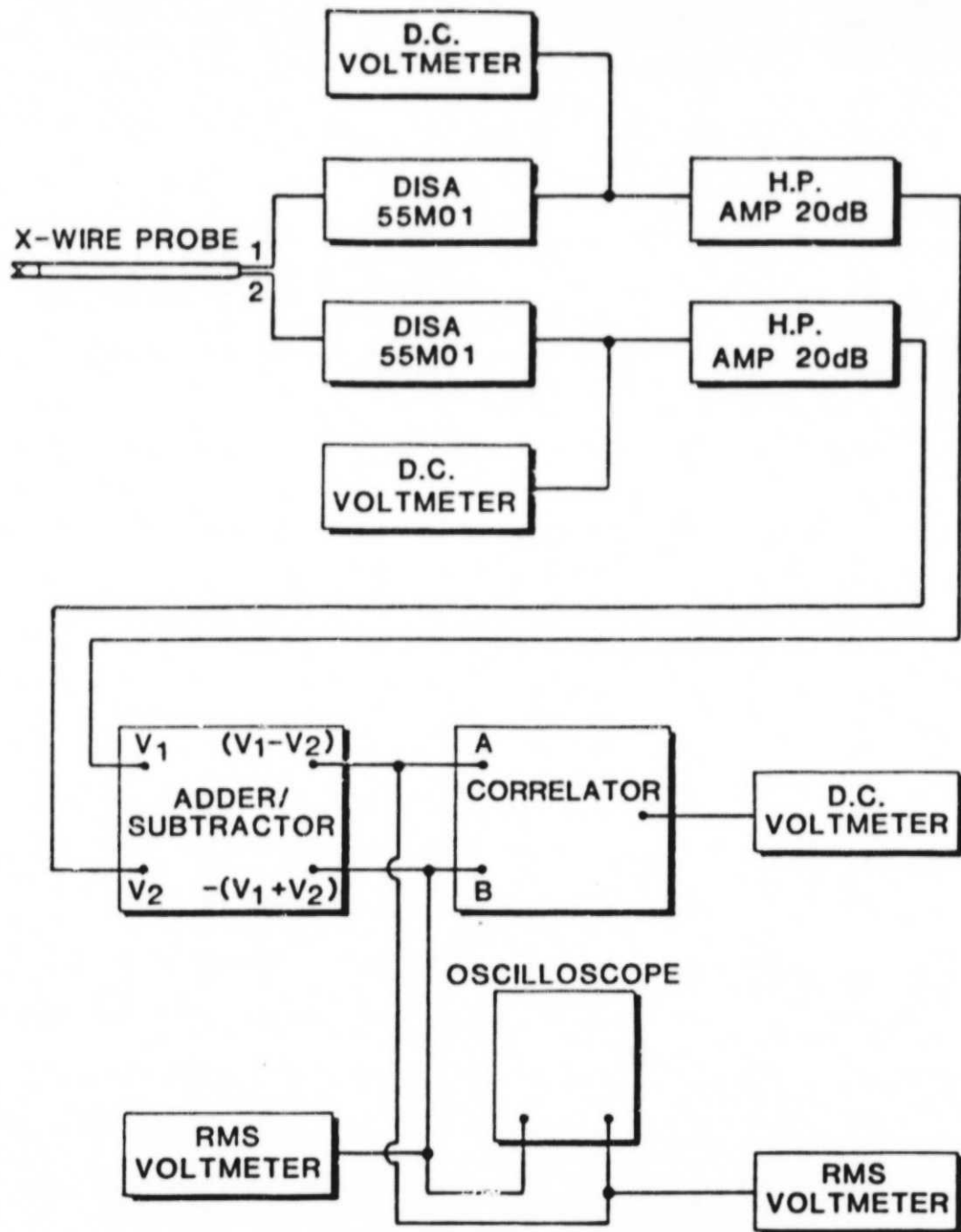


Fig. 2 Schematic of instrumentation layout

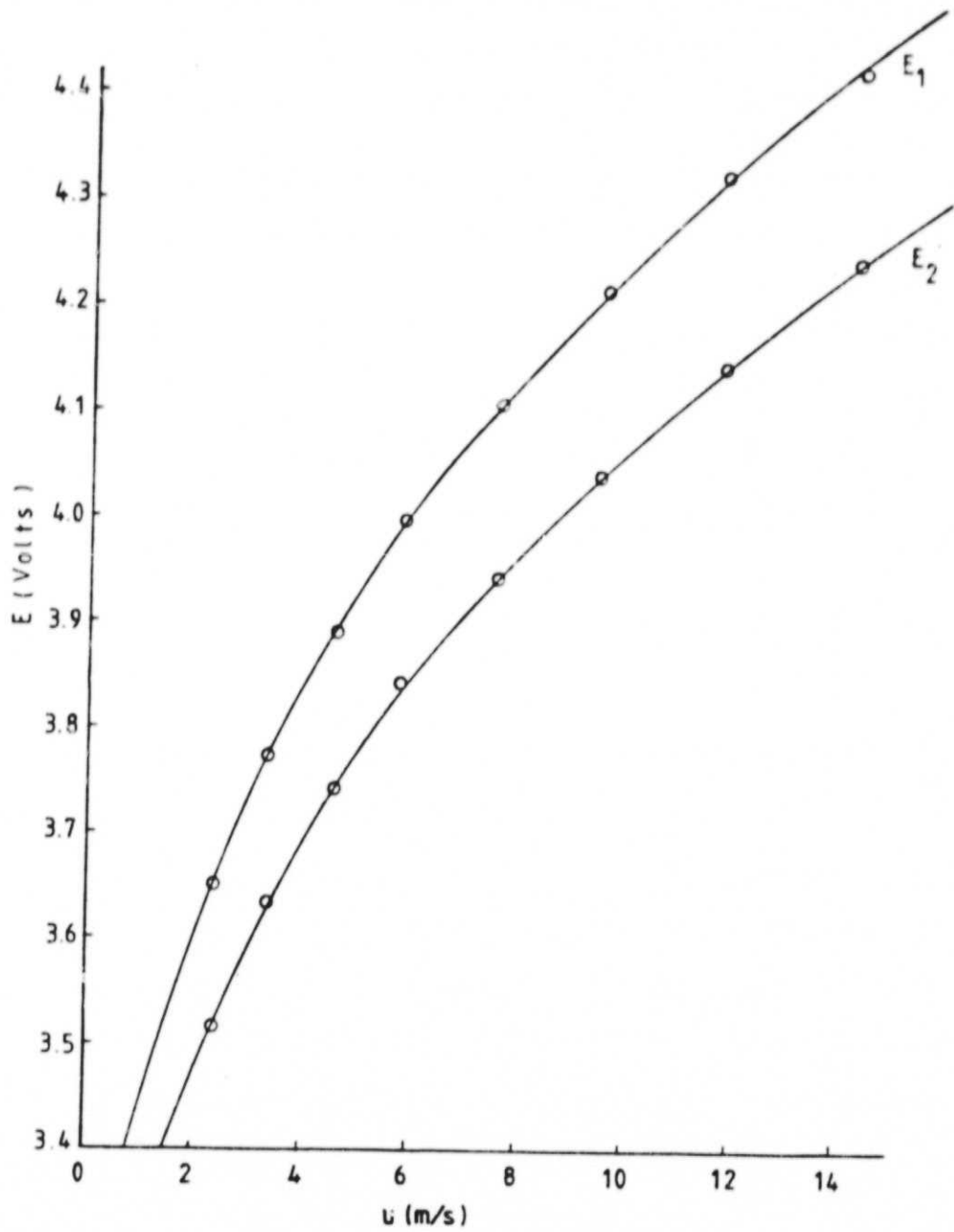


Fig. 3 Calibration plot of  $E$  versus  $u$

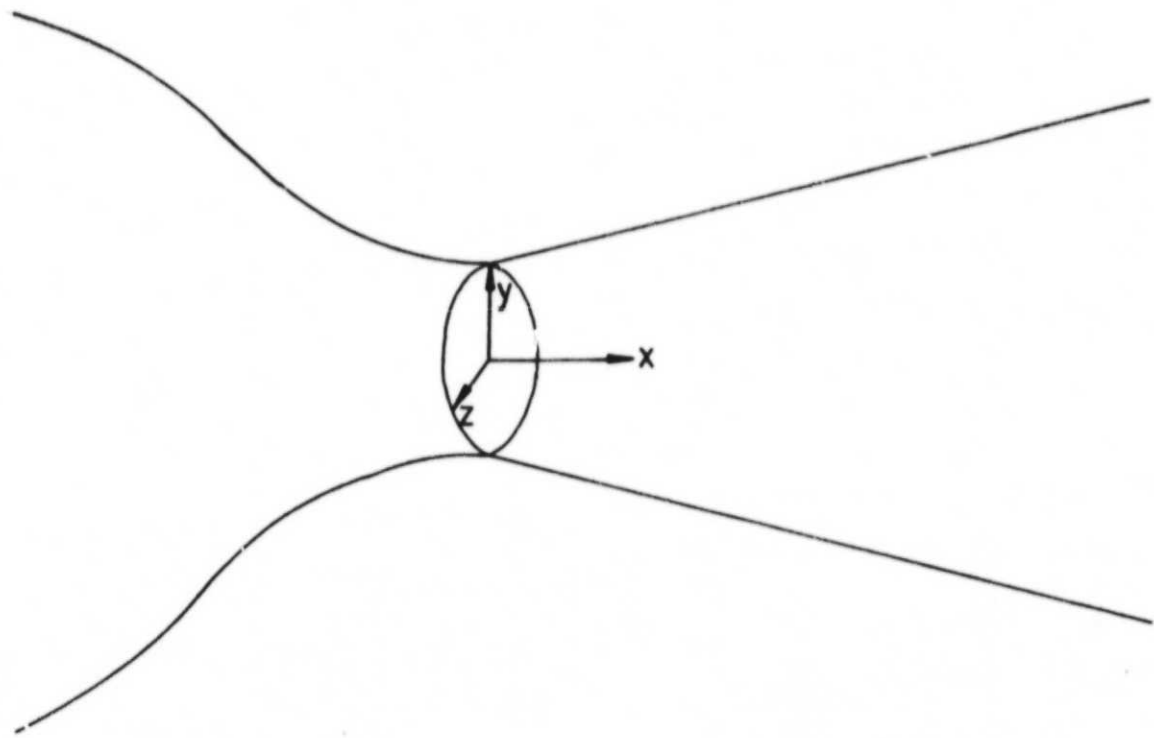


Fig. 4. Coordinate system of free and confined jet.

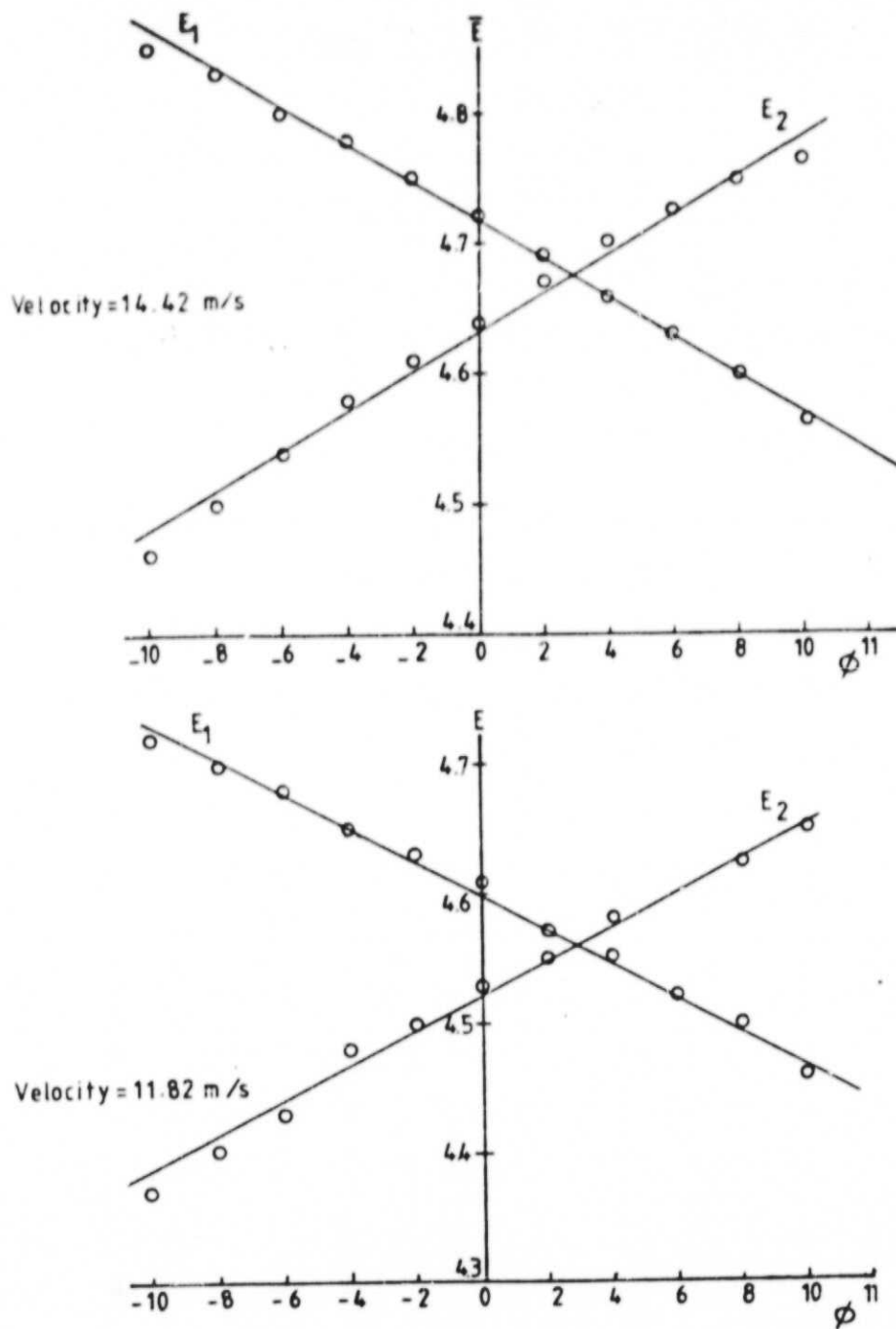


Fig. 5 Calibration plot for sensitivity for angulation

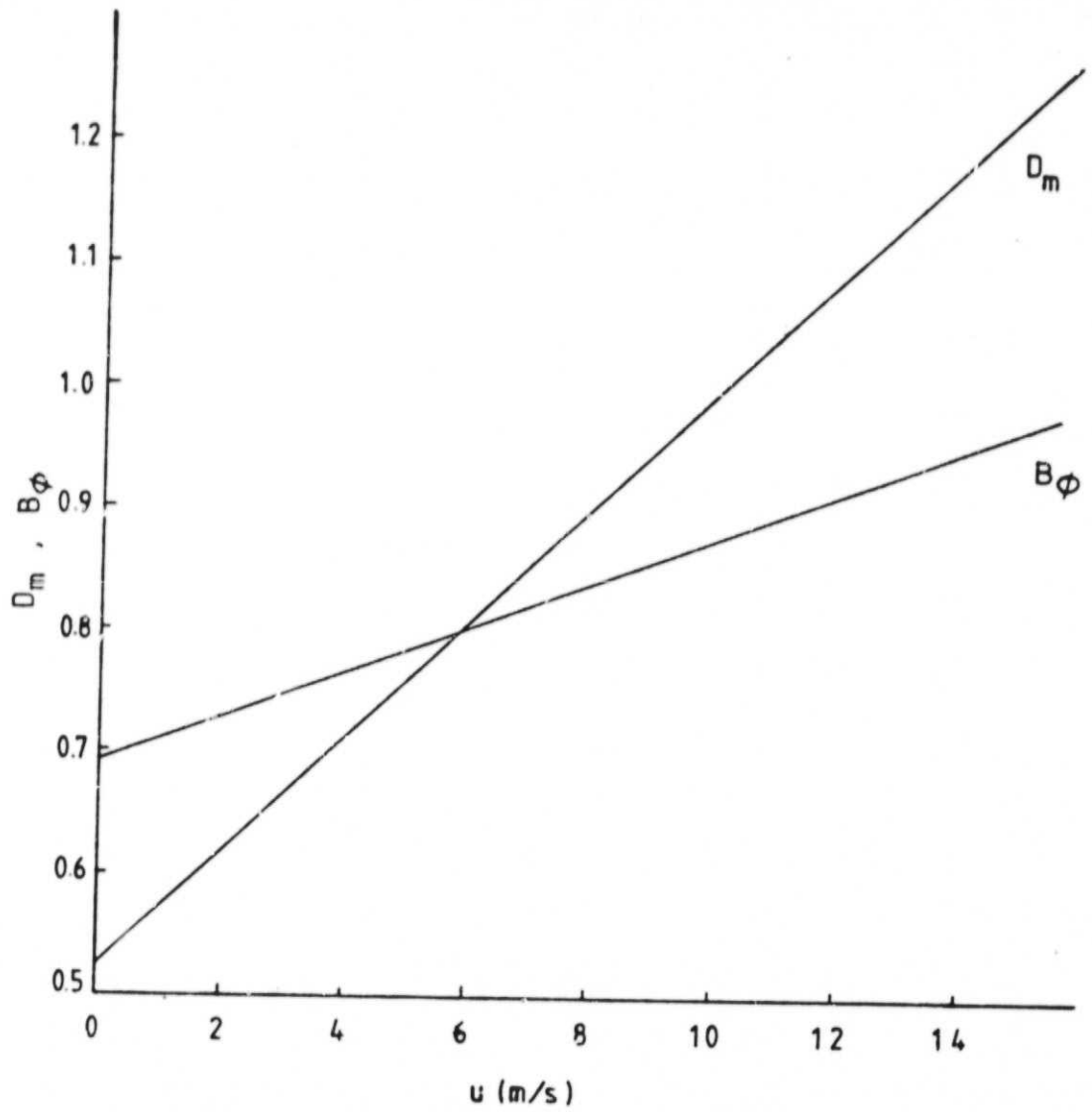


Fig. 6 Parameters  $D_m$  and  $B_\phi$  versus  $u$

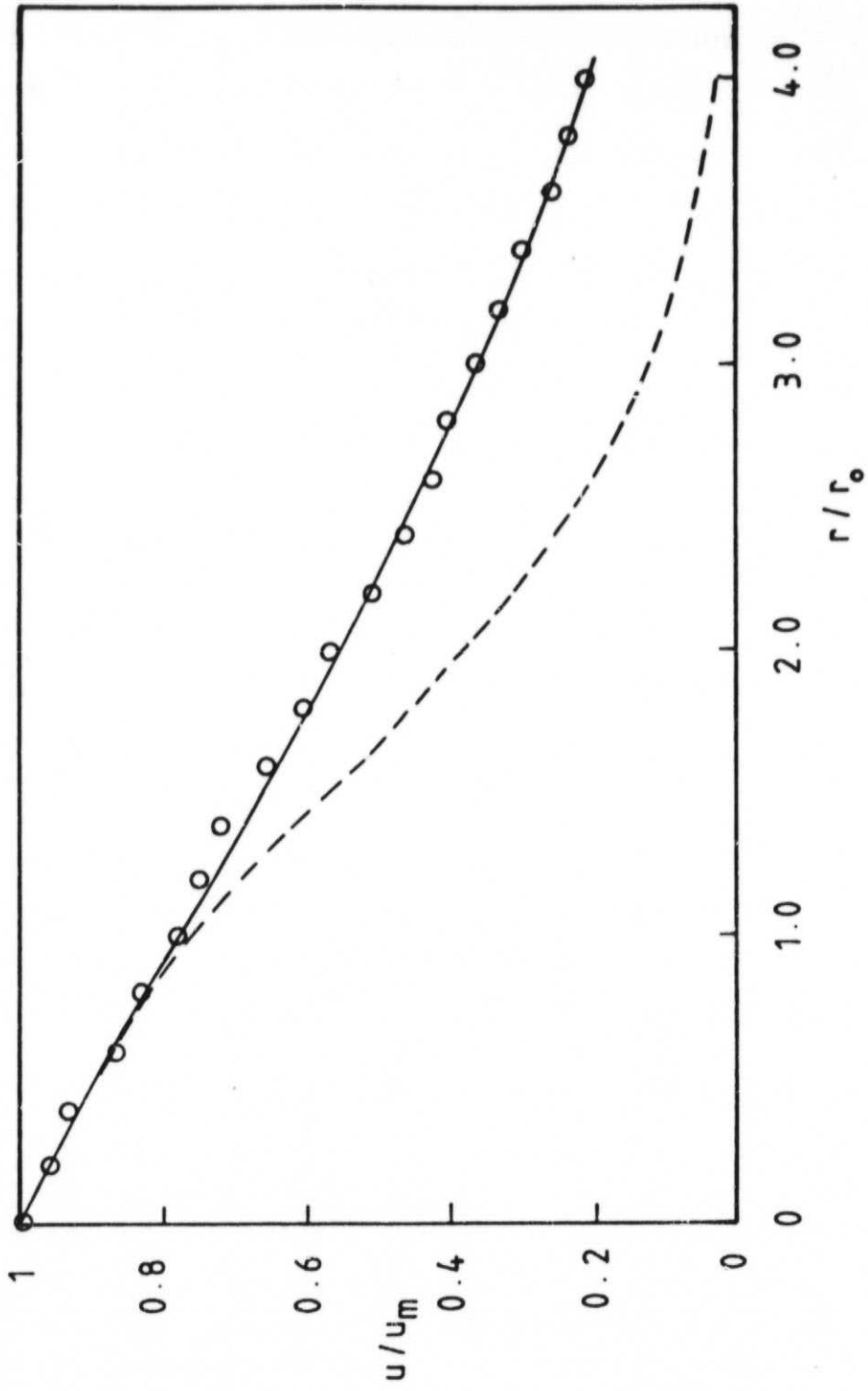


Fig. 7 Radial distribution of time-mean axial velocity at  $x/d = 20$ . [----- Ref. 7]

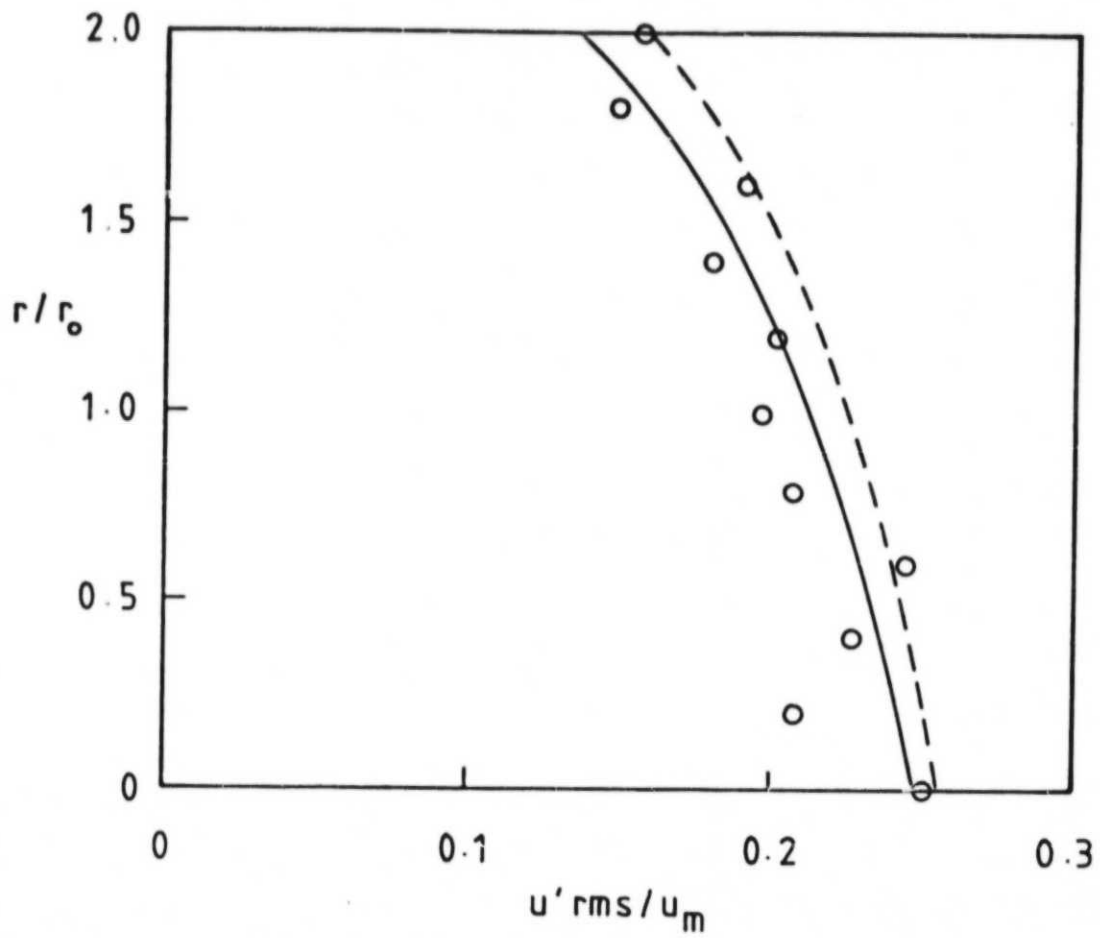


Fig. 8 Radial distribution of axial velocity fluctuation at  $x/d = 20$ . [ ---- Ref. 7]

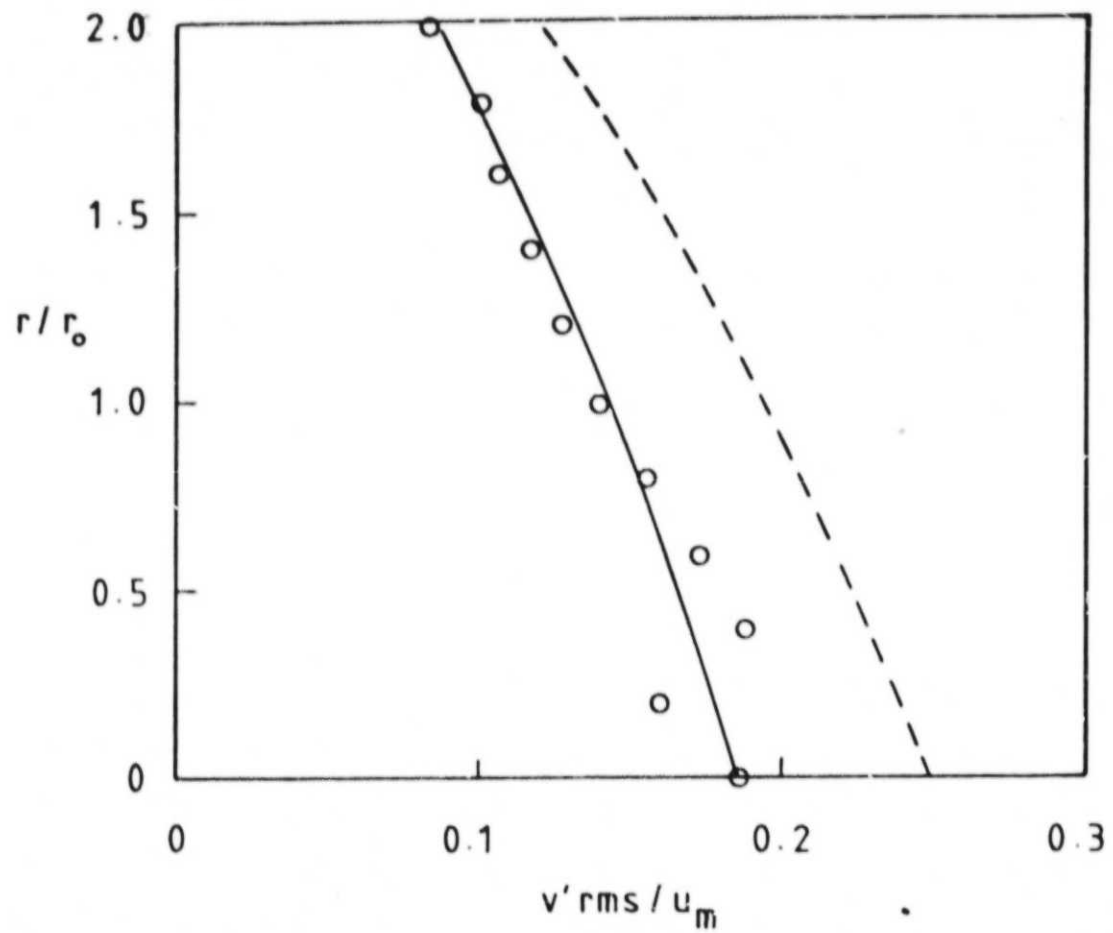


Fig. 9 Radial distribution of radial velocity fluctuation at  $x/d = 20$ . [ ---- Ref. 7]

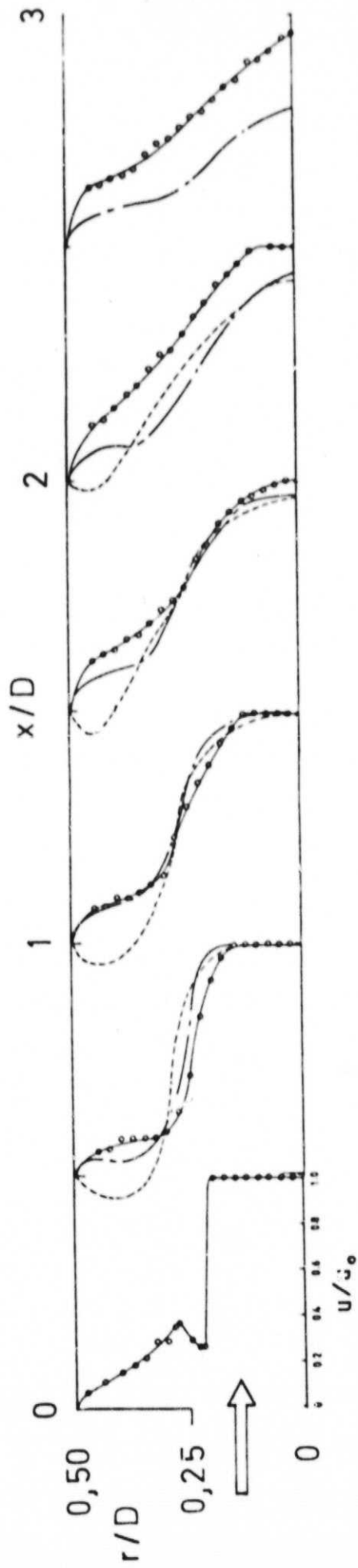


Fig. 10 Time-mean axial velocity profiles in nonswirling confined jet  
 [o—o present study, - - - - - Ref. 10, — · — · — Ref. 11]

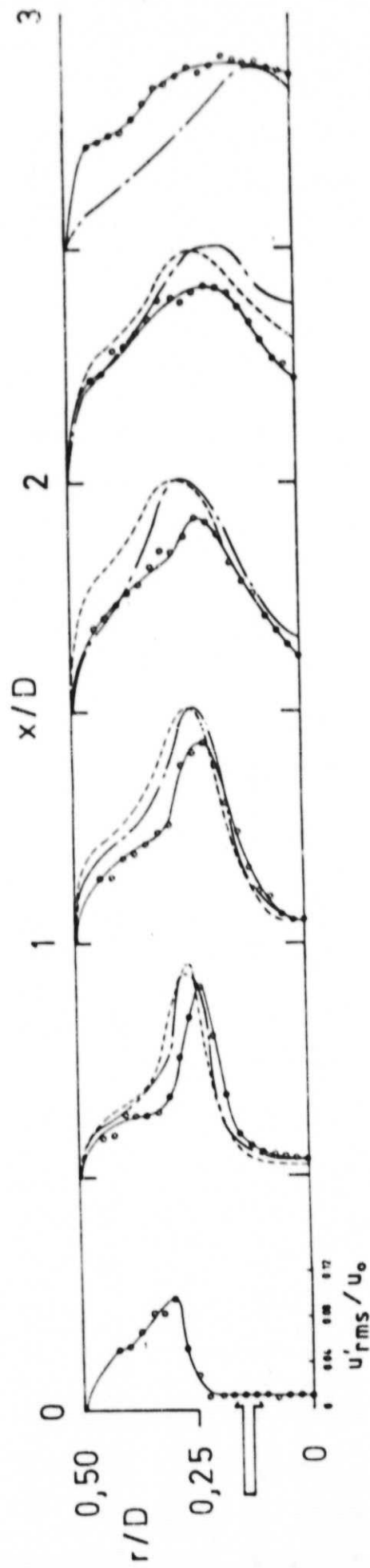


Fig. 11 Axial velocity fluctuation profiles in nonswirling confined jet  
 [o—o present study, ----- Ref. 10, ——— Ref. 11]

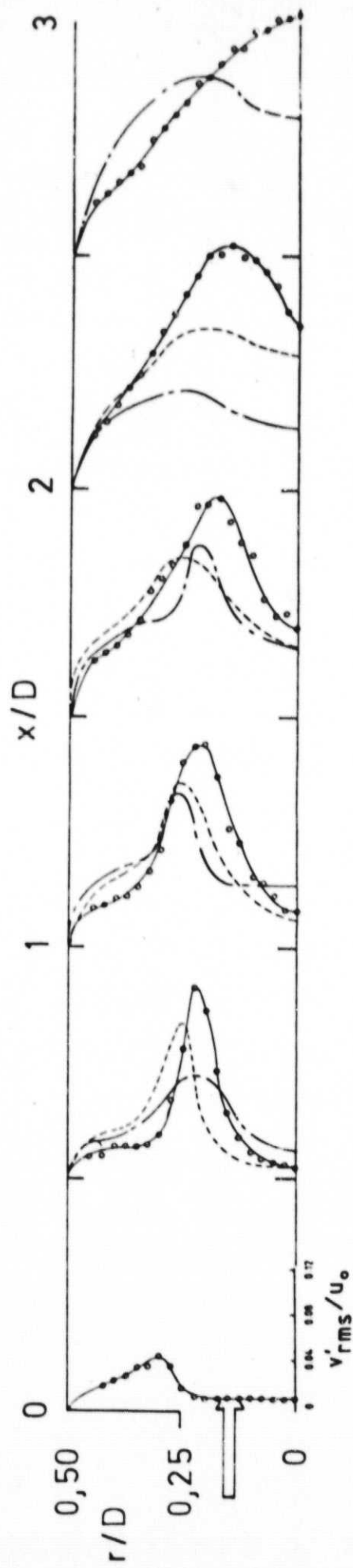


Fig. 12 Radial velocity fluctuation profiles in nonswirling confined jet  
 [o—o present study, - - - - - Ref. 10, - · - · - Ref. 11]

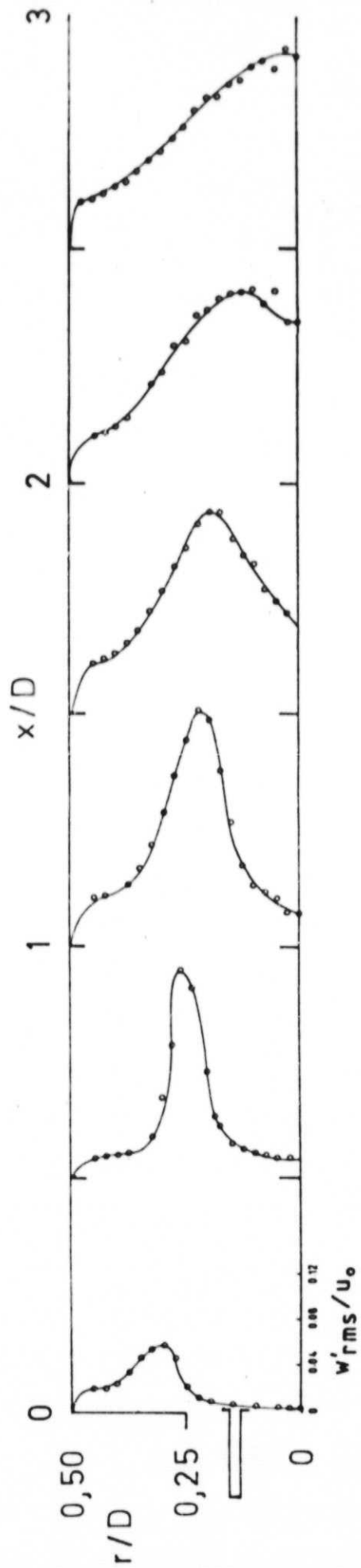


Fig. 13 Tangential velocity fluctuation profiles in nonswirling confined jet

APPENDIX C

A SIMPLE FINITE DIFFERENCE PROCEDURE FOR THE  
VORTEX CONTROLLED DIFFUSER

**AIAA-82-0109**

**A Simple Finite Difference Procedure for the  
Vortex Controlled Diffuser**

A.A. Busnaina and D.G. Lilley, Oklahoma  
State Univ., Stillwater, OK



**AIAA 20th Aerospace  
Sciences Meeting**

January 11-14, 1982/Orlando, Florida

# A SIMPLE FINITE DIFFERENCE PROCEDURE FOR THE VORTEX CONTROLLED DIFFUSER

A. A. Busnaina\* and D. G. Lilley\*\*  
Oklahoma State University, Stillwater, Okla.

## Abstract

The effect of bleed on short vortex controlled diffusers is considered numerically. The transient Navier-Stokes equations are solved via their associated finite difference equations, directly in terms of the primitive pressure-velocity variables, and the technique is based on the two-dimensional Los Alamos SOLA prediction procedure. A short simple computer code has been developed, using a laminar flow simulation with 'free slip' or 'no slip' wall boundary conditions. The simplified code represents a basic tool to which user-oriented complexities and sophistications can easily be added as required.

## 1. Introduction

### 1.1 The Phenomenon Considered

Recent emphasis has been placed on the requirement for a short efficient diffuser to be placed between the compressor and combustor components of the aircraft gas turbine engine.<sup>1,2</sup> The vortex-controlled diffuser VCD employs bleed at the step location of a dump diffuser, so as to obtain a low-pressure loss in a short length. Figure 1 shows a schematic of the VCD in its simplest form. Here, the view may be considered as a slice of an annular path with inner and outer bleeds or as an axisymmetric situation with circumferential bleed. In practice, the flow diffuses from the primary duct into an abruptly-enlarged secondary duct. Interaction between the VCD bleed and the main flow is stabilized via a vortex fence, also shown in the figure. Without bleed, there is jet flow with very little lateral diffusion - a long duct is needed to obtain uniform air-flow properties at the diffuser exit. Conversely, with sufficient bleed, the main flow diffuses rapidly and fills the secondary duct - the corner recirculation zone is considerably shorter.

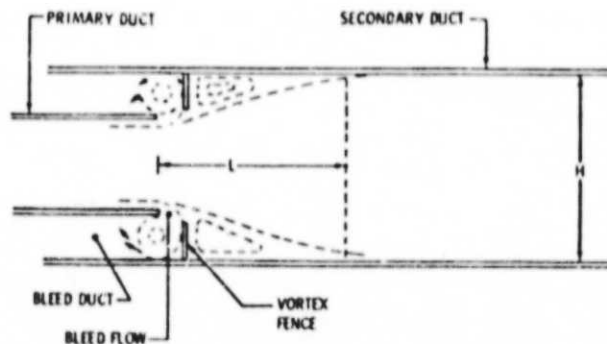


Fig. 1 Schematic of the VCD geometry<sup>2</sup>

\* Graduate Student, School of Mechanical and Aerospace Engineering, Member AIAA.

\*\* Associate Professor, School of Mechanical and Aerospace Engineering, Associate Fellow AIAA.

### 1.2 Previous Studies

Early ideas of the VCD placed cusps in the diffuser wall to locate vortices rotating preferentially in the direction of flow, so as to reduce the boundary layer shear stress experienced by the flow in the region of high adverse pressure gradients.<sup>3</sup> Only limited success was obtained because of difficulty in retaining a stable vortex system. Recent extensive studies at Cranfield Institute of Technology overcame this problem by featuring bleed off directly from the vortex.<sup>4,5,1</sup> It was also found that the quantity of bleed required could be kept at reasonable levels by locating a fence directly downstream of the vortex, thereby creating a partially enclosed vortex chamber. Figure 2 shows the mechanism deduced from experimental data, where a layer of high turbulence forms between the drawn off stream tube 'a' and the diffusing stream tube 'b'. The mainstream flow is further aided on its path by the formation of a Coanda bubble immediately downstream of the lateral fence.

This work suggested a potential performance payoff in practical engine applications. Detroit Diesel Allison Division of General Motors applied the above laboratory concepts to a realistic gas turbine annular combustion system flow path.<sup>2</sup> The performance was confirmed to be a strong function of several variables including:

1. Secondary duct length  $L/H$
2. Bleed quantity  $B$  (flow fraction)
3. VCD area ratio  $A_2/A_1$
4. VCD inlet flow distortion  $\alpha$
5. Bleed slot axial and radial gaps
6. Bleed cavity geometry.

Other workers considered applications to variable geometry combustors<sup>6-8</sup> and inlet flow distribution effects.<sup>9</sup>

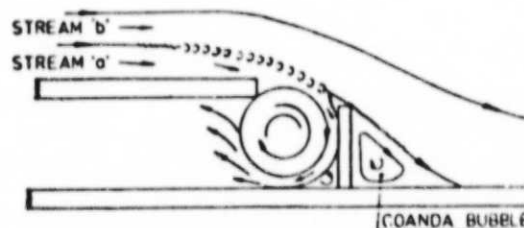


Fig. 2 Vortex control flow mechanism<sup>1</sup>

### 1.3 The Computational Problem

Mathematically the governing equations are elliptic in character and a relaxation method of

solution is appropriate (if solving directly for the steady-state); they are parabolic (in time) and a marching method of solution is appropriate (if solving for the steady-state via the time evolution of the transient flow process). Consideration is given here to a primitive, pressure-velocity variable, finite difference code which has been developed to predict 2-D axisymmetric transient flows. The technique used here incorporates the following:

- (i) A finite difference procedure is used in which the dependent variables are the velocity components and pressure, formulated in axisymmetric cylindrical polar coordinates.
- (ii) The pressure is deduced from the continuity equation and the latest velocity field, using a guess-and-correct procedure for the latter.
- (iii) The procedure incorporates displaced grids for the two velocity components, which are placed between the nodes where pressure is stored.

The code is designed for persons with little or no experience in numerical fluid dynamics with the purpose of demonstrating that many useful and difficult problems can be solved without resorting to large, complicated computer programs. As specific complexities can be added easily, the program provides a basis for developing many new numerical capabilities. The present work has grown out of previous ideas about solving 2-D flows using so-called Los Alamos<sup>10-12</sup> and Imperial College<sup>13,14</sup> methods, solving for the primitive pressure-velocity variables, the former treating the transient case and the latter treating the steady state case directly.

The present study illustrates the use of a short simple computer code, using a laminar flow simulation with 'free slip' or 'no slip' wall boundary conditions. The simplified code provides an alternative to a more sophisticated code applied to a similar dump flowfield with bleed which is discussed as one of the gas turbine combustor design challenges of the 1980's.<sup>15</sup>

#### 1.4 Outline of the Contribution

The computational procedure described in Section 2 is based on Los Alamos SOLA 2-D ideas.<sup>12</sup> The technique is for incompressible fluid flow, and complexities are restrained to a minimum so as to facilitate the use of the code. User-oriented complexities can be added as required and details of many such extensions may be obtained elsewhere: control volume and flux approach to obtaining the FDEs, non-uniform grid system, semi-implicit method for each time-step, etc.<sup>14,16,17</sup> Predictions for the VCD are given in Section 3 showing the influence of several design parameters. The final conclusions illustrate that a useful and valuable tool, based on conceptually simple ideas, is now becoming available, and on to which any user-oriented complexities can easily be added.

### 2. Simulation and Solution Procedure

#### 2.1 The Technique

The computational code solves directly for the primitive pressure and velocity variables, and is based on the Marker and Cell MAC Los Alamos techni-

que. This is one of the most well-known methods to solve time-dependent incompressible fluid flow problems; its conceptual simplicity is one of the main attributes. A 2-D version is described in Ref. 12, upon which the present work is based. In the present work, and Eulerian finite difference formulation is used with pressure and velocity as the main dependent variables. In addition, the velocity components are positioned between the nodes where pressure and other variables are stored. At each step, the time-advanced expressions for  $u$  and  $v$  are substituted into the finite difference form of the continuity equation for each cell, and the guess and correct iterative process on pressure and velocity corrections is done until the continuity equations is sufficiently well satisfied. This section continues with a full discussion of the partial differential equations, mesh system, finite difference equations, stability and accuracy, and boundary condition insertion.

#### 2.2 The Partial Differential Equations

The governing partial differential equations PDEs of the incompressible flowfield are the continuity equation, and conservation of momentum in the  $x$  (= radial) and  $y$  (= axial) directions. These may be taken in axisymmetric cylindrical coordinates in conservative form<sup>18,19</sup> as:

$$\frac{\partial u}{\partial x} + \frac{\partial v}{\partial y} + \frac{u}{x} = 0$$

$$\frac{\partial u}{\partial t} + \frac{\partial}{\partial x} (u^2) + \frac{\partial}{\partial y} (vu) + \frac{u^2}{x} = -\frac{\partial p}{\partial x} + v(\nabla^2 u - \frac{u}{x^2}) \quad (1)$$

$$\frac{\partial v}{\partial t} + \frac{\partial}{\partial x} (uv) + \frac{\partial}{\partial y} (v^2) + \frac{uv}{x} = -\frac{\partial p}{\partial y} + v\nabla^2 v$$

where

$$\nabla^2 \phi = \frac{\partial^2 \phi}{\partial x^2} + \frac{\partial^2 \phi}{\partial y^2} + \frac{1}{x} \frac{\partial \phi}{\partial x}$$

The above simulation indicates that the problem is simply treated as a laminar viscous problem with unrealistic 'free slip' or 'no slip' wall boundary conditions. In this manner of formulation, much of the flow is controlled by the inlet and outlet conditions, together with the confining constraint. As recommended in Ref. 12, when computations are made in a large chamber, it is often a complicated and lengthy task to resolve thin boundary layers along the confining walls. But in many cases, the presence of these is unimportant and free slip boundary conditions can be justified as a good approximation. On the question of turbulence modeling, it is known that the time-mean behavior of a certain turbulent flows may sometimes be simulated via a constant large viscosity.<sup>20,21</sup> This is the approach taken here and predictions have been made with a range of values given to the constant viscosity  $\mu$  with minor effect on the flowfield produced. In view of this minor effect of the viscosity magnitude, computations given later are obtained merely with the laminar viscosity being used. The results show that, even with this limitation, a useful simulation of the actual problem is obtained.

The present simulation and solution procedure is a short simplified approach [approximately 350 Fortran statements] with good capability. Of course, other more lengthy [approximately 2000 Fortran statements] and sophisticated [nonuniform grid, implicit solution procedure, two-equation turbulence model and wall functions] approaches are available.

### 2.3 The Mesh System

The x-y domain is divided into rectangular cell divisions, with uniform  $\Delta x$  and  $\Delta y$  spacings. In the case of an annular diffuser, the left hand boundary represents a symmetry plane with radius  $x_L = (r_i + r_o)/2$  where  $r_i$  and  $r_o$  are inner and outer primary duct annulus radii. This assumed symmetry implies that only half of the problem is being solved. In the case of an axisymmetric diffuser, the left hand boundary is the symmetry axis with radius  $x_L = 0$ .

This domain is also complemented by a layer of cells on all sides, so as to allow easy simulation of the required boundary conditions (BCs). These fictitious cells increase the total number of cells in each direction. Figure 3 illustrates the total mesh arrangement, while Fig. 4 portrays a single cell and shows the location of each field variables  $p$ ,  $u$  and  $v$  relative to this (I,J)-cell. The pressure  $p$  is located at the center of each cell, while the radial and axial velocities ( $u$  in the radial x-direction and  $v$  in the axial y-direction) are on the right and top boundaries, respectively. Thus normal velocities lie *directly* on the physical boundaries of the solution domain, while the tangential velocities and pressure are *displaced half a cell interval* inside the flowfield. In this way the exterior fictitious cells are particularly convenient when applying the boundary conditions BCs.

### 2.4 The Finite Difference Equations

In formulating finite difference representations of the governing partial differential equations PDEs, the usual intuitive estimates of one-sided first-derivatives, centered first-derivatives and centered second-derivatives are used. Superscripts  $n$  and (blank) are used to denote values at time-level  $t$  and  $t + \Delta t$ , respectively. Portrayed now are equations enabling one such forward time-step to be accomplished. Thus, starting from initial field values throughout the domain of interest, a time-march process is used so as to advance toward the final steady-state solution, which is usually of special interest as opposed to the en route calculations.

In Eq. (1) the time-derivatives are approximated by forward one-sided derivatives; most spatial derivatives are approximated by central differences based on values at time-level  $t$ . Special techniques are required in computational fluid dynamics, however, in the representation of the convection terms, and a certain amount of upstream differencing is required. The difference equations representing the conservation of momentum Eq. (1) in directions  $x$  and  $y$  may be written and used to accomplish one forward time-step as follows:

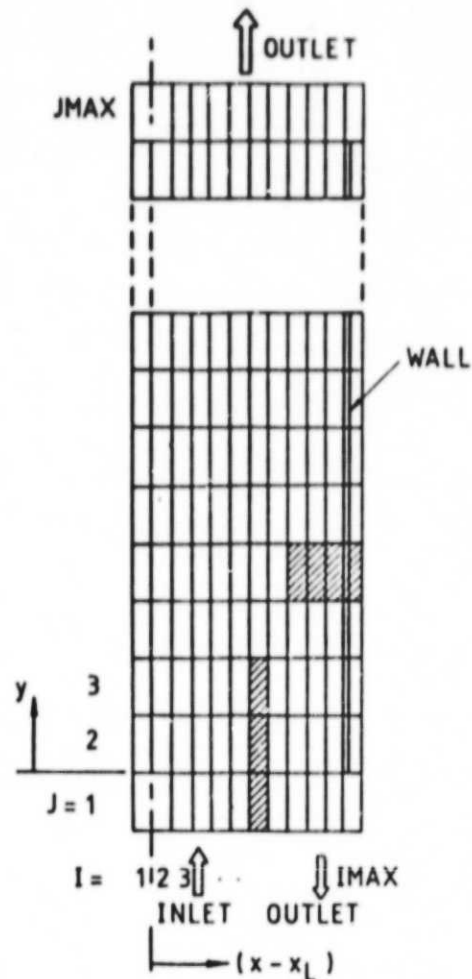


Fig. 3 General grid system covering the flow domain.

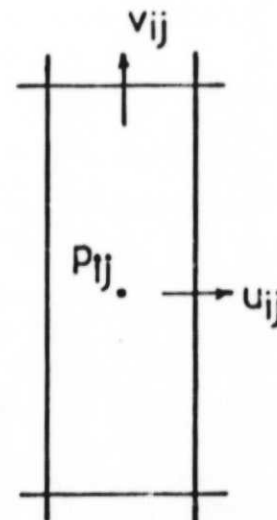


Fig. 4 Arrangement of finite difference variables in a typical cell.

$$\begin{aligned}
u_{ij} &= u_{ij}^n + \Delta t \left[ \frac{1}{\Delta x} (p_{ij}^n - p_{i+1,j}^n) \right. \\
&\quad \left. - FUX - FUY - FUC - VISX \right] \\
v_{ij} &= v_{ij}^n + \Delta t \left[ \frac{1}{\Delta y} (p_{ij}^n - p_{i,j+1}^n) \right. \\
&\quad \left. - FVX - FVY - FVC + VISY \right]
\end{aligned} \tag{2}$$

where the 4 terms on the right of each of these equations are defined in Appendix A. The Coefficient  $\alpha$  in these equations (see Appendix A) is a constant taking a value between 0 and 1, and so giving the desired amount of upstream (donor cell) differencing in the convection terms.<sup>12</sup> A value of 0 gives merely central differencing as in the original MAC codes<sup>10,11</sup> and numerical instability problems arise; a value of 1 gives the full upstream or donor cell form which, though introducing errors, is stable provided the fluid is not allowed to pass through more than one cell in one time-step, see the stability criterion of Eq. (6) later.

Although Eq. (2) accomplishes one forward time-step based on conservation of momentum principles, the newly calculated velocities will not, in general, satisfy the continuity requirement, as expressed by the central finite difference form of the continuity equation (see the first of Eq. (1)):

$$\begin{aligned}
\frac{1}{\Delta x} (u_{ij} - u_{i-1,j}) + \frac{1}{\Delta y} (v_{ij} - v_{i,j-1}) \\
\frac{1}{2\Delta x} (u_{ij} + u_{i-1,j}) = 0
\end{aligned} \tag{3}$$

where

$$x = x_L + \Delta x(i-1.5)$$

Terms here are evaluated at time-level  $t + \Delta t$ . This incompressibility condition is imposed by iteratively adjusting the cell pressure. That is, if the divergence  $D$  of a cell is positive (the left hand side of Eq. (3) is positive) there is a net mass outflow from that cell. This is corrected by reducing the cell pressure. If the divergence is negative, an increase in cell pressure is appropriate.

When a cell pressure changes from  $p$  to  $p + \Delta p$ , the velocity components on the 4 faces of that cell change, given from a linear analysis from Eq. (2), by an amount:

$$\begin{aligned}
u_{i,j} &= u_{i,j} + \Delta t \Delta p / \Delta x \\
u_{i-1,j} &= u_{i-1,j} - \Delta t \Delta p / \Delta x \\
v_{i,j} &= v_{i,j} + \Delta t \Delta p / \Delta y \\
v_{i,j-1} &= v_{i,j-1} - \Delta t \Delta p / \Delta y
\end{aligned} \tag{4}$$

Substitution of these in Eq. (3) yields the amount of correction to  $p$  required as:

$$\Delta p = -D / (2 \Delta t (1/\Delta x^2 + 1/\Delta y^2)) \tag{5}$$

where  $D$  is the current (nonzero) value of the left hand side of Eq. (3).

At each time-step, pressure and velocity update iteration continues until the  $D$ s of all the cells are less than some prescribed small positive quantity  $\epsilon$ . The Eq. (4) are applied with an over-

relaxation parameter  $\omega$  between 1 and 2, a value near 1.8 often being optimal, in order to speed up the convergence of the pressure iteration process. Convergence to the steady-state solution is established by taking many forward time-steps.

## 2.5 Stability and Accuracy

The steady state solution is evolved from taking many forward time-steps, a recommendation being at least twice the average residence time of a typical particle passing through the flow domain, based on a simple 1-D flow analysis. Accuracy is enhanced by using small spatial and time intervals, at the expense of large computer time. When total time requirements necessitate a large grid size, it is not possible to resolve thin boundary layers along confining walls and free-slip BCs for tangential velocities are more appropriate than the more intuitively correct no-slip BCs.

Once the spatial subdivision is chosen, the time increment must be restricted in two ways. Firstly, it must be less than (typically equal to 0.25 to 0.33 times) the minimum cell transit time taken over all cells:

$$\Delta t < \min \left[ \frac{\Delta x}{|u|}, \frac{\Delta y}{|v|} \right] \tag{6}$$

Secondly, with a nonzero kinematic viscosity, momentum must not diffuse more than approximately one cell in one time-step, for which an estimate is:

$$v \Delta t < \frac{1}{2} \left[ \frac{\Delta x^2 + \Delta y^2}{\Delta x^2 + \Delta y^2} \right] \tag{7}$$

When the time-step is so restricted, the required amount of upstream (donor cell) differencing must be achieved by choosing  $\alpha$  slightly larger than (typically 1.2 to 1.5 times) the largest of the right hand side member of:

$$1 \geq \alpha > \max \left[ \frac{|u| \Delta t}{\Delta x}, \frac{|v| \Delta t}{\Delta y} \right] \tag{8}$$

where the maximum is taken over all cells. If  $\alpha$  is chosen to be too large, stability is being achieved at the expense of the introduction of an unnecessarily large amount of diffusion-like truncation errors (called numerical smoothing).

## 2.6 Boundary Conditions

Finite difference equations FEDs simulating the PDEs are set up and solved by way of a time-march process applied to cells within the flow domain of interest. Cells touching the boundary thus utilize the value on or just beyond the boundary.

Interior *normal* velocity calculations take the zero normal wall values, the given normal inlet or outlet values, or the yet-to-be-determined outlet values as appropriate BCs during their calculations.

Interior *tangential* velocity calculations use the fictitious values which are placed in the surrounding layer of complementary cells. Specification of these is after each time-step and after each sweep of the cell's during the pressure iteration. With a coarse grid, *free-slip* BCs are appropriate for tangential velocities, and external values are set equal to their associated immediately interior values. On the other hand, with a fine grid computing through the boundary layer, *no-slip* BCs are appropriate for tangential velocities and

external values are set equal to the negative of their associated immediately interior values.

Specification of normal velocities at an outflow boundary often poses a problem as it can have detrimental upstream influence. One might merely impose the zero-normal gradient or continuative condition and set these values equal to their immediately upstream values.<sup>12</sup> When primary interest is being focused on the final steady-state solution, it has been found<sup>13</sup> that a suitable constant may be added to each such extrapolated value, with advantage to the rapidity of convergence. This constant value is chosen so as to make the total outlet flux equal to the total inlet flux, thus ensuring the requirement of a macroscopic mass balance. Outlet boundary specification is imposed only after each time-step as computed via Eq. (2) and not after each pass through the mesh during the pressure iteration.

On an axis or plane of symmetry the usual zero normal velocity and free-slip axial velocity specification are applicable.

### 3. Predictions and Discussion

#### 3.1 Diffuser Effectiveness

Experimental tests<sup>1,2</sup> have included both non-uniform inlet profiles and varying quantities of bleed. Modifications to the usual effectiveness parameter are needed to characterize the situation correctly. Flow distortion is characterized by the flow distortion parameter,  $\alpha$ . This is defined as the kinetic energy flux of the given profile divided by the kinetic energy flux of the same flow quantity with a flat profile. Values larger than unity indicate flow distortion. The following equation may be used to compute  $\alpha$ :

$$\alpha = \frac{\int \rho V^3 dA / \rho dA^2}{[\int \rho V dA]^3} \quad (9)$$

where the integrations are taken across the flow passage. This parameter is of fundamental importance since it establishes the ideal diffuser static pressure rise coefficient, which for incompressible flow is:

$$C_{P_1} = \alpha_1 - \alpha_2 \left[ \frac{1-B}{A_R} \right]^2 \quad (10)$$

The diffuser effectiveness is the actual diffuser static pressure rise, divided by the ideal static pressure rise. Typically, the inlet flow to the diffuser is highly distorted with  $\alpha_1 = 1.22$  and  $u_m/u_{av} = 1.2$  [the maximum axial velocity is near the center], while the exit flow is far more uniform with  $\alpha_2$  and  $u_m/u_{av}$  taken near unity.

#### 3.2 Predictions

To demonstrate the capabilities of the solution scheme just described, predictions are now made and discussed for the case of the sudden expansion annular VCD with area ratio  $A_R = 3, 2$  and  $1.5$ . The inflow is taken to be highly distorted with  $\alpha_1 = 1.22$  as in the experimental data used for comparison.<sup>2</sup>

Predictions are first discussed for the case  $A_R = 2$ . The flow domain is overlaid with  $10 \times 28$  internal cell divisions in the  $x$ - and  $y$ -directions respectively, with aspect ratio  $\Delta y/\Delta x = 4$ . Transient computations are continued until steady state conditions establish themselves, roughly two flow-

field residence times later, corresponding to 300 time-steps, and requiring about 70 s of IBM 370/168 CP time. The number of pressure-velocity iterations required per time-step depends on the inlet nonuniformities and bleed magnitudes. Typically, it is initially about 150 and decreases to 1 as the final steady state solution is approached.

Figure 5 shows predictions of the velocity vector patterns in the  $xy$ -domain, with 0% and 16% bleed in Parts (a) and (b), respectively. Notice that with no bleed, there is a rather large corner

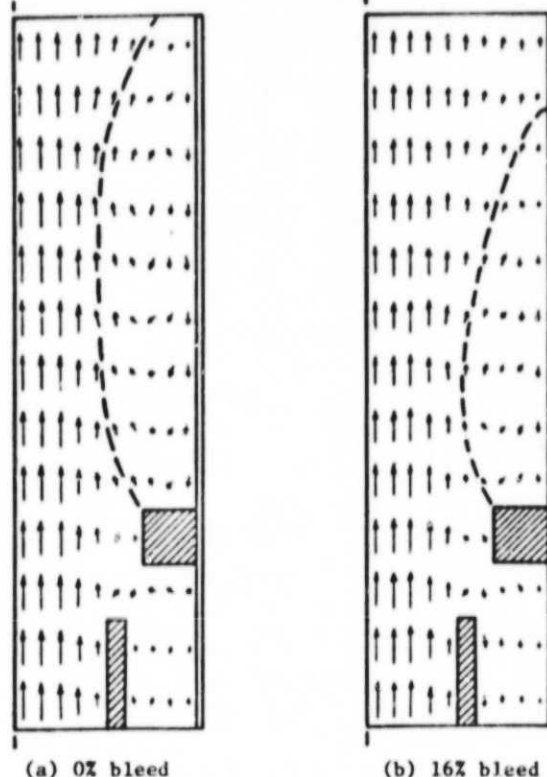


Fig. 5 Predicted velocity vector patterns with:  
(a) 0% bleed  
(b) 16% bleed  
[--- recirculation bubble boundary]

recirculation zone provoked by the sudden expansion. It is some distance downstream before the axial velocity profiles become more uniform. On the other hand, with 16% bleed, the inflow is encouraged to expand into the larger cross-sectional area and only a relatively small corner vortex region is to be seen. Axial velocity profiles become more uniform much more quickly in the downstream direction than was the case with no bleed. The dashed line on these vector velocity plots is approximately the zero streamline, which enclosed the corner recirculation bubble.

Vortex controlled diffuser performance prediction is illustrated in Figs. 6-8 for the area expansion ratios  $A_R = 3, 2$  and  $1.5$  respectively. In each case, VCD effectiveness is plotted as a function of downstream distance  $L/H$ , measured from the end of the primary duct. Each of the figures has three lines drawn, representing the cases of 0%, 8% and 12% bleed. The open symbols and solid lines are predicted; the closed symbols are corresponding experimental evidence.<sup>2</sup> The agreement is very

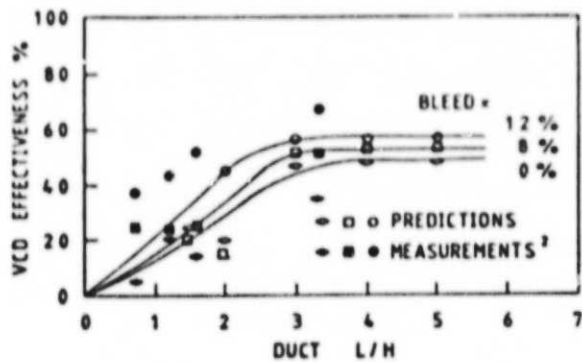


Fig. 6 VCD performance with area ratio  $A_R = 3$  and inlet flow distortion  $\alpha = 1.22$ .

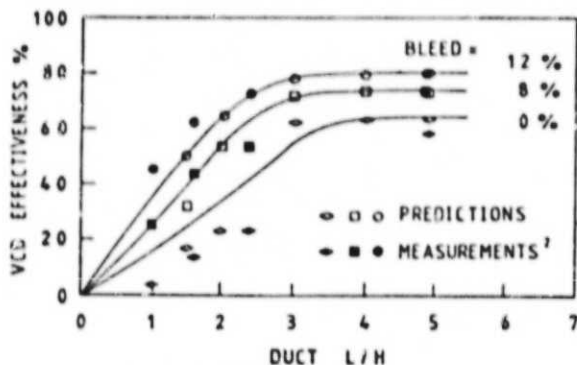


Fig. 7 VCD performance with area ratio  $A_R = 2$  and inlet flow distortion  $\alpha = 1.22$ .

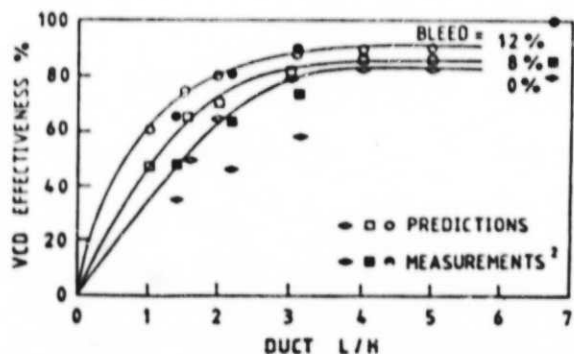


Fig. 8 VCD performance with area ratio  $A_R = 1.5$  and inlet flow distortion  $\alpha = 1.22$ .

satisfactory in view of the simplicity of the computer code being used for the simulation and the general trends are clearly evident.

An earlier study<sup>1</sup> asserts [but does not clearly

document] that when effectiveness is plotted against the percentage of main flow that is bled from the diffuser, there is a 'minimum bleed requirement'. Bleed percentages below this value are ineffective and, as this level is reached, there is a rather sudden increase in performance. Above this value only a slight further improvement is obtained. The present predicted results do not show this abrupt trend, and the onset of performance increase is far less dramatic. There is a continuous improvement in performance as the bleed percentage is increased. Figure 9 shows the details for the area ratio equal to two case, with curved of performance versus bleed. The two lines represent performance being characterized by values at locations  $L/H = 2$  and 3.

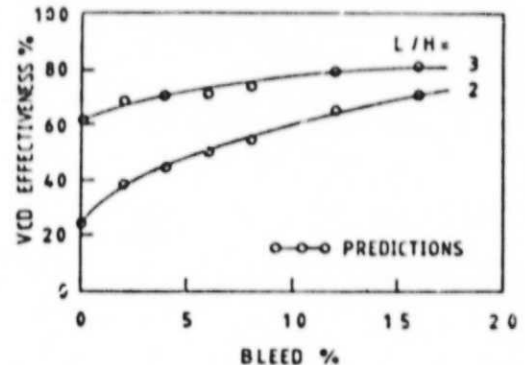


Fig. 9 VCD performance with area ratio  $A_R = 2$  and inlet flow distortion  $\alpha = 1.22$ .

#### 4. Conclusions

A simple prediction procedure for sudden expansion incompressible flows has been developed and applied to the vortex controlled diffuser. Based on the Los Alamos 2-D SOIA ideas, the transient Navier-Stokes equations of an incompressible fluid are solved via their associated finite difference equations directly in terms of primitive pressure-velocity variables. The technique is simplified to facilitate its use by persons with little or no experience in computational fluid dynamics, and boundary conditions, for example, are particularly simple to specify. The code thus represents a basic tool, to which user-oriented complexities and sophistications can easily be added as required. The results presented and discussed are extremely useful to the designer of vortex controlled diffusers for pre-combustor applications. Predicted results confirm that effectiveness increases with increases in duct length and bleed flow rate.

Other developments and applications of this finite difference technique currently in progress at Oklahoma State University include: inclusion of swirl and the two-equation  $k-\epsilon$  turbulence model into the present 2-D code, and laminar and turbulent 3-D codes for application to local destratification and dilution air cross-jets into main streams.

#### Acknowledgments

The authors wish to express their appreciation to NASA Lewis Research Center and Air Force Wright Aeronautical Laboratories for support via grant NAG 3-74.

References

1. Adkins, R. C., A Short Diffuser with Low Pressure Loss, in Fluid Mechanics of Combustion, (J. L. Dussourd, R. P. Lohmann and E. M. Uram, eds.) ASME, New York, 1974, pp. 155-169. [See also ASME J. of Fluids Engng., Sept. 1975.]
2. Verdouw, A. J., Performance of the Vortex-Controlled Diffuser (VCD) in an Annular Combustor Flowpath, in Gas Turbine Combustor Design Problems, (A. H. Lefebvre, ed.), Hemisphere-McGraw-Hill, New York, 1980, pp. 13-25.
3. Ringleb, F. O., Flow Control by Generation of Standing Vortices and the Cusp Effect, Report No. 317, Dept. of Aeronautical Engng., Princeton University, Princeton, NJ, July 1955.
4. Beatty, C. G., Diffuser Control by Trapped Vortices. Thesis, Cranfield Inst. of Tech., Cranfield, England, 1970.
5. Sutherland, G. D., An Investigation into the Flow of Vortex Diffusers. Thesis, Cranfield Inst. of Tech., Cranfield, England, 1972.
6. Kwan, W. C. T., The Use of Vortex Flow Control in Variable Geometry Combustion. Thesis, Cranfield Inst. of Tech., Cranfield, England, 1976.
7. Odgers, J. and Kreschmer, D., Design Features for a Pre-mixed Variable Area Combustor. Paper presented at 48th PEP AGARD Conf. on Variable GEometry and Multi-cycle Engines, Paris, France, Sept. 1976.
8. Adkins, R. C. and Elsaftawy, A. S., A Double Acting Variable Geometry Combustor. ASME Paper No. 79-GT-197, 24th Int. of Gas Turbine Conf., San Diego, CA., March 12-15, 1979.
9. Adkins, R. C., The Effect of Compressor Exit Flow Distribution on Air Placement in Annular Combustors, ASME Paper No. 78-GT-84, 23rd Int. Gas Turbine Conf., London, England, April 9-13, 1978.
10. Harlow, F. H., and Welch, J. E., Numerical Calculation of Time-Dependent Viscous Incompressible Flow of Fluid with Free Surface, (The MAC Method), Physics of Fluids, Vol. 8, 1965, pp. 2182-2189.
11. Amsden, A. A., and Harlow, F. H., The SMAC Method: A Numerical Technique for Calculating Incompressible Fluid Flows, Report LA-4379, 1970, Los Alamos Scientific Laboratory, Los Alamos, NM.
12. Hirt, C. W., Nichols, B. D., and Romero, N. C., SOLA: A Numerical Solution Algorithm for Transient Fluid Flows, Report LA-5882, Los Alamos Scientific Laboratory and the University of California, Los Alamos, NM, 1975.
13. Gosman, A. D. and Pun, W. M., Lecture Notes for course entitled "Calculation of Recirculating Flows," Report ETS/74/2, Dept. of Mechanical Engineering, Imperial College, London, 1974.
14. Patankar, S. V., Numerical Heat Transfer and Fluid Flow, McGraw-Hill, New York, 1980.
15. Sturgess, G. J., Gas Turbine Combustor Design Challenges for the 1980's, Paper AIAA-80-1285, Hartford, Conn., June 30-July 2, 1980.
16. Croft, D. R. and Lilley, D. G., Heat Transfer Calculations Using Finite Difference Equations, Applied Science Publishers, London, 1977.
17. Gupta, A. K. and Lilley, D. G., Flowfield Modeling and Diagnostics, Abacus Press, Tunbridge Wells, Kent, England, 1982 (in press).
18. Roache, P. J., Computational Fluid Dynamics, Hermosa, Albuquerque, NM, 1972.
19. Chow, C.-Y., An Introduction to Computational Fluid Mechanics, Wiley, New York, 1979.
20. Hinze, J. O., Turbulence, 2nd ed., McGraw-Hill, New York, 1975, p. 539.
21. Schlichting, H., Boundary Layer Theory, 6th ed., McGraw-Hill, New York, NY, 1968, p. 699.

Appendix A

The finite difference form of the Navier-Stokes equations is given as Eq. (2) with donor cell differencing in some of the terms. For completeness, the appropriate expressions are appended.

u-equation

$$FUX = \frac{1}{4\Delta x} [(u_{1,j} + u_{1+1,j})^2 + \alpha |u_{1,j} + u_{1+1,j}| (u_{1,j} - u_{1+1,j}) - (u_{1-1,j} + u_{1,j})^2 - \alpha |u_{1-1,j} + u_{1,j}| (u_{1-1,j} - u_{1,j})]$$

$$FUY = \frac{1}{4\Delta y} [(v_{1,j} + v_{1+1,j})(u_{1,j} + u_{1,j+1}) + \alpha |v_{1,j} + v_{1+1,j}| (u_{1,j} - u_{1,j+1}) - (v_{1,j-1} + v_{1+1,j-1})(u_{1,j-1} + u_{1,j}) - \alpha |v_{1,j-1} + v_{1+1,j-1}| (u_{1,j-1} - u_{1,j})]$$

$$FUC = \frac{1}{8(x_L + \Delta x(1-1))} [(u_{1,j} + u_{1+1,j})^2 + (u_{1-1,j} + u_{1,j})^2 + \alpha |u_{1,j} + u_{1+1,j}| (u_{1,j} - u_{1+1,j}) + \alpha |u_{1-1,j} + u_{1,j}| (u_{1-1,j} - u_{1,j})]$$

$$VISX = \nu \left[ \frac{1}{\Delta x^2} (u_{1+1,j} - 2u_{1,j} + u_{1-1,j}) + \frac{1}{\Delta y^2} (u_{1,j+1} - 2u_{1,j} + u_{1,j-1}) + \frac{1}{2\Delta x(x_L + \Delta x(1-1))} (u_{1+1,j} - u_{1-1,j}) - \frac{u_{1,j}}{(x_L + \Delta x(1-1))^2} \right]$$

v - equation

$$FVX = \frac{1}{4\Delta x} [(u_{i,j} + u_{i,j+1})(v_{i,j} + v_{i+1,j}) + \alpha |u_{i,j} + u_{i,j+1}| (v_{i,j} - v_{i+1,j}) - (u_{i-1,j} + u_{i-1,j+1})(v_{i-1,j} + v_{i,j}) - \alpha |u_{i-1,j} + u_{i-1,j+1}| (v_{i-1,j} - v_{i,j})]$$

$$FVY = \frac{1}{4\Delta y} [(v_{i,j} + v_{i,j+1})^2 + \alpha |v_{i,j} + v_{i,j+1}| (v_{i,j} - v_{i,j+1}) - (v_{i,j-1} + v_{i,j})^2 - \alpha |v_{i,j-1} + v_{i,j}| (v_{i,j-1} - v_{i,j})]$$

$$FVC = \frac{1}{8(x_L + \Delta x(1-1.5))} [(u_{i,j} + u_{i,j+1})(v_{i,j} + v_{i+1,j}) + (u_{i-1,j} + u_{i-1,j+1})(v_{i-1,j} + v_{i,j}) + \alpha |u_{i,j} + u_{i,j+1}| (v_{i,j} - v_{i+1,j}) + \alpha |u_{i-1,j} + u_{i-1,j+1}| (v_{i-1,j} - v_{i,j})]$$

$$VISY = \nu [\frac{1}{\Delta x^2} (v_{i+1,j} - 2v_{i,j} + v_{i-1,j}) + \frac{1}{\Delta y^2} (v_{i,j+1} - 2v_{i,j} + v_{i,j-1}) + \frac{1}{2\Delta x(x_L + \Delta x(1-1.5))} (v_{i+1,j} - v_{i-1,j})]$$

R	Ratio
1	Inlet
2	Outlet

Superscripts

n	Value at time-level t
(blank)	Value at time-level t + Δt

Nomenclature

A	Flow area, m <sup>2</sup>
A <sub>R</sub>	Diffuser area expansion ratio
B	Diffuser bleed flow fraction
C <sub>P1</sub>	Ideal diffuser static pressure rise coefficient
D	Divergence of velocity field, s <sup>-1</sup>
H	Channel height (width), m
i, j	Mesh point
L	Channel length, m
p	Ratio of pressure to constant density, Nm/kg
t	Time coordinate, s
u, v	Velocity components in x(=r), y coordinate directions, m/s
x, y	Cylindrical polar coordinates, m
Δp	Small finite p increment, Nm/kg
Δt	Small finite time increment, s
Δx, Δy	Small finite radial and axial distances, m
α	Donor cell upstream differencing parameter, flow distortion factor
ε	Small positive number
ν	Kinematic viscosity, m <sup>2</sup> /s
ρ	density, kg/m <sup>3</sup>
ω	Over-relaxation parameter
∇ <sup>2</sup>	Laplacian operator

Subscripts

av	Station average
ch	Chamber
i, j	Mesh point indexes
i	Inner
m	Station maximum
o	Outer

APPENDIX D

A BASIC CODE FOR THE PREDICTION OF TRANSIENT  
THREE-DIMENSIONAL TURBULENT FLOWFIELDS

A BASIC CODE FOR THE PREDICTION OF  
TRANSIENT THREE-DIMENSIONAL TURBULENT FLOWFIELDS

A. A. Busnaina  
Graduate Student  
School of Mechanical and Aerospace Engineering  
Oklahoma State University  
Stillwater, OK 74078                  Student Member ASME

and

D. G. Lilley  
Associate Professor  
School of Mechanical and Aerospace Engineering  
Oklahoma State University  
Stillwater, OK 74078                  Member ASME

ABSTRACT

A primitive pressure-velocity finite difference code has been developed to predict transient three-dimensional turbulent flow. The code is a simplified yet effective prediction procedure for use by persons with little experience in computational fluid dynamics, and into which user-oriented complexities can easily be added. The method is based on the transient two-dimensional Los Alamos SOLA prediction technique for laminar flows. Turbulence is simulated by means the two-equation  $k-\epsilon$  turbulence model; species diffusion and buoyancy are also included. Two applications of the code are presented to local destratification near the release structure of a reservoir and to the deflection of a jet entering normally into a uniform cross-flow. Predicted results exhibit good agreement with experimental data, showing that a useful characterization of fully three-dimensional flows is now available.

Paper for presentation at the Symposium on 3-D Turbulent Shear Flows to be held at the ASME Fluids Engineering Division 1982 Spring Meeting in St. Louis, Missouri, June 7-10, 1982.

NOMENCLATURE

$C_1$  k- $\epsilon$  model constant  
 $C_2$  k- $\epsilon$  model constant  
 $C_D$  k- $\epsilon$  model constant  
 $C_\mu$  k- $\epsilon$  model constant  
 $D_p$  Propeller diameter, m  
 $D^*$  Nondimensional propeller diameter,  $D^* = D_p/H$   
 $DF$  Dilution factor,  $DF = (\rho_r - \rho_2)/(\rho_1 - \rho_2)$   
 $E$  Constant in the log-law  
 $Frd$  Densimetric Froude number,  
 $Frd = v_p/[g(\Delta\rho/\rho_1)H]^{1/2}$   
 $g$  Gravitational acceleration,  $m/s^2$   
 $G$  Generation rate of turbulence energy,  
 $J/kg-s$   
 $H$  Total depth of model, m  
 $k$  Kinetic energy of turbulence per unit mass,  
 $J/kg$

$k_p$  Kinetic energy at point P  
 $K$  Constant in the log-law  
 $K^*$  Nondimensional propeller distance, normalized with respect to H.  
 $L$  Propeller depth below the surface, m  
 $l$  Length scale of turbulence, m  
 $L^*$  Nondimensional propeller depth,  $L^* = L/H$   
 $m_1$  Mass fraction of fluid of density  $\rho_1$   
 (epilimnion)  
 $m_2$  Mass fraction of fluid of density  $\rho_2$   
 (hypolimnion)  
 $p$  Time-mean static pressure deviation from hydrostatic pressure, Pa  
 $P$  Typical point in flowfield  
 $Q_p$  Propeller flow rate, kg/s  
 $Q_r$  Release flow rate, kg/s  
 $Q^*$  Nondimensional flow rate,  $Q^* = Q_p/Q_r$   
 $R$  Jet-to-crossflow velocity ratio,  $R = u_j/u_{in}$   
 $r_o$  Deflected jet radius, m  
 $S_k$  Source term for k  
 $S_\epsilon$  Source term for  $\epsilon$   
 $t$  Time, s

$u, v, w$	Time-mean velocity components in $x, y, z$ coordinate directions, m/s
$v_p$	Propeller velocity, m/s
$V_p$	Component of velocity parallel to the wall in the near wall region, m/s
$x, y, z$	Cartesian coordinates, m
$y_p$	Normal distance from nearby wall to point P, m
$Z_T$	Thermocline location (measured from the bottom), m
$Z_T^*$	Nondimensional thermocline location, $Z_T^* = Z_T/H$
$\epsilon$	Turbulent energy dissipation rate, $m^2/s^3$
$\mu$	Absolute viscosity, Pa.s
$\mu_t$	Turbulent viscosity, Pa.s
$\nu$	Kinematic viscosity, $m^2/s$
$\rho_1$	Epilimnion or top fluid density, $kg/m^3$
$\rho_2$	Hypolimnion or bottom fluid density, $kg/m^3$
$\rho_r$	Release fluid density, $kg/m^3$
$\sigma_k$	Schmidt number for $k$
$\sigma_\epsilon$	Schmidt number for $\epsilon$
$\sigma_{sc}$	Schmidt number
$\tau$	Turbulent stress tensor, $N/m^2$
$\phi$	General dependent variable

## INTRODUCTION

Existing 3-D turbulent flowfields prediction codes, although incorporating many complexities and being efficient in their solution algorithms, present a major struggle to the code user who is faced with the task of understanding, amending, and utilizing the available codes (1). There is a need for simplified techniques for persons with little or no experience in computational fluid dynamics CFD, and into which user-oriented complexities can easily be added. This paper presents a method which, in a computer program of approximately 450 statements, solves the fully 3-D time-dependent turbulent flow equations in cartesian coordinates. Turbulence is simulated by means of the two-equation  $k-\epsilon$  turbulence model (2), and species diffusion and buoyancy effects are properly simulated. The computational method is based on the transient 2-D Los Alamos SOLA prediction technique (3) [for laminar flows], which is a finite difference scheme based on the marker and cell method.

Consideration is given here to a primitive, pressure-velocity variable, finite difference code which has been developed to predict turbulent 3-D

transient flows. The technique used here incorporates the following:

1. A finite difference procedure is used in which the dependent variables are the velocity components and pressure, formulated in cartesian coordinates.
2. The pressure is deduced from the continuity equation and the latest velocity field, using a guess-and-correct procedure for the latter.
3. The procedure incorporates displaced grids for the three velocity components, which are placed between the nodes where pressure and other variables are stored.
4. The code is designed for persons with little or no experience in numerical fluid dynamics with the purpose of demonstrating that many useful and difficult problems can be solved without resorting to large, complicated computer programs. As specific complexities can be added easily, the program provides a basis for developing many new numerical capabilities. The present code incorporates the two-equation  $k-\epsilon$  turbulence model (4).

The paper presents recent work in the finite difference solution, via a primitive pressure-velocity code, of 3-D recirculating transient turbulent flowfields. The technique is for incompressible flow, and the complexities are restrained to a minimum so as to facilitate the use of the code and user-oriented complexities can be added as required. Two applications of the code are presented. The first is prediction of local destratification of reservoirs (5,6) which includes species diffusion and buoyancy forces, and the second application is prediction of the velocity field generated by a deflected turbulent jet, injected normally into a uniform cross-flow (7).

## THE PREDICTION PROCEDURE

### Governing Equations

Equations representing conservation of mass, momentum, species diffusion, turbulent kinetic energy and its dissipation rate are taken in conservative form in Cartesian coordinates (6) as:

$$\frac{\partial u_i}{\partial x_i} = 0 \quad (1)$$

$$\frac{\partial \phi}{\partial t} + \frac{\partial}{\partial x_i} (u_i \phi) = \frac{1}{\rho_1} \left[ \frac{\partial}{\partial x_i} \left( \frac{\mu_t}{\sigma} \frac{\partial \phi}{\partial x_i} \right) + S_\phi \right]$$

where  $\phi$  stands for any of the dependent variables  $u, v, w, m_1, k$  and  $\epsilon$ . The first three of these are time-mean velocity components  $u_i$  in the  $x_i$  directions [ $x, y$  and  $z$ ], respectively. A buoyancy term occurs in the vertical  $z$ -direction equation (6). The local mass fraction  $m_1$  of fluid of density  $\rho_1$  allows the local density to be found using

$$m_1 + m_2 = 1 \quad (2)$$

$$\rho = m_1 \rho_1 + m_2 \rho_2$$

Density changes are slight and allow incompressible equations to be used, with the addition of an upward buoyancy force. The viscosity is calculated from the standard  $k-\epsilon$  turbulence model (4)

$$\mu_t = C_\mu \rho k^2 / \epsilon \quad (3)$$

where  $k$  is the turbulence energy and  $\epsilon$  [ $= C_D k^{3/2} l$ ] is the energy dissipation rate, both of these being obtained from solution of partial differential equations.

The equations differ primarily in their Schmidt numbers  $\sigma_\phi$  and final 'source' terms  $S_\phi$ , as indicated in Table 1. The rate of generation of  $k$  by the action of velocity gradients is taken as

$$G = \mu_t \left( \frac{\partial u_i}{\partial x_j} + \frac{\partial u_j}{\partial x_i} \right) \frac{\partial u_i}{\partial x_j} \quad (4)$$

Turbulence and other constants appearing are given the usual recommended values:  $C_D = 1.0$ ,  $C_\epsilon = 0.09$ ,  $C_1 = 1.44$ ,  $C_2 = 1.92$ . These have been used in a wide variety of turbulent flow situations and exhibit good predictive capability (4).

TABLE 1

SCHMIDT NUMBERS AND SOURCE TERMS IN THE GENERAL EQUATION

$\phi$	$\sigma_\phi$	$S_\phi$
$u$	1	$-\frac{\partial p}{\partial x} + \frac{\partial}{\partial x_i} \left( \mu_t \frac{\partial u_i}{\partial x} \right)$
$v$	1	$-\frac{\partial p}{\partial x} + \frac{\partial}{\partial x_i} \left( \mu_t \frac{\partial u_i}{\partial y} \right)$
$w$	1	$-\frac{\partial p}{\partial z} + \frac{\partial}{\partial x_i} \left( \mu_t \frac{\partial u_i}{\partial z} \right) - g(\rho - \rho_1)$
$m_1$	1	0
$k$	1	$G - C_D \rho \epsilon$
$\epsilon$	1.3	$(C_1 G \epsilon - C_2 \rho \epsilon^2) / k$

#### The Grid System

The rectangular 3-D region to be considered is divided into rectangular cell divisions, with uniform  $\Delta x$ ,  $\Delta y$  and  $\Delta z$  spacings. This solution domain is complemented by a layer of cells on all sides, so as to allow easy simulation of the required boundary conditions. These fictitious cells increase the total number of cells in each direction. Figure 1 illustrates the total mesh arrangement, while Figure 2 portrays a single cell and shows the location of each field variable  $p$ ,  $u$ ,  $v$ ,  $w$  and  $m_1$  relative to this (I,J,K)-cell. Notice that pressure  $p$  and  $m_1$  are cell centered, as also are the turbulence quantities  $k$  and  $\epsilon$ . Velocities are located on the faces of the cell such that appropriate pressure gradients in their differential equations are readily found. Notice also that normal velocities lie directly on the physical boundaries of the solution domain, while the tangential velocities and pressure are displaced half a cell interval inside the flowfield. In this way the exterior fictitious cells are particularly convenient when applying the boundary conditions.

Figure 1 also represents the physical problem of the first application which contains a downward flowing jet of fluid from a propeller. Initially two fluids occupy positions above and below the interface [called 'thermocline'] as shown, so that their initial mass fractions are  $m_1 = 1$  and  $m_2 = 0$  (for  $z > Z_T$ , the height of the interface) and vice versa. Also shown is how the inlet and outlet flows are handled. The exit release flow is via a rectangular area in the release structure with the flow rate

specified a priori.

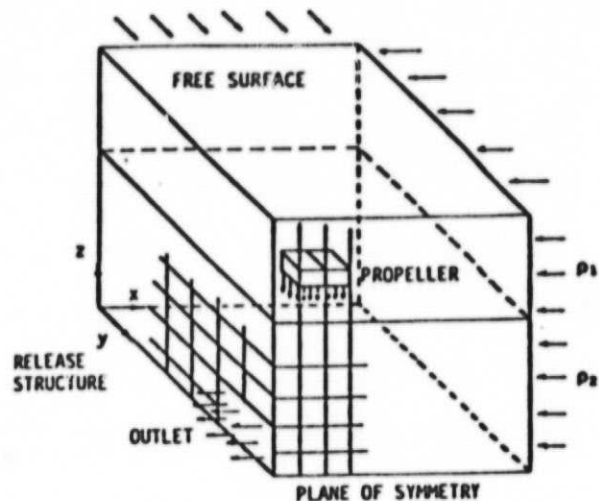


Fig. 1 Fully 3-D Cartesian Grid Schematic.

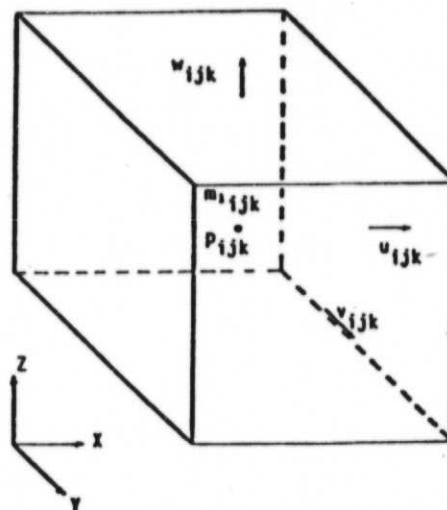


Fig. 2 Arrangement of Finite Difference Variables in a Typical Cell.

#### The Boundary Conditions

Finite difference equations simulating the problem are set up and solved by way of a time-march process applied to cells within the flow domain of interest. Cells touching the boundary thus utilize the value on the boundary (in the case of a normal velocity) or values half a cell distant beyond the boundary (in the case of tangential velocities).

Interior normal velocity calculations take the zero normal wall values, the given normal inlet values, on the yet-to-be-determined outlet values as appropriate boundary conditions during their calculations. Interior tangential velocity calculations use the fictitious values which are placed in the surrounding layer of complementary cells. Specification of these is after each time-step and after each sweep of the cells during the pressure iteration. With a coarse grid, free-slip boundary conditions are appropriate for tangential velocities, and external values are set

equal to their associated immediately interior values. On the other hand, with a fine grid computing through the boundary layer, *no-slip* boundary conditions are appropriate for tangential velocities and external values are set equal to the negative of their associated immediately interior values.

Specifications of normal velocities at an outflow boundary often poses a problem, as it can have detrimental upstream influence. One might merely impose the zero-normal gradient or continuative condition and set these values equal to their immediately upstream values (3). When primary interest is being focused on the final steady-state solution, it has been found (5) that a suitable constant may be added to each such extrapolated value, with advantage to the rapidity of convergence. This constant value is chosen so as to make the total outlet flux equal to the total inlet flux, thus ensuring the requirement of a macroscopic mass balance. Outlet boundary specification is imposed only after each time-step and not after each pass through the mesh during the pressure iteration.

At planes of symmetry the usual zero normal velocity and free-slip tangential velocity specification are applicable.

The inlet value for the turbulent kinetic energy  $k$  is taken as  $0.03u^2$  and the dissipation  $\epsilon$  is calculated from its definition [ $\epsilon = C_D k^{3/2}/l$ ] and the length scale of turbulence  $l$ , taken typically as 3 per cent of the characteristic size of the passage.

At a plane of symmetry both  $k$  and  $\epsilon$  are given the zero-gradient condition. At a wall,  $k$  is treated similarly but  $\epsilon$  values are specified just inside the computational field at a point  $P$  in the terms of the local value of  $k$  via (4)

$$p = \frac{C_\mu^{3/4} k_p^{3/2}}{K \cdot y_p} \quad (5)$$

Wall shear stress is evaluated via the modified log-law with the assumption of a constant shear region near the wall. Wall functions are employed in  $u$ ,  $v$ ,  $w$ ,  $k$  and  $\epsilon$  equations, using the recommended expressions (4)

$$v_p \frac{(C_\mu^{1/4} k_p^{1/2})}{(\tau/\rho)_w} = \frac{1}{K} \ln \left[ EC_\mu^{1/4} k_p^{1/2} y_p / \nu \right] \quad (6)$$

$$\frac{k_p}{(\tau/\rho)_w} = \frac{1}{C_\mu^{1/2}}$$

where the suffices  $w$  and  $p$  refer to the conditions at the wall and at the near-wall grid node respectively.  $K$  and  $E$  are constants used in the log-law of the wall, and possess the values 0.4186 and 9.793, respectively.

#### Solution Procedure

Finite difference representations are required of the governing partial differential equations. The usual intuitive estimates of one-sided first-derivatives, centered first-derivatives and centered second-derivatives are used in representing the momentum equations. Superscripts  $n$  and (blank) are used to denote values at time-level  $t$  and  $t + \Delta t$ , respectively. Portrayed now are equations enabling one such forward time-step to be accomplished. Thus, starting from initial field values throughout the domain of interest, a time-march process is used so as to advance toward the final steady-state solution,

which is usually of special interest as opposed to the en route calculations. In Eq. (1) the time-derivatives are approximated by forward one-sided derivatives; most spatial derivatives are approximated by central differences based on values at time-level  $t$ . Special techniques are required in computational fluid dynamics, however, in the representation of the convection terms, and a certain amount of upstream differencing is required.

The difference equations representing the partial differential equations may be written explicitly as:

$$\phi = \phi^n + \Delta t [---] \quad (7)$$

where  $\phi = u, v, w, m_1, k$  and  $\epsilon$ . Convection, diffusion and source terms occur in the parentheses on the right hand side. For the momentum equations the appropriate forms are given in Ref. 6. For the turbulence quantities  $k$  and  $\epsilon$ , similar terms occur and source term linearization is effected in the manner recommended for always positive variables [see Ref. 7, p. 145]. In all six of these forward marching equations, donor cell differencing is used with the convection terms. In this a coefficient  $\alpha$  takes a constant value between 0 and 1, so giving the desired amount of upstream differencing (3). A value of 0 gives merely central differencing as in the original MAC code and numerical instability problems arise; a value of 1 gives the full upstream or donor cell for which, although less accurate, is stable provided among other things that the fluid is not allowed to pass through more than one cell in one time-step, see the stability criterion of Eq. (11) and other conditions later.

Although Eq. (5) accomplishes one forward time-step based on conservation of momentum principles, the newly calculated velocities will not, in general, satisfy the continuity requirement, as expressed by the central finite difference form of the continuity equation (the first of Eq. (1)):

$$\frac{1}{\Delta x} (u_{ijk} - u_{i-1,j,k}) + \frac{1}{\Delta y} (v_{ijk} - v_{i,j-1,k}) + \frac{1}{\Delta z} (w_{ijk} - w_{i,j,k-1}) = 0 \quad (8)$$

Terms here are evaluated at time-level  $t + \Delta t$ . This incompressibility condition is imposed by iteratively adjusting the cell pressure. That is, if the divergence  $D$  of a cell is positive (the left hand side of Eq. (8) is positive) there is a net mass outflow from that cell. This is corrected by reducing the cell pressure. If the divergence is negative, an increase in cell pressure is appropriate.

When a cell pressure changes from  $p$  to  $p + \Delta p$ , the velocity components on the 6 faces of that cell change, given from a linear analysis from Eq. (7), by the amounts:

$$\begin{aligned} u_{i,j,k} &= u_{i,j,k} + \Delta t \Delta p / (\Delta x \rho_1) \\ u_{i-1,j,k} &= u_{i-1,j,k} - \Delta t \Delta p / (\Delta x \rho_1) \\ v_{i,j,k} &= v_{i,j,k} + \Delta t \Delta p / (\Delta y \rho_1) \\ v_{i,j-1,k} &= v_{i,j-1,k} - \Delta t \Delta p / (\Delta y \rho_1) \\ w_{i,j,k} &= w_{i,j,k} + \Delta t \Delta p / (\Delta z \rho_1) \\ w_{i,j,k-1} &= w_{i,j,k-1} - \Delta t \Delta p / (\Delta z \rho_1) \end{aligned} \quad (9)$$

Substitution of these in Eq. (8) yields the amount of correction to  $p$  required as:

$$p = -\rho_1 D / [2 \Delta t (1/\Delta x^2 + 1/\Delta y^2 + 1/\Delta z^2)] \quad (10)$$

where  $D$  is the current (nonzero) value of the left hand side of Eq. (8). Pressure update iteration until the  $D$ s of all the cells are less than some prescribed small positive quantity. The Eq. (9) are applied with an over-relaxation factor  $\omega$  between 1 and 2, a value near 1.8 often being optimal, in order to speed up the convergence of the pressure iteration process. After the continuity equation is sufficiently well satisfied, the values are accepted as new-time values and preparation for the next step of the time-march can begin.

#### Stability and Accuracy

Accuracy is enhanced by using small spatial and time intervals, at the expense of large computer time. When total time requirements necessitate a coarse grid, it is not possible to resolve thin boundary layers along confining wall and free-slip BCs for tangential velocities are more appropriate with linear finite difference approximations than the expected viscous flow no-slip BCs.

Once the spatial subdivision is chosen, the time increment must be restricted in two ways. Firstly, it must be less than (typically equal to 0.25 to 0.33 times) the minimum cell transit time taken over all cells:

$$\Delta t < \min \left\{ \frac{\Delta x}{|u|}, \frac{\Delta y}{|v|}, \frac{\Delta z}{|w|} \right\} \quad (11)$$

Secondly, with a nonzero kinematic viscosity, momentum must not diffuse more than approximately one cell in one time-step, for which an estimate (3) is:

$$\nu \Delta t < \frac{1}{2} \min \left\{ \Delta x^2, \Delta y^2, \Delta z^2 \right\} \quad (12)$$

A similar criterion is given in Ref. 6.

When the time-step is so restricted, the required amount of upstream (donor cell) differencing must be achieved by choosing  $\alpha$  slightly larger than (typically 1.2 to 1.5 times) the largest of the right hand side member of:

$$1 \geq \alpha > \max \left\{ \frac{|u|\Delta t}{\Delta x}, \frac{|v|\Delta t}{\Delta y}, \frac{|w|\Delta t}{\Delta z} \right\} \quad (13)$$

where the maximum is taken over all cells. If  $\alpha$  is chosen to be too large, stability is being achieved at the expense of the introduction of an unnecessarily large amount to diffusion-like truncation errors (called numerical smoothing).

#### APPLICATIONS AND DISCUSSION

In order to demonstrate the capability of the code just described, two applications are now given. In each case, predictions are given via the use of the recommended values (4) of the empirical constants in the turbulence model. Typically a rather coarse grid system is used in the demonstrations, although clearly finer meshes are needed if accuracy is paramount. Approximately 10 minutes of IBM 370/168 CP time is required to allow the final steady state solution to evolve. Results presented are demonstrative of the qualitative predictions currently available.

#### Local Destratification of Reservoirs

The Garton pump consists of a low-energy axial flow propeller placed just below the surface so as to provide a downward directed jet of fluid and thereby locally mix reservoirs near the release structure of

the dam. In this way high-quality epilimnion water is transported downwards, so obtaining local destratification and improved release water quality in the vicinity of low-level release structures. The flowfield is fully three-dimensional and the solution procedure needs to include species diffusion and buoyancy forces. Figure 3 shows a schematic of the mixing so produced when there is no exit beneath the propeller. The jet

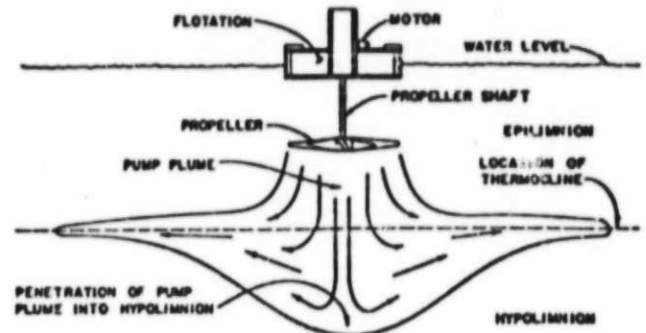


Fig. 3 Schematic of a Typical Propeller Pump and the Flowfield Produced Without Exit Flow.

or plume penetrates some distance below the level of the thermocline. Figure 4 illustrates the practical application of localized mixing in the proximity of the release structure of a dam with low-level release gate. The flowfield so produced is fully three-dimensional. Earlier work by the authors (5) was restricted to this axisymmetric formulation about a vertical

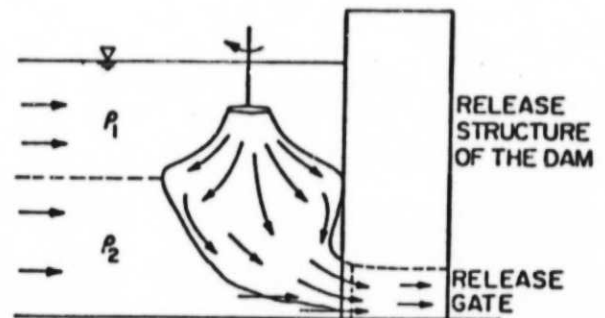


Fig. 4 Schematic of a Typical Propeller Pump and the Flowfield Produced With Exit Flow Via a Low Level Release Structure.

axis; and good results were portrayed for cases in which the propeller was close to the release structure. More recently, a three-dimensional version (6) has been developed using a constant eddy viscosity model, based on round turbulent free jet theory. Comparison of those predictions with the main source of experimental data (8) confirmed that the main dynamic effects are modeled better than the previous two-dimensional predictions. The present study extends the three-dimensional simulation to include turbulent mixing via the two-equation  $k-\epsilon$  turbulence model.

For the numerical simulation, a grid system of

7x5x9 internal cells (in x, y and z directions, respectively) is employed. [This corresponds to 10x8x12 grid lines]. No slip boundary conditions with the wall function approach are taken at the vertical dam wall and the horizontal floor of the reservoir. Free slip conditions are taken at the free surface, which is also assumed to maintain a constant height. The propeller is positioned sufficiently far beneath the surface for surface effects to be neglected. Velocities are specified a priori with flat profiles at the propeller and exit locations. Use is made of the plane of symmetry through the center of the propeller and the exit; free slip conditions are applied there. The available volume of the flow domain is very limited. To allow the outlet of release water without dramatically decreasing the fluid level, there is a compensating incoming flow which is distributed among the top and bottom layers in amounts equal to the epilimnetic and hypolimnetic water released. The peripheral inflow is at all elevations in such a way that epilimnetic water enters into the upper layer and does not disturb the density profile. The large area of inflow allows it to be at a low velocity in order to avoid any disturbance to the flowfield. Similarly, hypolimnetic water is fed into the bottom layer.

The dilution factor DF (release water quality) is found to be a function of turbulent viscosity  $\mu_t$ , densimetric Froude number  $Fr_d$ , nondimensional thermocline height  $Z_T^*$ , nondimensional flow rate  $Q^*$ , and nondimensional propeller diameter  $D^*$ , horizontal distance  $K^*$  and depth  $L^*$ . Results are now discussed about the application of the present 3-D turbulent code to this problem with the following base values of the parameters:  $Fr_d = 2.0$ ,  $D^* = 0.131$ ,  $K^* = 0.211$ ,  $L^* = 0.211$ ,  $Q^* = 2.6$ ,  $Z_T^* = 0.6$ . These values are taken so as to represent the same conditions as the available experimental data (8).

The rate of progress of the transient computations toward the steady state solution is illustrated in Fig. 5. Prediction of the dilution factor DF as a function of iteration time is shown for both a laminar and a turbulent flow with k- $\epsilon$  model. The latter approach is closer to the experimental evidence. It may also be noted that steady state conditions have established themselves in approximately 17 seconds [corresponding to about 320 forward steps].

In Figure 6 the dilution factor DF is shown to be a strong function of the densimetric Froude number

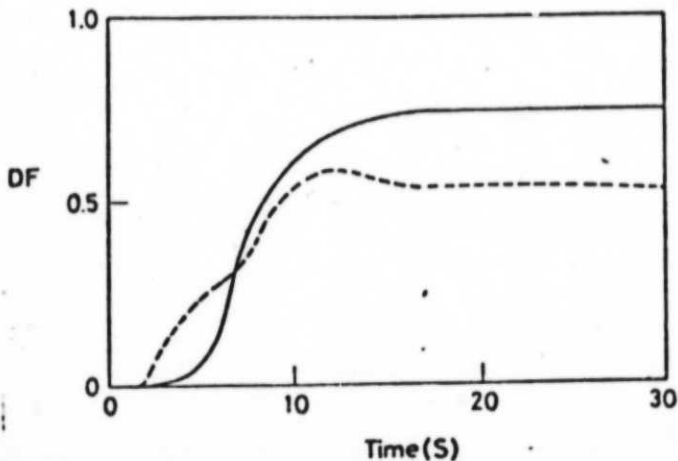


Fig. 5 Prediction of Dilution Factor DF as a Function of a Time [— Turbulent, --- Laminar]

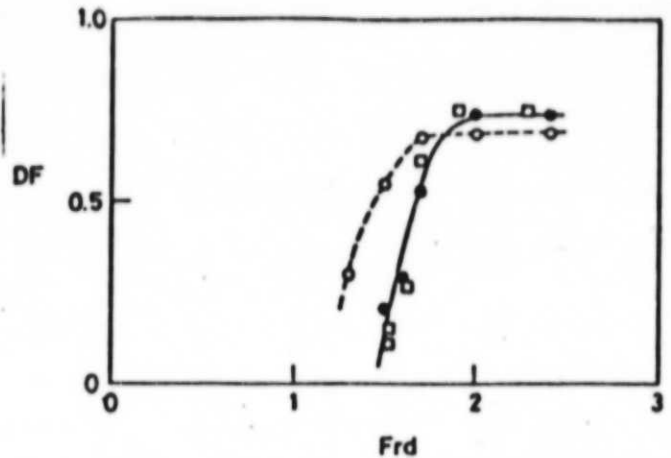


Fig. 6 Dilution Factor DF as a Function of Froude Number  $Fr_d$  [□ Experiments (8), ● Predictions with k- $\epsilon$  Model, ○ Predictions with Constant Viscosity].

$Fr_d$  in both predictive and laboratory data. The above base values are retained for the other parameters. The general result is that release water quality (fraction of epilimnetic (top) water in the exit stream) increases with higher values of the Froude number, such conditions being achieved with higher jet velocities from the propeller and/or a lower degree of stratification in the lake. The figure clearly shows the difference between the use of a constant eddy viscosity model and the k- $\epsilon$  turbulence model: the former under-predicting the release water quality and the latter giving more accurate predictions when compared to the experimental data. From the designer's view, the important result is the Froude number at which the dilution factor rises sharply, since that determines the velocity required at the propeller for the given conditions. Clearly the 3-D turbulent simulation is superior to the constant eddy viscosity model, and this Froude number is predicted better via this approach. The computations were performed with the standard k- $\epsilon$  turbulence model for the mixing. The influence of buoyancy was via the buoyancy term in the vertical momentum equation. No attempt has been made to include the effects of buoyancy on the generation rates of the turbulence parameters  $k$  and  $\epsilon$ , a practice advocated elsewhere (9,10), since there is as yet no adequate generalization of the rather meagre evidence.

#### Deflected Turbulent Jet

An interesting three-dimensional problem arises when a turbulent jet enters normally into a uniform steady cross-flow. Figure 7 shows a schematic of the problem, which has previously been discussed (7), predicted (11) and experimentally investigated (12-15). Such problem configurations arise in chimney plumes, flow under a V/STOL aircraft, film cooling and dilution air mixing in combustor applications. Clearly the problem is more complicated than corresponding free jet flows into quiescent surroundings, which are axisymmetric parabolic problems. Earlier predictions (11) utilized a proprietary three-dimensional implicit computer code to obtain steady state predictions. This sophisticated code is more complicated to use than the present code. Moreover, it is not generally available. Hence the capability of the present straightforward explicit solution scheme is now illustrated for this problem.

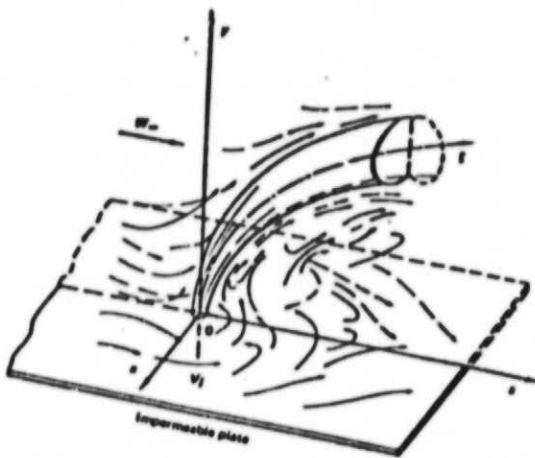


Fig. 7 Schematic of the Deflected-Jet Problem (7).

The simulation is for the turbulent jet of inlet velocity  $u_j$ , see Fig. 7. Use is made of the vertical symmetry plane. A horizontal top plane is located 18 jet radii above the bottom plane. A grid system of  $7 \times 9 \times 9$  internal cells (in  $x$ ,  $y$  and  $z$  directions, respectively) is used. Uniform steady cross-flow is specified at the upstream plane of the main inflow with velocity  $u_{in}$ . The usual zero normal gradients are taken at the exit plane. Free slip boundary conditions are used on the top, bottom, and side planes.

Figure 8 shows the predicted velocity vectors in the  $yz$ -plane through  $x = 0$ . This gives a clear indication of the behavior, magnitude and direction of the deflected jet. These predictions are for the jet to cross-flow velocity ratio  $R = u_j/u_{in} = 4$ , and the standard values in the  $k-\epsilon$  turbulence model are used (4). Velocity vector plots of this type allow the jet trajectory [the line joining points of maximum velocity] to be determined.

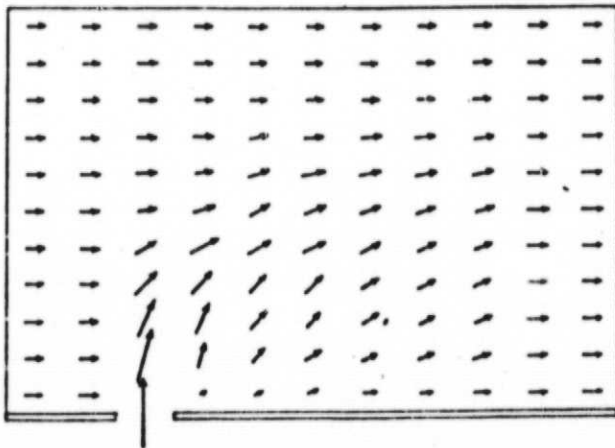


Fig. 8 Velocity Vectors in  $yz$ -Plane at  $x = 0$  Showing Magnitude and Direction of the Jet [for Velocity Ratio  $R = u_j/u_{in} = 4$ ].

Experimental work for comparison purposes includes Jordinson (12), Keffer and Baines (13) [who studied the structure of turbulence], Ramsey and Goldstein (14) [who presented velocity and temperature plots in cross-sectional and symmetry planes], and Chassaing et al (15) [who studied both cylindrical and co-axial jets]. The predicted effect of jet to cross-flow velocity ratio  $R$  on jet trajectories is illustrated in Figure 9 with appropriate experimental data for comparison. Earlier predictions (11) are very much in agreement with the present study. Considering the scatter in the data, the quality of the predictions is very good, thus confirming that the main dynamic and turbulence mixing effects are modeled adequately in the present code.

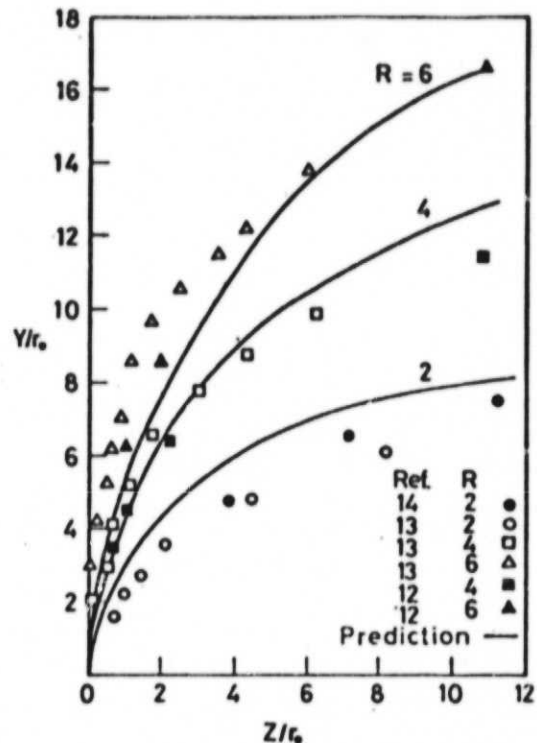


Fig. 9 Location of the Jet Centerline for Different Jet-to-Crossflow Velocity Ratios  $R = u_j/u_{in}$ .

#### CONCLUSIONS

A prediction procedure for fully 3-D transient turbulent flows has been developed. Based on the Los Alamos 2-D SOLA ideas, the transient Reynolds equations of an incompressible fluid are solved via their associated finite difference equations directly in terms of the primitive pressure velocity variables. Eddy viscosity is calculated via the  $k-\epsilon$  two-equation turbulence model. Species diffusion and buoyancy forces are included. The technique is simplified to facilitate its use by persons with little or no experience in computational fluid dynamics, and boundary conditions, for example, are particularly simple to specify. The code thus represents a basic tool, to which user-oriented complexities and sophistications can easily be added as required.

## ACKNOWLEDGMENTS

The authors wish to express their appreciation to OVRT/OWRRI, NASA and AFWAL for support of their research studies.

## REFERENCES

- 1 Lilley, D. G., "Flowfield Modeling in Practical Combustors: A Review," Journal of Energy, Vol. 3, No. 4, July-August 1979, pp. 193-210.
- 2 Launder, B. E. and Spalding, D. G., Mathematical Models of Turbulence, Academic Press, London, 1972.
- 3 Hirt, C. W., Nichols, B. D. and Romero, N. C., "SOLA - A Numerical Solution Algorithm for Transient Fluid Flows," Report LA-5852, 1975, Los Alamos Scientific Laboratory, Los Alamos, NM.
- 4 Launder, B. E. and Spalding, D. G., "The Numerical Computation of Turbulent Flow," Computer Methods in Applied Mechanics and Engineering, Vol. 3, 1974, pp. 269-289.
- 5 Busnaina, A. A., Lilley, D. G., and Moretti, P. M., "Prediction of Local Destratification of Lakes," Journal of Hydraulics Division, ASCE, HY3, Proc. Paper 16094, March 1981, pp. 259-272.
- 6 Busnaina, A. A. and Lilley, D. G., "Computer Prediction of Local Destratification Near Low-Level Release Structures of Reservoirs," Paper No. 81-FE-11 presented at the ASME Fluids Engineering Division 1981 Spring Meeting, Boulder, Colorado, June 22-24, 1981.
- 7 Patankar, S. V., Numerical Heat Transfer and Fluid Flow, Hemisphere-McGraw-Hill, New York, 1980.
- 8 Moon, J. J., "Enhancement of Release Water Quality by Localized Mixing - A Hydraulic Model Study," Thesis presented to the Oklahoma State University at Stillwater, OK, in 1978, in partial fulfillment of the requirements for the degree of Master of Science.
- 9 Hossain, M. S. and Rodi, W., Influence of Buoyancy on the Turbulence Intensities in Horizontal and Vertical Jets in Heat Transfer and Turbulent Buoyant Convection, Studies and Applications for Natural Environment, Buildings, Engineering Systems, (D. B. Spalding and N. Afgan, eds.) Hemisphere Publishing Corp., Washington, DC, USA, 1977.
- 10 Rodi, W., Turbulence Models and Their Application in Hydraulics, Book Publication of the International Association for Hydraulic Research, Delft, The Netherlands, 1980.
- 11 Patankar, S. V., Basu, D. K., and Alpay, S. A., "Prediction of the Three-Dimensional Velocity Field of a Deflected Turbulent Jet," Journal of Fluids Engineering, Vol. 99, 1977, pp. 758-762.
- 12 Jordinson, R., "Flow in a Jet Directed Normal to the Wind," Aeronautical Research Council, R&M No. 3074, 1958.
- 13 Keffer, J. F. and Baines, W. D., "The Round Turbulent Jet in a Cross-Wind," Journal of Fluid Mechanics, Vol. 15, Pt. 4, 1963, pp. 481-496.
- 14 Ramsey, J. W. and Goldstein, R. S., "Interaction of a Heated Jet with Deflecting Stream," NASA CR-72613, HTL TR No. 92, April 1970.
- 15 Chassaing, P., "Physical Characteristics of Subsonic Jets in a Cross-Stream," Journal of Fluid Mechanics, Vol. 62, Part 1, 1973, pp. 41-64.

APPENDIX E

COMPUTER MODELING IN RAMJET COMBUSTORS

AIAA 80-1189R

# Computer Modeling in Ramjet Combustors

ORIGINAL PAGE IS  
OF POOR QUALITY.

David G. Lilley\*

Oklahoma State University, Stillwater, Okla.

## Abstract

**P**ROBLEMS and progress in the simulation and solution of complex turbulent reacting flows for ramjet combustor applications are surveyed. The full paper reviews the difficulties, discusses developments, and demonstrates that useful predictions are already being made to aid designers. Areas in which further detailed numerical prediction research will be most useful include (for the nonreacting case) recirculation zone characterization, turbulence simulation in swirling recirculation flow, irregular boundary representation (via analytical or numerical transformation techniques or finite element methods), and further complexities and parameter influences; and (for the reacting case) the simulation of complex chemistry, the turbulence/chemistry/spray interaction problem, and application to realistic three-dimensional problems.

## Contents

The basic ramjet combustor configuration is the so-called sudden expansion dump combustor. In this type of combustor, liquid fuel is sprayed into the ram air upstream of the dump station, although it may also be injected directly into the chamber via side-wall inlets. Primary flame stabilization is provided by the flow recirculation regions, which may be supplemented, at the expense of total pressure loss, with mechanical flameholding devices at the air inlet/combustor interface and/or the presence of inlet air swirl, obtained by the use of tangential injection or swirl vanes. The flow throughout is multiphase, subsonic, turbulent, and involves large-scale corner recirculation zones. With strong swirl in the inlet flow a central toroidal recirculation zone (a recirculation bubble in the middle of the chamber near the inlet) also presents itself. Even gross features of the flow are not known quantitatively with certainty: for example, factors affecting the existence, size, and shape of the recirculation zones.<sup>1</sup>

The designer has a formidable problem in aerothermochemistry, and the modeling task is to provide a route which leads to the accomplishment of design objectives more quickly and less expensively than current practice permits. Some combustor modeling problems are 1) physical processes: turbulence, radiation, combustion, and multiphase effects; 2) computer programs: 0-, 1-, 2-, and 3-D approaches in steady-state and transient cases; 3) unresolved problems: irregular boundary representation, effect of swirl, recirculation, and wall proximity on turbulence, turbulence—reaction interaction, multiphase simulation.

Current combustor design and development problems, the needs of the combustion engineer in practice, and proposed research tasks which will assist in the attainment of design

objectives are becoming clear. Improvements and new developments (both experimental and theoretical) can and should be made, theoretical modeling being aided by specific carefully chosen experiments being performed.

Mathematical models of steadily increasing realism and refinement are being developed, both in the dimensionality of the model (together with the computational procedures) and in problems associated with the simulation of the physical processes occurring. In the modeling and prediction of swirl flow combustion, one is involved with simulating the problem via simultaneous nonlinear partial differential equations. These may be parabolic (boundary layer type) but are more often elliptic (recirculating type) and the solution scheme differs according to the category.

Because application of the general partial differential equations is complex, time-consuming, and in a development stage, simplified approaches to the problem are extremely popular. The most common models include perfectly stirred reactors (PSRs), well-stirred reactors (WSRs), and plug flow reactors (PFRs). Models differ in how these are interrelated to simulate various aspects of the mixing/reaction taking place. An important problem in finite rate chemistry is choosing an appropriate level of complexity, in view of the large number of species and chemical reactions taking place. One solution to this problem is the use of the quasiglobal reaction scheme whose key element is a unidirectional subglobal oxidation step. Coupled with this are a number of intermediate reversible reactions. The model affords a useful computer time saving as compared to a full finite-rate chemical kinetics formulation. Well-known models are categorized as integral, modular, or hybrid. Modular<sup>2,3</sup> methods give useful qualitative trend predictions and, when amalgamated with finite difference flowfield predictions via 2-D axisymmetric<sup>4</sup> or fully 3-D approaches,<sup>5</sup> excellent results are available.

Most combustion systems exhibit recirculation, and full flowfield prediction requires iterative solution techniques. Axisymmetric simulations give rise to 2-D elliptic problems and involve 2-D storage, stream function-vorticity  $\psi-\omega$  or primitive pressure-velocity  $p-u-v$  formulation, and Gauss-Seidel point-by-point iteration or line-by-line SIMPLE (semi-implicit method for pressure linked equations) iteration procedures, the line methods involving the TDMA (tridiagonal matrix algorithm). The essential differences between the various available computer codes include the following: the complexity of the equation set for the simulation of the physical processes, the storage requirements, the location of variables in the grid space system, the method of deriving the finite-difference equations that are incorporated, and the solution technique. In primitive pressure-velocity variable formulations a staggered grid system is normally used, as recommended by Los Alamos for its special attributes. In computational fluid dynamics the "best" representation of the convection and diffusion terms is essential to the accuracy and convergence of the iteration scheme. At high cell Reynolds numbers a certain degree of "upstream differencing" is essential, using, for example, these techniques: upwind differencing, a hybrid formulation or the Los Alamos zip, donor cell, etc. Sample recent numerical prediction studies include Refs. 6 and 7 for the  $\psi-\omega$  approach and Refs. 8 and 9 for the  $p-u-v$  approach. Excellent trade-off between code complexity and quality of flowfield

Presented as AIAA Paper 80-1189 at AIAA/SAE/ASME 16th Joint Propulsion Conference, Hartford, Conn., June 30-July 2, 1980; submitted Sept. 11, 1980; synoptic received May 28, 1981. Copyright © 1980 by David G. Lilley. Published by the American Institute of Aeronautics and Astronautics with permission. Full paper available from AIAA Library, 555 West 57th St., New York, N.Y. 10019. Price: Microfiche, \$3.00; hard copy, \$7.00. Remittance must accompany order.

\*Associate Professor, School of Mechanical and Aerospace Engineering, Associate Fellow AIAA.

patterns is available via the axisymmetric approach. For example, in Ref. 9 computational results show the interesting effects of several combustor design parameters, such as degree of swirl, performance of a recirculation zone amplifier ("trip"), and effect of laterally induced secondary air supply on subsequent flowfield development and combustor performance (for example, velocity, temperature, and composition distributions, the occurrence of recirculation zones, and flame size, shape, and combustion intensity).

Practical ramjet combustor designs exhibit many nonaxisymmetric features mainly because of air and fuel inlets at discrete circumferential locations. The requirement to predict a fully 3-D flowfield arises. Recent significant contributions to 3-D combustor flowfield prediction are exemplified in Refs. 5 and 10-13, where application has been to the furnace and gas turbine fields. Computationally, the techniques are very similar, except handling very high combustion intensities in the latter case causes additional problems. Implicit techniques for 3-D flows with recirculation have the advantage of efficiency and stability in their computations. All the work cited is implicit in character and solves directly for pressure and velocities; a staggered mesh system is used and some degree of upstream differencing is used for the convection terms at high cell Reynolds numbers. Perhaps Ref. 5 is the most ambitious in being a hybrid technique. The finite difference solution of some 30 partial differential equations on a  $27 \times 18 \times 7$  grid system provides input to a modular approach which handles realistic chemical kinetics, with presently 13 species undergoing 18 reactions. Encouraging results are portrayed for a variety of flow types.

In deciding and justifying the use of a particular procedure, one has some deliberation. One of the objectives of the present full paper was to clarify the choice and give appropriate advice, emphasizing computer application where appropriate. For example, at the present time the usefulness of a fully 3-D computer code in practice is not clear. Again, recent discussions have doubted the industrial value of this, especially when current practice and many problem areas involve use of 0-D and 1-D models, as successful application of modular and hybrid schemes reveal. The 2-D and 3-D approaches do possess the possibility of being eventually capable of a higher degree of realism, but model accuracy is in doubt, time and cost requirements are large and, more specifically, many current needs do not demand them.

Model experiments designed to highlight specific subproblems and their interactions (and not complex combustor flows) should receive attention for model development and validation. Computational results show some of the interesting effects of combustor design parameters on subsequent flowfield development and combustor performance. Computational experiments can be, should be, and have been performed which complement test cell data describing the internal flowfield characteristics. Theoretically, it is in the area of parameter influences that computer programs show their supremacy in terms of time and cost savings as compared

with experimental work. Progress will lead to more realistic and cost-effective practical combustor modeling. This, and continued development on the accuracy of the simulation of the physical processes involved, should elevate computer modeling to an established place in practical combustor design and development programs.

## References

- <sup>1</sup>Gupta, A. K., Lilley, D. G., and Syred, N., *Swirl Flows*, Abacus Press, London, England, to be published, 1982.
- <sup>2</sup>Hammond, D. C. Jr. and Mellor, A. M., "A Preliminary Investigation of Gas Turbine Combustor Modelling," *Combustion Science and Technology*, Vol. 2, 1970, p. 67.
- <sup>3</sup>Mosier, S. A. and Roberts, R., "Low-Power Turbo-Propulsion Combustor Exhaust Emissions," Vol. III Analysis, AFAPL-TR-73-36, Vol. III, 1974 [see also Vols. I and II].
- <sup>4</sup>Harsha, P. T. and Edelman, R. B., "Application of Modular Modeling to Ramjet Performance Prediction," AIAA Paper 78-944, July 1978.
- <sup>5</sup>Swithenbank, J., Turan, A., and Felton, P. G., "3-Dimensional 2-Phase Mathematical Modeling of Gas Turbine Combustors," *Gas Turbine Combustor Design Problems*, edited by A. H. Lefebvre, Hemisphere-McGraw-Hill, New York, 1980, pp. 249-314.
- <sup>6</sup>Anasoulis, R. F., McDonald, H., and Buggeln, R. C., "Development of a Combustor Flow Analysis, Part 1: Theoretical Studies," Tech. Rept. AFAPL-TR-98, Part 1, Air Force Aero Prop. Lab., Air Force Systems Command, Wright-Patterson AFB, Ohio, Jan. 1974 (see also Parts 2 and 3).
- <sup>7</sup>Peck, R. E. and Samuelsen, G. S., "Eddy Viscosity Modeling in the Prediction of Turbulent Backmix Combustion Performance," *16th Symposium (International) on Combustion*, The Combustion Institute, Pittsburgh, Pa., 1977, pp. 1675-1687.
- <sup>8</sup>Khalil, E. E., Spalding, D. B., and Whitelaw, J. H., "The Calculation of Local Flow Properties in Two-Dimensional Furnaces," *International Journal of Heat and Mass Transfer*, Vol. 18, 1975, pp. 775-791.
- <sup>9</sup>Novick, A. S., Miles, G. A., and Lilley, D. G., "Modeling Parameter Influences in Gas Turbine Combustor Design," *Journal of Energy*, Vol. 3, Sept.-Oct. 1979, pp. 257-262.
- <sup>10</sup>Patankar, S. V. and Spalding, D. B., "Simultaneous Predictions of Flow Pattern and Radiation for Three-Dimensional Flames," *Heat Transfer in Flames*, edited by N. H. Afgan and J. M. Beer, Scripta Book Co. (Hemisphere-Wiley), Washington, D.C., 1974, pp. 73-94.
- <sup>11</sup>Abou Ellail, M.M.M., Gosman, A. D., Lockwood, F. C., and Megahed, I.E.A., "Description and Validation of a Three-Dimensional Procedure for Combustion Chamber Flows, Turbulent Combustion," *AIAA Progress in Astronautics and Aeronautics—Turbulent Combustion*, edited by L. A. Kennedy, Vol. 58, New York, 1978, pp. 163-190.
- <sup>12</sup>Mongia, H. C. and Reynolds, R. S., "Combustor Design Criteria Validation Vol. III—User's Manual," Rept. USARTL-TR-78-55C, U.S. Army Res. & Tech. Lab., Ft. Eustis, Va., Feb. 1979 (see also Vols. I and II).
- <sup>13</sup>Serag-Eldin, M. A. and Spalding, D. B., "Computations of Three-Dimensional Gas-Turbine Combustion Chamber Flows," *Journal of Engineering for Power, Transactions of ASME*, Vol. 101, July 1979, pp. 326-336.

APPENDIX F

SUB-CONTRACT ACTIVITY AT DYNAMICS TECHNOLOGY

# Dynamics Technology, Inc.

---

DTN-8178-01

SEMI-ANNUAL STATUS REPORT  
EXPERIMENTS ON SWIRLING,  
CONFINED JET FLOWFIELDS

A Subcontract To:  
Oklahoma State University

Principal Investigator:  
Dennis K. McLaughlin

February, 1982

As Part Of:

"Investigations of Flowfields Found in Typical  
Combustor Geometries" NASA Lewis Research  
Center Grant No. NAG-3-74

Dynamics Technology, Inc.  
22939 Hawthorne Blvd.  
Torrance, CA 90505  
(213) 373-0666

This report has undergone an extensive internal review before publication, both for technical and non-technical content, by the Program Manager and an independent internal review committee.

Program Manager:

Duane Howe

Internal Review:

Robert L. Green

## 1. SUMMARY OF PROJECT ACTIVITY

Through the subcontract project number 8178 Dynamics Technology has contributed to the Oklahoma State University project "Investigation of Flowfields Found in Typical Combustor Geometries" in the following two areas:

- (1) Facility assembly in preparation for turbulence measurements in a swirling confined jet using a three-wire hot-wire probe.
- (2) Consultation by D. K. McLaughlin on student work at Oklahoma State University.

## 2. SUMMARY OF PROGRESS

### Activity 1.

Considerable effort has been expended in assembling the confined, swirling jet facility. Several of the major components of this facility: the nozzle, turbulence management section and fan diffuser, were constructed by students at Oklahoma State University this past summer. Dynamics Technology personnel have been assembling these components on framework constructed for that purpose and mating it to the fan supplied by Dynamics Technology.

A problem with the diffuser downstream of the fan has demanded our attention. The flow exiting the fan has residual swirl. When this passes into the expansion flow in the diffuser a central recirculation regions forms. This is very similar to the flowfield experienced in the test section of the swirling confined jet, which is the basic phenomenon under study. The recirculating flow is very unsteady and undesirable in

the flowfield upstream of the facility nozzle.

The recirculation region in the diffuser flow has been eliminated by inserting a section of short straws just downstream of the fan, which eliminates the swirl component of the flow. The nonswirling flow then separates from the walls of the diffuser as normally expected in diffusers with larger than  $6^\circ$  expansion half angle. This separated flow has been eliminated by inserting perforated plates across the flow at three locations equally spaced in downstream locations.

Finishing work on the nozzle and turbulence management sections are presently underway. Final facility assembly should take place in early March. At that time the swirl pack and probe drive being constructed by Oklahoma State University students, will be incorporated with the main facility.

Planning has begun for the computer software required to control the acquisition of data from the three hot-wires on the probe. Analog to digital convertors (ADC's) will be controlled with our Tektronics 4051 computer terminal so that numerous batches of digitized signals will be input to computer memory and then transferred to magnetic tape. Programs will be written to convert these digitized data into three instantaneous components of velocity from which statistical estimates of mean velocities, and turbulent normal and shear stresses will be obtained. Distributions of these quantities will be plotted on the Tektronics 4051 CRT screen from which hard copies will be directly obtained.

The three-wire hot-wire probe requires three channels of anemometer electronics which will be supplied by Dynamics Technology. The three-wire probe will require extensive calibration at the start, and periodic calibration during the series of production experiments. The results of

these calibrations are used in the data reduction to convert raw hot-wire signals into the individual velocity components. We anticipate beginning the first calibrations in mid-March.

Activity 2.

Dr. McLaughlin has provided consultation services to students at Oklahoma State University during the past several months. The bulk of this activity has focused on the MS thesis work of Salim Janjua and the crossed hot-wire experimental program of Trevor Jackson. This activity will continue on an as needed basis.